

THE FINITE ELEMENT METHOD OVER A SIMPLE STABILIZING GRID APPLIED TO
FLUID FLOW PROBLEMS

SELÇUK HAN AYDIN

MAY 2008

THE FINITE ELEMENT METHOD OVER A SIMPLE STABILIZING GRID APPLIED TO
FLUID FLOW PROBLEMS

A THESIS SUBMITTED TO
THE GRADUATE SCHOOL OF APPLIED MATHEMATICS
OF
THE MIDDLE EAST TECHNICAL UNIVERSITY

BY

SELÇUK HAN AYDIN

IN PARTIAL FULFILLMENT OF THE REQUIREMENTS FOR THE DEGREE OF
DOCTOR OF PHILOSOPHY
IN
THE DEPARTMENT OF SCIENTIFIC COMPUTING

MAY 2008

Approval of the Graduate School of Applied Mathematics

Prof. Dr. Ersan AKYILDIZ
Director

I certify that this thesis satisfies all the requirements as a thesis for the degree of Doctor of Philosophy

Prof. Dr. Bülent KARASÖZEN
Head of Department

This is to certify that we have read this thesis and that in our opinion it is fully adequate, in scope and quality, as a thesis for the degree of Doctor of Philosophy.

Prof. Dr. Münevver TEZER-SEZGİN
Advisor

Assoc. Prof. Dr. Ali İhsan NESLİTÜRK
Co-Advisor

Examining Committee Members

Prof. Dr. Bülent KARASÖZEN

Prof. Dr. Münevver TEZER-SEZGİN

Assoc. Prof. Dr. Ali İhsan NESLİTÜRK

Prof. Dr. Haluk AKSEL

Prof. Dr. Tanıl ERGENÇ

I hereby declare that all information in this document has been obtained and presented in accordance with academic rules and ethical conduct. I also declare that, as required by these rules and conduct, I have fully cited and referenced all material and results that are not original to this work.

Name, Last name :

Signature :

ABSTRACT

THE FINITE ELEMENT METHOD OVER A SIMPLE STABILIZING GRID APPLIED TO FLUID FLOW PROBLEMS

Aydın Selçuk Han

Ph.D., Department of Scientific Computing

Institute of Applied Mathematics

Advisor: Prof. Dr. Münevver Tezer-Sezgin

Co-Advisor: Assoc. Prof. Dr. Ali İhsan Neslitürk

May 2008, 125 pages

We consider the stabilized finite element method for solving the incompressible Navier-Stokes equations and the magnetohydrodynamic (MHD) equations in two dimensions. The well-known instabilities arising from the application of standard Galerkin finite element method are eliminated by using the stabilizing subgrid method (SSM), the streamline upwind Petrov-Galerkin (SUPG) method, and the two-level finite element method (TLFEM). The domain is discretized into a set of regular triangular elements. In SSM, the finite-dimensional spaces employed consist of piecewise continuous linear interpolants enriched with the residual-free bubble functions. To find the bubble part of the solution, a two-level finite element method with a stabilizing subgrid of a single node is described and its applications to the Navier-Stokes equations and MHD equations are displayed. This constitutes the main original contribution of this thesis. Numerical approximations employing the proposed algorithms are presented for some benchmark problems. The results show that the proper choice of the subgrid node is crucial to get stable and accurate numerical approximations consistent with the physical configuration of the problem at a cheap computational cost. The stabilized finite element method of SUPG type is applied to the unsteady Navier-Stokes equations together with a finite element discretization in the time domain. Thus, oscillations in the solution and the need of very small time increment are avoided in obtaining stable solutions.

Keywords: Stabilized FEM, Stabilizing subgrid, Two-level finite element method, Navier-Stokes Equations, Magnetohydrodynamic equations.

ÖZ

STABİLİZE EDİLMİŞ GRİD ÜZERİNDE SONLU ELEMANLAR YÖNTEMİNİN AKIŞKAN AKIM PROBLEMLERİNE UYGULAMASI

Aydın, Selçuk Han

Doktora, Bilimsel Hesaplamalar Bölümü

Uygulamalı Matematik Enstitüsü

Tez Danışmanı: Prof. Dr. Münevver Tezer-Sezgin

Ortak Danışman: Doç. Dr. Ali İhsan Neslitürk

Mayıs 2008, 125 sayfa

Bu tezde, iki boyutlu uzayda, Navier-Stokes denklemleri ve magnetohidrodinamik (MHD) denklemlerinin stabilize edilmiş sonlu elemanlar yöntemleri ile çözümleri verilmektedir. Standart Galerkin yönteminden kaynaklanan ve bilinen kararsızlıklar, stabilize edilmiş alt grid yöntemi (SSM), streamline upwind Petrov-Galerkin (SUPG) yöntemi ve iki aşamalı sonlu elemanlar yöntemleri (TLFEM) kullanılarak giderilmektedir. Problem tanım bölgesi, düzgün bir yapıda üçgen elemanlara ayrıklaştırılır. SSM yönteminde, sonlu elemanlar uzayı, parçalı, sabit ve doğrusal enterpolasyon fonksiyonlarının yanında kalansız ampul fonksiyonları kullanılarak genişletilmektedir. Çözümün ampul fonksiyon kısmı, stabilize edilmiş tek noktalı alt grid üzerinde iki aşamalı sonlu elemanlar yöntemi kullanılarak elde edilmekte ve Navier-Stokes denklemleri ile MHD denklemlerine uygulamaları gerçekleştirilmektedir. Bunlar, tezdeki en önemli yenilikler olarak ön plana çıkmaktadır. Verilen algoritmaların sayısal çözüm uygulamaları örnek problemler üzerinde gerçekleştirilir. Elde edilen sonuçlara göre, alt grid noktasının uygun seçimi problemin fiziksel konfüğürasyonu ile uyumlu, kararlı ve verimli sayısal sonuçların ucuz olarak elde edilmesinde önem göstermektedir. Zaman bağımlı Navier-Stokes denklemlerinin çözümü, SUPG türü stabilize edilmiş sonlu elemanlar yöntemine ilave olarak zaman boyutunda da sonlu elemanlar yöntemi kullanılarak elde edilmektedir. Böylelikle kararlı çözüm elde edilmesinde görülen salınımlar ve küçük zaman aralığı kullanımı sorunları giderilmektedir.

Anahtar Kelimeler : Stabilize sonlu elemanlar yöntemi, stabilize edilmiş alt grid, iki aşamalı sonlu elemanlar yöntemi, Navier-Stokes denklemleri, magnetohidrodinamik denklemleri.

To my wife,
Burcu

ACKNOWLEDGMENTS

I would like to express my sincere appreciation to the members of the Institute of Applied Mathematics of Middle East Technical University, especially to Prof. Dr. Münevver TEZER-SEZGİN and Assoc. Prof. Dr. Ali İhsan NESLİTÜRK for their valuable guidance and helpful suggestions in every aspect from the very beginning onwards.

Deepest thanks and regards to my family who have provided me the love, support and educational background that has enabled me to be successful both in my personal and academic life.

Finally, I would also like to thank the members of the Computer Center and my friends for their support during the preparation of this thesis.

TABLE OF CONTENTS

PLAGIARISM	iii
ABSTRACT	iv
Öz	vi
ACKNOWLEDGMENTS	ix
TABLE OF CONTENTS	ix
LIST OF FIGURES	xiii
LIST OF TABLES	xvii

CHAPTER

1 INTRODUCTION	1
1.1 Basic equations	1
1.1.1 Conservation of mass	2
1.1.2 Conservation of momentum	3
1.2 The Navier-Stokes equations	4
1.3 The Magnetohydrodynamic equations	7
1.4 Plan of the thesis	10
2 SOLUTION OF THE NAVIER-STOKES EQUATIONS	12
2.1 Stabilized Finite Element Methods	18

2.1.1	Convection-diffusion equation	18
2.1.2	SUPG formulation of the Navier-Stokes equations	19
2.2	Stabilizing Subgrid Method (SSM)	21
2.3	Two-Level Finite Element Method (TLFEM)	24
2.3.1	TLFEM for the convection-diffusion equation	24
2.3.2	TLFEM for the Navier-Stokes equations	26
2.4	Numerical Results	28
2.4.1	L-Shape flow	32
2.4.2	Rotating flow field	35
2.4.3	Lid-Driven Cavity flow	36
2.4.4	Backward facing step flow	50
2.4.5	Flow past a cylinder	55
3	SOLUTION OF THE UNSTEADY NAVIER-STOKES EQUATIONS	61
3.1	Finite Element Method in Time	61
3.1.1	Diffusion equation	62
3.1.2	Convection-diffusion equation	64
3.1.3	Unsteady Navier-Stokes equations	64
3.2	Finite Difference Method in Time	66
3.2.1	Convection-diffusion equation	67
3.2.2	Unsteady Navier-Stokes equation	68
3.3	Numerical Results	69
3.3.1	Diffusion equation	69
3.3.2	Convection-diffusion equation	70
3.3.3	Taylor vortex flow	70
3.3.4	Flow around a cylinder	71
4	SOLUTION OF THE MAGNETOHYDRODYNAMIC EQUATIONS	78
4.1	FEM formulation of the MHD equations	80
4.2	SUPG formulation for the MHD equations	81

4.3	TLFEM for the MHD equations	82
4.4	SSM for the MHD equations	87
4.5	Magnetic pressure in the MHD equations	89
4.6	Numerical Results	91
4.6.1	Test problem	91
4.6.2	MHD Cavity flow	99
4.6.3	MHD flow over a step	106
4.6.4	MHD Duct flow	109
5	CONCLUSION	114
	REFERENCES	116
	VITA	123

LIST OF FIGURES

1.1	Control volume and surface	2
2.1	Types of inflow boundary	22
2.2	Submesh for rectangle and quadrangle elements	29
2.3	Bubble functions for rectangular elements	30
2.4	3-D view of bubble function for rectangular elements	30
2.5	Two different types of submesh generations and corresponding bubble functions for triangular elements	31
2.6	Definition of L-shape flow problem	32
2.7	Standard Galerkin FEM and SUPG solutions of L-Shape flow	33
2.8	Stabilization effect in L-shape flow near boundary layers for $\epsilon = 5 \times 10^{-4}$	34
2.9	Comparison of SUPG and TLFEM solutions of rotating flow field	35
2.10	The problem statement of the lid-driven cavity flow	36
2.11	The problem meshes tested for the cavity flow: 800 and 3200 elements	37
2.12	Pressure elevation and streamlines for the cavity flow, $Re = 100$	37
2.13	Solutions of the cavity flow with 3200 elements of Q2-Q1 type	38
2.14	Comparison of Q2-Q1 elements with SUPG method for the cavity flow, $Re = 400$	40
2.15	Comparison of Q2-Q1 elements with SUPG method for the cavity flow, $Re = 5200$	41
2.16	Pressure contours and elevations for the cavity flow with SSM, TLFEM and Q2- Q1, $Re = 400$	42
2.17	Pressure contours and elevations for the cavity flow with SSM, TLFEM and Q2- Q1, $Re = 5200$	43
2.18	Pressure contours and elevations for the cavity flow with SP, GP and TLFEM, $Re = 5200$	44

2.19	Adaptation of the subgrid points in SSM as the problem mesh is refined at $Re = 5200$: The problem meshes are $e800$ and $e3200$	45
2.20	Adaptation of the subgrid points in SSM as the problem becomes convection dominated on a fixed mesh $e800$: $Re = 400$ and $Re = 5200$	46
2.21	Streamlines for the cavity flow with SSM, $Re = 5200$	46
2.22	Velocity profiles for the cavity flow with SSM, $Re = 400$ and $Re = 5200$	47
2.23	Randomly generated non-uniform mesh and pressure contours for the cavity flow	48
2.24	Modified non-uniform mesh and pressure contours for the cavity flow	48
2.25	Unstructured, quadratically distributed mesh and streamlines for the cavity flow: $Re = 1000, 2500$ and 5000	49
2.26	The statement of the backward facing step flow	50
2.27	The problem meshes tested for the backward facing step flow	51
2.28	Pressure contours for the backward facing step flow with SP, GP and TLFEM, $Re = 150$	51
2.29	Pressure elevations for the backward facing step flow with SP, GP and TLFEM, $Re = 150$	52
2.30	Streamline details for the backward facing step flow behind the step with SP, GP and TLFEM, $Re = 150$	53
2.31	Changes in the flow as Reynolds number increases for the backward facing step flow with SSM	54
2.32	The statement of the flow past a cylinder	55
2.33	The problem meshes tested for the flow past a cylinder	56
2.34	Pressure contours for the flow past a cylinder, $Re = 26$	57
2.35	Pressure detail behind the cylinder for $Re = 26$	58
2.36	Mesh detail around the cylinder for $Re = 26$ with $e=1700$ and $e=6800$	59
2.37	Streamlines details behind the cylinder for $Re = 26$	60
3.1	A sample bilinear-linear element in the spatial-time domain	63
3.2	FEM, FDM and exact solutions of diffusion problem at $t = 0.05$	70
3.3	Solution of convection-diffusion problem at $t = 0, 0.25$ and $t = 2.0$	71
3.4	Pressure and Streamlines for Taylor vortex flow($t = 1.0$)	71

3.5	The velocity contours for Taylor vortex flow ($t = 1.0$)	72
3.6	The problem mesh tested for flow around a cylinder: 5404 triangular elements . .	72
3.7	Pressure contours for flow around a cylinder	73
3.8	Streamlines for flow around a cylinder	74
3.9	Pressure contours for unsteady flow around a cylinder using FDM in time at $t = 1, 2, 4, 6$ and 8	75
3.10	Velocity (u) component for unsteady flow around a cylinder using FDM in time at $t = 1, 2, 4, 6$ and 8	76
3.11	Flow vectors for unsteady flow around a cylinder using FDM in time at $t =$ $1, 2, 4, 6$ and 8	77
4.1	Pressure contours and elevations obtained from standard Galerkin FEM and exact solutions	92
4.2	Standard Galerkin FEM and exact solutions for the velocity(u_1, u_2)	93
4.3	Standard Galerkin FEM and exact solutions for the magnetic field(B_1, B_2) . . .	94
4.4	Pressure contours obtained from FEM with Babuska-Brezzi condition and exact solutions	95
4.5	Magnetic pressure contours and elevations obtained from standard Galerkin FEM and Babuska-Brezzi condition (Q2-Q2-Q2-Q1 elements)	96
4.6	Pressure contours obtained from SUPG, SSM and exact solutions	97
4.7	Zoom for the pressure contours obtained from SUPG, SSM	97
4.8	Velocity flow vectors and adaption of the position of the subgrid point	98
4.9	The problem statement and a uniform mesh with 3200 triangular elements for MHD cavity flow	99
4.10	Pressure contours obtained from SUPG, SSM and Babuska-Brezzi formulations for $Ha = 0$, $Ha = 10$ and $Ha = 100$; applied magnetic field is through $+x$ direction	100
4.11	Pressure elevations obtained from SUPG, SSM and Babuska-Brezzi formulations for $Ha = 0$, $Ha = 10$ and $Ha = 100$; applied magnetic field is through $+x$ direction	101
4.12	Velocity component (u_1) contours for $Ha = 0$ and $Ha = 100$ with SSM; applied magnetic field is through $+x$ direction	102
4.13	Streamlines of the velocity for $Ha = 0$ and $Ha = 100$ with SSM; applied magnetic field is through $+x$ direction	102

4.14	Flow vectors of the magnetic field for $Ha = 0$ and $Ha = 100$ with SSM; applied magnetic field is through $+x$ direction	103
4.15	Pressure, first component of the velocity and magnetic field contours for $Ha = 10$ and $Ha = 100$ with SSM; applied magnetic field is through $+y$ direction	104
4.16	Streamlines of the velocity and flow vectors of the magnetic field for $Ha = 100$ with SSM; applied magnetic field is through $+y$ direction	105
4.17	The problem statement and a uniform mesh with 7168 triangular elements for the MHD step flow	106
4.18	Pressure contours for $Ha = 0$, $Ha = 5$ and $Ha = 10$	107
4.19	x-component (B_1 contours) of the magnetic field for $Ha = 5$ and $Ha = 10$	107
4.20	Velocity flow vectors and streamlines (zoom in behind the step) for $Ha = 0$, $Ha = 5$ and $Ha = 10$	108
4.21	Velocity and induced magnetic field contours at $t = 0.01$ and $t = 0.03$ for $M = 100$	111
4.22	Velocity and induced magnetic field contours at $t = 0.001$ and $t = 0.003$ for $M = 1000$	112
4.23	Velocity and induced magnetic field contours at $t = 0.001$ for $M = 10000$	113

LIST OF TABLES

- 2.1 Velocity values at some selected points through the geometric center of the cavity 47

CHAPTER 1

INTRODUCTION

Because of the applications in many different areas, fluid dynamics and solution of the fluid flow problems gain importance among researchers. However, both the simulation with experiments and finding the exact solution of the fluid flow problems are not easy. Therefore, finding the numerical solutions of the fluid flow problems which is the most important computational approach, is the popular branch of the applied mathematics.

Some of the important properties of the fluids are the density and viscosity. Also, depending on some other properties of the fluids, they are classified as compressible/incompressible, Newtonian/non-Newtonian, laminar/turbulent, etc.

Fluid dynamics is dealing about the behaviour of fluids such as its motion, velocity and its changes. Fluid flow is caused by the action of externally applied forces, compression or stress. Analysis of the motion is concentrated on the velocity of the fluid, changes in the pressure, effect of the applied magnetic field and some other changes.

1.1 Basic equations

An analysis of fluid flow problems is based on some laws. The mathematical modelling of the fluid flow problems are derived from the following principles [57];

1. Conservation of mass
2. Newton's second law of motion (conservation of momentum)
3. Conservation of energy.

Derivation of continuity equation which results from the conservation of mass, and equations of motion resulting from the conservation of momentum are given in the next subsections over

a control volume using integral approach [57]. These equations can also be obtained by using derivative approach.

1.1.1 Conservation of mass

The most important property in Newtonian fluid dynamics is that mass is conserved. The law of conservation of mass is stated as "mass is not created nor destroyed".

Consider a fluid element of a finite volume V (control volume) surrounded by surface area S (control surface) (Figure 1.1).

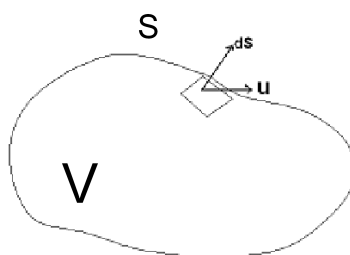


Figure 1.1: Control volume and surface

Then, the mass balance is written as:

$$\left\{ \begin{array}{l} \text{The rate of flow} \\ \text{of mass into } V \end{array} \right\} = \left\{ \begin{array}{l} \text{The rate of increase} \\ \text{of mass in } V \end{array} \right\}$$

Let ρ be the density and \mathbf{u} the velocity of the fluid and the normal vector on the surface S is through out of V . Then, the net rate of flow of mass through the control surface S is

$$-\int_S \rho \mathbf{u} \cdot d\mathbf{S} \quad (1.1)$$

and the net rate of increase of mass within the control volume V is

$$\int_V \frac{\partial \rho}{\partial t} dV. \quad (1.2)$$

Using the divergence theorem

$$\int_V \left\{ \frac{\partial \rho}{\partial t} + \nabla \cdot (\rho \mathbf{u}) \right\} dV = 0. \quad (1.3)$$

Note that, this equality is valid for any volume V . Therefore, we will obtain the main equation of the fluid flow problems called "**the continuity equation**" as

$\frac{\partial \rho}{\partial t} + \nabla \cdot (\rho \mathbf{u}) = 0. \quad (1.4)$
--

For incompressible flows, ρ is constant. Therefore, whether the flow is steady or unsteady, the continuity equation is written as

$$\nabla \cdot \mathbf{u} = 0. \quad (1.5)$$

1.1.2 Conservation of momentum

The second governing equation for the fluid dynamics is based on the "momentum balance" property. The conservation of momentum for the fluid flows is derived similarly over a control volume V as

$$\left\{ \begin{array}{l} \text{The rate of increase} \\ \text{of momentum} \\ \text{inside volume } V \end{array} \right\} = \left\{ \begin{array}{l} \text{The rate of} \\ \text{momentum inflow} \\ \text{through } S \end{array} \right\} + \left\{ \begin{array}{l} \text{Total forces} \\ \text{acting inside } V \end{array} \right\} + \left\{ \begin{array}{l} \text{Total forces} \\ \text{acting on } S \end{array} \right\}.$$

Thus the equation of motion for the fluid inside S is

$$\frac{\partial}{\partial t} \int_V \rho u_i dV = - \int_S \rho u_i \mathbf{u} \cdot d\mathbf{S} + \int_V \rho f_i dV + \int_S \sigma_{ij} dS_j \quad (1.6)$$

where u_i is the i^{th} component of the velocity \mathbf{u} , f_i is the i^{th} component of the body force \mathbf{f} and σ_{ij} is the stress tensor. Using the divergence theorem and the identity

$$\rho u_i \mathbf{u} \cdot d\mathbf{S} = \rho u_i u_j dS_j \quad (1.7)$$

all the terms are collected under volume integral

$$\int_V \left\{ \frac{\partial}{\partial t}(\rho u_i) + \frac{\partial}{\partial x_j}(\rho u_i u_j) - \rho f_i - \frac{\partial}{\partial x_j} \sigma_{ij} \right\} dV = 0 \quad (1.8)$$

where x_j is the j^{th} component of the space coordinate. Finally, because V is arbitrary, "**the equation of motion**" is obtained as

$$\frac{\partial}{\partial t}(\rho u_i) + \frac{\partial}{\partial x_j}(\rho u_i u_j) = \rho f_i + \frac{\partial}{\partial x_j} \sigma_{ij}. \quad (1.9)$$

There are two types of forces to be included, body forces and surface forces. Body force is due to the gravity. Surface forces arise from the pressure and viscous stresses. Therefore, the stress σ_{ij} includes the pressure p and the normal viscous stress τ_{ij} . Since the pressure is acting through inward direction, it appears with negative sign in the equation.

A full form for σ_{ij} in terms of the constants μ and K is given as

$$\sigma_{ij} = -P\delta_{ij} + 2\mu(e_{ij} - \frac{1}{3} e_{kk} \delta_{ij}) \quad (1.10)$$

where

$$e_{ij} = \frac{1}{2} \left(\frac{\partial u_i}{\partial x_j} + \frac{\partial u_j}{\partial x_i} \right), \quad e_{kk} = \frac{\partial u_k}{\partial x_k} = \nabla \cdot \mathbf{u} \quad \text{and} \quad P = p - K e_{kk} \quad (1.11)$$

with p and P as thermodynamic and mechanical pressures, respectively.

Substituting for σ_{ij} in the equation of motion (1.9), we obtain the full Navier-Stokes equations

$$\rho \frac{Du_i}{Dt} = \rho f_i - \frac{\partial p}{\partial x_i} + \frac{\partial}{\partial x_j} \left\{ \mu \frac{\partial u_i}{\partial x_j} + \mu \frac{\partial u_j}{\partial x_i} \right\} + \frac{\partial}{\partial x_i} \left\{ \left(K - \frac{2}{3}\mu \right) \frac{\partial u_k}{\partial x_k} \right\}. \quad (1.12)$$

We write the equation in vector form as

$$\rho \left(\frac{\partial \mathbf{u}}{\partial t} + \mathbf{u} \cdot \nabla \mathbf{u} \right) = \rho \mathbf{f} - \nabla p + \mu \nabla^2 \mathbf{u} + \left(K - \frac{2}{3}\mu \right) \nabla \nabla \cdot \mathbf{u} \quad (1.13)$$

where μ is the dynamic viscosity and K has a value near that of μ . For incompressible fluids the Navier-Stokes equations take the form

$$\rho \left(\frac{\partial \mathbf{u}}{\partial t} + \mathbf{u} \cdot \nabla \mathbf{u} \right) = \rho \mathbf{f} - \nabla p + \mu \nabla^2 \mathbf{u} \quad (1.14)$$

where ∇^2 is the Laplace operator

1.2 The Navier-Stokes equations

The Navier-Stokes equations, named after Claude-Louis Navier (1827) and George Gabriel Stokes (1845), describe the motion of viscous fluid substances such as liquids and gases. The Navier-Stokes equations for the incompressible fluids are obtained in the previous subsection as

$$\begin{aligned} \frac{\partial \mathbf{u}}{\partial t} + \mathbf{u} \cdot \nabla \mathbf{u} &= -\frac{1}{\rho} \nabla p + \nu \nabla^2 \mathbf{u} + \mathbf{f} \\ \nabla \cdot \mathbf{u} &= 0 \end{aligned} \quad (1.15)$$

where $\nu = \frac{\mu}{\rho}$ is the kinematic viscosity. In non-dimensional form, it is written as

$$\begin{aligned} \frac{\partial \mathbf{u}}{\partial t} + \mathbf{u} \cdot \nabla \mathbf{u} &= -\nabla p + \frac{1}{Re} \nabla^2 \mathbf{u} + \mathbf{f} \\ \nabla \cdot \mathbf{u} &= 0 \end{aligned} \quad (1.16)$$

where $Re = \frac{\rho \mathbf{U}_0 L}{\mu}$ with \mathbf{U}_0 and L are characteristic velocity and length, respectively.

The nonlinear character makes difficult finding the exact solution of the Navier-Stokes equations. However, many researchers are interested in the solution of the equations with numerical methods especially by the finite element method (FEM) which is one of the most valuable numerical tool used in the solution of many engineering problems.

Applications of the Galerkin finite element method to incompressible Navier-Stokes equations in velocity-pressure form were carried out in the early 1970's. It was soon recognized that the use of equal-order interpolations for both the velocity and pressure variables, which is the most desirable choice from the implementation point of view, generates numerical approximation

that is inconsistent with the physical configuration of the problem. The difficulty is two-folded. In the first layer, the finite element formulation of the problem is of mixed form and the appropriate pair of the function spaces satisfying the Babuška-Brezzi condition (the order of pressure approximation is less than the order of velocity approximation) must be employed [1, 4, 59]. However, the problem may still exhibit numerical instabilities at high Reynolds numbers even the appropriate pair of approximation spaces are employed. A considerable amount of scientific work has been devoted to developing numerical algorithms that are able to cope with both of these problems simultaneously.

One of the most popular of such numerical methods is referred to as the streamline upwind Petrov-Galerkin (SUPG) method [13]. The finite element method of the SUPG type reduces the oscillations in the standard Galerkin method of piecewise linears and achieves stability by adding mesh-dependent perturbation terms to the formulation. These terms enhance the coercivity of the formulation by acting like artificial diffusion in the direction of streamlines and enables the usage of the equal order velocity-pressure pairs which are known to produce approximations not consistent with the exact solution of the problem [43]. However, the amount of perturbation or the value of the stability parameters which should be chosen by user is not known a priori and needs to be adjusted by means of error analysis and/or experiments.

Later, it has been shown that the SUPG type stabilized methods for the equations modelling the flow problems can be derived by adding the bubble functions (functions defined on the interior of the finite element that vanish on the element boundary [19]) to the velocity space in the standard Galerkin finite element formulation and then eliminating the bubbles by using the static condensation approach [5, 6, 12, 23, 37, 60]. In this approach, the optimal choice of the stabilization parameter in the SUPG method was simply translated into the problem of the optimal choice of the bubble space. Therefore the bubble functions should be chosen appropriately to cope with the difficulties arising in the numerical simulation of the equations. In that context, the residual-free bubble (RFB) functions whose description is based on a local boundary value problem related to the strong form of the equation in each element were introduced in [12]. The numerical methods employing the RFB functions were investigated in different element configurations mostly for convection-dominated flows. It can be verified that the RFB method enhances the stability of the discrete problem and satisfies a priori error estimates similar to the ones for the SUPG method [7, 8, 11, 28, 63].

Bubble functions are defined on element level for each element and vanish on the element boundary. Although, the stabilization can be performed by using polynomial bubble functions, they don't change its shape and characteristics as problem getting convection-dominated. Therefore, a special case of the bubble functions called residual-free bubble (RFB) functions give better accuracy in convection-dominated case since they change both height and shape depending on the flow direction. The RFB functions minimize the residual inside each element by satisfying

the strong form of the problem locally. The RFB functions are first introduced by Brezzi and Russo [12] and applied in many flow problems.

Since the residual-free bubble method is based on the classical solution of a local problem of convection-diffusion type, finding its exact solution is usually difficult as much as the original system of differential equations. Therefore, an accurate numerical algorithm to obtain the approximate solution of the bubble problem inside each element has to be designed. This can be done by the two-level finite element method (TLFEM). The two-level finite element method was first introduced by Franca and Macedo in [26] for the Helmholtz equation. It was later extended to the convection-diffusion equation by Franca et.al. [28] and to the incompressible Navier-Stokes equations in [52, 27]. TLFEM consists of two parts: On the one at the global mesh level, the problem will be in the Galerkin framework while the bubble part of the solution is still unknown. Before solving the problem on the global mesh, we have to compute the bubble functions which is accomplished in the second part of the method. To do this, we set another layer of mesh (subgrid) inside each element on which we calculate the approximate solution of bubble functions by using a non-standard finite element method. Then, these approximations are used instead of the exact bubble functions in the global mesh level of the formulation. However, the implementation of the TLFEM can be expensive from the computational point of view and a cheap efficient algorithm that generates qualitatively the same bubble functions as the TLFEM thus is sought.

Recently, some numerical algorithms were proposed in the context of convection-diffusion equation to provide a cheap approximate solution to the bubble problem with the use of a subgrid consisting of very few nodes [9, 10]. The method can be viewed as a variant of the TLFEM where the subgrid is consisted of a single internal node plus three vertices induced by the global mesh, per element. The internal node is taken over one of the medians of the triangle and the precise location of the subgrid node is determined so that a residual value becomes minimum in the sense of L_1 . With the use of suitably chosen internal subgrid node, it can be proven that the resulting numerical method, called Stabilizing Subgrid Method (SSM), has qualitatively similar stability features of the classical stabilized methods and satisfies the same a priori error estimates as the SUPG or the RFB methods do. However, these results hold only if the convection field is piecewise-constant inside each element.

Application of spatial discretization using the FEM to transient field problems governed by convection-diffusion type partial differential equations yields a system of ordinary differential equations of the first order. This initial value problem can be solved by a finite difference approximation of the time derivative [16, 18, 41, 42, 48, 78], weighted residual methods in the context of one time element representing the entire time domain [65, 79], least squares schemes [69, 70]. The space-time finite element formulation has been used for various problems by Hughes et al. [39, 40]. The finite element interpolation functions are discontinuous in time so that the fully

discrete equations are solved one space-time slab at a time. Mittal and Tezduyar [50] presented numerical results for certain unsteady flows past oscillating cylinders and aerofoils with computations based on the stabilized space-time FE formulation. They have also used the deforming-spatial-domain/space-time (DSD/ST) for computation of unsteady viscous incompressible flows which involve moving boundaries and interfaces [71, 72]. Similarly, FE computations in the space domain based on the standard Galerkin formulation of incompressible unsteady flows can involve numerical instabilities due to the presence of dominating convection terms in the governing equations and due to the use of inappropriate combinations of interpolation functions to represent velocities and the pressure. To stabilize the computations, the consistent Streamline Upwind Petrov-Galerkin (SUPG) FEM should be used to handle the convective terms. Other approaches are also in use as projection and fractional Q -scheme [48]. Codina et al. [16] have implemented a stabilized FE formulation for the incompressible Navier-Stokes equations based on a pressure gradient projection.

In our study, we apply the stabilizing subgrid method (SSM) to obtain approximate solution of the incompressible Navier-Stokes equations on a triangular discretization of the domain. We employ the space of continuous piecewise-linear interpolation functions plus bubbles for velocity variable and the continuous piecewise-linear interpolation functions for pressure variable in a framework of the mixed finite element method. The nonlinearity emanating from the nature of the equation is treated through an iteration. We assume the convection field is uniform (constant) inside each element by taking the average value of the velocity variable at the vertices of the triangle. The resulting numerical scheme gives accurate and stable solutions. Furthermore, it is computationally cheap and able to adapt itself for different flow regimes.

1.3 The Magnetohydrodynamic equations

Magnetohydrodynamics (MHD) is the theory of the macroscopic interaction of electrically conducting fluid and electromagnetic fields. Applications arise in astronomy and geophysics and as well as in connection with numerous engineering problems, such as liquid-metal cooling of nuclear reactors, electromagnetic casting of metals, MHD power generation, and MHD ion propulsion. In MHD problems we deal with a flow of viscous, incompressible fluid which has a property of electric current conduction and interacting with electromagnetic fields. The conducting fluid flow can induce electric current and interact with the magnetic field. This interaction in turn produces Lorentz force on the fluid and can greatly change the fluid behaviour. Thus, MHD flow is governed by the Navier-Stokes and pre-Maxwell equations coupled via the Lorentz force. The theory and the mathematical modelling of the equations can be found in [20, 67].

Analysis of electromagnetic in liquid metals involves solving the Maxwell equation for the non-existence of a magnetic monopole, Faraday's law, pre-Maxwell Ampere's law and Gauss law

as

$$\nabla \cdot \mathbf{B} = 0 \quad (1.17)$$

$$\nabla \times \mathbf{E} = -\frac{\partial \mathbf{B}}{\partial t} \quad (1.18)$$

$$\nabla \times \mathbf{B} = \mu_0 \mathbf{J} \quad (1.19)$$

$$\nabla \times \mathbf{D} = q \quad (1.20)$$

where \mathbf{B} is the magnetic induction, \mathbf{D} is the electric displacement, \mathbf{E} is the electric field, \mathbf{J} is the electric current density ($\mathbf{J} \equiv \sigma \mathbf{E}$) and q is the electric charge density. Actually, the Ampere's law is given as $\nabla \times \mathbf{H} = \mathbf{J} + \frac{\partial \mathbf{D}}{\partial t}$ with the magnetic field density \mathbf{H} . However, the displacement current $\frac{\partial \mathbf{D}}{\partial t}$ is assumed to be negligibly small in comparison with other terms.

For a free-space (non-magnetizable or non-polarizable) electromagnetic medium, define $\mathbf{H} = \mathbf{B}/\mu_0$ and $\mathbf{E} = \mathbf{D}/\epsilon_0$ with the free-space magnetic permeability $\mu_0 = 4\pi \times 10^{-7} \text{Hs/m}$ and free-space electric permittivity $\epsilon_0 = 8.854 \times 10^{-12} \text{F/m}$. Then, Ohm's law is written as

$$\mathbf{J} = \sigma(\mathbf{E} + \mathbf{u} \times \mathbf{B}) \quad (1.21)$$

where σ is the electrical conductivity of the material and \mathbf{u} is the velocity of the fluid in motion. Notice that, Ohm's law characterizes the ability of the investigated conducting fluid to transport electric charges under the influence of applied electric field.

If we perform the curl operator on each term in the Ohm's law

$$\begin{aligned} \text{curl}(\mathbf{J}) &= \sigma \text{curl}(\mathbf{E}) + \sigma \text{curl}(\mathbf{u} \times \mathbf{B}) \\ \frac{1}{\mu_0} \text{curl}(\nabla \times \mathbf{B}) &= -\sigma \frac{\partial \mathbf{B}}{\partial t} + \sigma \text{curl}(\mathbf{u} \times \mathbf{B}) \\ \frac{1}{\mu_0} \nabla(\nabla \cdot \mathbf{B}) - \frac{1}{\mu_0} \nabla^2 \mathbf{B} &= -\sigma \frac{\partial \mathbf{B}}{\partial t} + \sigma \nabla \times (\mathbf{u} \times \mathbf{B}) \end{aligned}$$

using the vector identity $\nabla \times (\nabla \times \mathbf{B}) = \nabla(\nabla \cdot \mathbf{B}) - \nabla^2 \mathbf{B}$.

Final form of the magnetic induction which enlightens the coupling of hydrodynamics and electromagnetic two fields, is written as

$$\frac{\partial \mathbf{B}}{\partial t} = \nabla \times (\mathbf{u} \times \mathbf{B}) + \frac{1}{\sigma \mu_0} \nabla^2 \mathbf{B}. \quad (1.22)$$

Also, under an applied magnetic field, the momentum equation is rewritten in non-dimensionalized form with the fluid Reynolds number Re , the magnetic Reynolds number Rem and the Hartmann number Ha , and an additional Lorentz force [46, 61, 68] as

$$\frac{\partial \mathbf{u}}{\partial t} + \mathbf{u} \cdot \nabla \mathbf{u} = -\nabla p + \frac{1}{Re} \nabla^2 \mathbf{u} + \mathbf{f} - \frac{Ha^2}{Re Rem} (\nabla \times \mathbf{B}) \times \mathbf{B} \quad (1.23)$$

where $Re = \frac{\rho \mathbf{U}_0 L}{\mu}$, $Rem = \mu_0 \sigma \mathbf{U}_0 L$, $Ha = \sqrt{Re Rem S}$ with the Coupling number $S = \frac{\mathbf{B}_0^2}{\mu_0 \rho \mathbf{U}_0}$, a characteristic value \mathbf{U}_0 for the velocity field, a characteristic value \mathbf{B}_0 for the magnetic field and a characteristic length L .

Several papers have been devoted to the analysis of numerical schemes for the simulation of MHD flows by using finite difference method (FDM). A nine-node grid, FD approximation was applied to solving MHD equations inside a channel with a rapidly expanded section in [44]. A description is made using two vector potentials and the vorticity vector, which form a system of three simultaneous, quasilinear equations of the elliptic type. Sekhar et al. [66] have obtained FD solutions in terms of stream function-vorticity for solving the steady MHD flow past a sphere with an applied magnetic field parallel to the main flow at low and moderate Reynolds number. In the paper written by Shue and Lin [68], a primitive variable approach for solving the magnetic field and hydrodynamic field equations has been given with the alternating direction implicit (ADI) solution algorithm. An extension of the generalized Peaceman and Rachford ADI scheme was presented in [51]. The discretized conservation equations are solved in stream function-vorticity formulation for low magnetic Reynolds number. 3-D numerical calculations on liquid-metal MHD flow through a rectangular channel in the inlet region, have been performed by Kumamaru et al [46] using the FDM.

Most of the numerical solutions of the MHD equations are performed by using the finite element method (FEM) because of its advantage in nonlinear equations. The existence of solutions of both continuous and discrete MHD problems without any condition on the boundary data of the velocity was derived in [77] and Gunzburger et al. [33] has shown that the existence and uniqueness of the solution of a weak formulation of the MHD equations can be guaranteed. Meir and Schmidt [49] and Schötzau [64] have carried out error analysis on their finite element solutions of MHD problems and established optimal order error bounds. Mixed FE approximation of incompressible MHD problems based on weighted regularization has been analyzed by Hasler et al [34]. Well-posedness of this approach and existence and uniqueness results, quasi-optimal error bounds were also provided. By using a two-level FEM for discretizing the stationary MHD equations, Layton et al. [47] have proved well-posedness of their algorithm and gave optimal error bounds. In their study, they have solved the nonlinear problem first on a coarse mesh and then the linear one on a fine mesh.

The study of MHD duct flows has great relevance for nuclear reactor cooling systems, MHD flowmeters, MHD micropumps. Such MHD flows have been studied under the assumption that the flow is fully developed. Then the problem dimensionality reduces from three to two and the application of the governing equations is allowed only in a transversal section of the duct. Verardi et al. [75, 76], Krzeminski [45], Tezer-Sezgin and Köksal [74] have given FE solutions of MHD equations in rectangular ducts. A stabilized FEM using the residual-free bubble (RFB) functions has been proposed by Neslitürk and Tezer-Sezgin [54, 55] for solving steady MHD duct flow problems. The FEM employing RFB functions was capable of solving the equations for high values of Hartmann number.

It is known that the small hydrodynamic diffusion may induce some well-known numerical

instabilities. It is therefore natural to use some stabilizing techniques for the Navier-Stokes equations. It may be also useful to stabilize the magnetic equation in spite of the high values of magnetic diffusivity. Several stabilized FEM studies are available for the full MHD equations. Gerbeau [31] has carried out a stabilized FEM procedure in terms of velocity (\mathbf{u}), the pressure (p) in the fluid and the magnetic field (\mathbf{B}), including a convergence proof. A stabilization technique is used in order to allow equal order interpolation on tetrahedral elements of all variables. In the papers by Salah et al. [61, 62], Codina and Silva [17], they have presented a stabilized FEM for the full MHD equations by including a magnetic pressure as unknowns to enforce the divergence free condition for the numerical approximation of the magnetic field.

As is done in the Navier-Stokes equations, numerical instabilities due to the coupled formulation and the existence of the coefficients in the MHD equations (the fluid Reynolds number Re , the magnetic Reynolds number Rem and the Hartmann number Ha), are eliminated by considering stabilized finite element methods. The application of the stabilizing subgrid method (SSM) to the solution of the MHD equations is given for the first time in this thesis. Obtained results have shown the accuracy of the SSM compared to SUPG type stabilization.

1.4 Plan of the thesis

We organize the thesis as follows. In Chapter 2, we introduce the finite element method first for the convection-diffusion type problems. Then, the numerical instabilities in the convection dominated flow problems, in obtaining solutions by standard Galerkin FEM formulation, are handled with stabilized finite element methods. These are Streamline Upwind Petrov Galerkin (SUPG), Stabilizing Subgrid Method (SSM) and Two-Level Finite Element Method (TLFEM). Then for the incompressible Navier-Stokes equations the same stabilization methods are applied. Demonstration of the mentioned methods is performed on the numerical solution of some test problems as L-shape flow, rotating flow field, cavity flow, backward facing step flow and flow past a cylinder.

In Chapter 3, transient field problems containing convection-diffusion terms are solved by using FEM in both space and time directions with a separation of variables idea and then FEM in space - FDM in time direction in order to make comparison. The separation of variables idea enables to express the temporal and space derivatives independently in terms of the derivatives of corresponding shape functions which may be taken equal order since the SUPG stabilization is performed. In this way, we take into account the deformation due to the convection terms (spatial domain) and also protect the computations against numerical oscillations in the time domain. The resulting discretized equations are solved iteratively in the time domain without the need of very small time increments. The application problems considered include diffusion and convection-diffusion problems, unsteady incompressible flow governed by Navier-Stokes equa-

tions.

Chapter 4 gives the FEM formulation of the incompressible MHD equations. The unknowns in the equations are the primitive variables as the velocity (\mathbf{u}), the magnetic field (\mathbf{B}) and the pressure in the fluid (p). Then, standard Galerkin, SUPG, TLFEM and SSM methods are all implemented. Existence of the magnetic pressure case is also considered. Then, numerical experiments are performed on a test problem having exact solution, MHD cavity flow problem and MHD flow over a step problem. A simplified form of the unsteady MHD equations describing the flow in a rectangular duct is also solved using the FEM formulation given in Chapter 3.

Finally, Chapter 5 contains the concluding remarks for the presented methods and obtained numerical results.

CHAPTER 2

SOLUTION OF THE NAVIER-STOKES EQUATIONS

In this Chapter, we describe stabilized finite element method, stabilizing subgrid method and two-level finite element method for solving the Navier-Stokes equations. The methods are explained first on convection-diffusion equations since the nonlinear terms in the Navier-Stokes equations are in the form of convection-diffusion. Applications of each method are given in Section (2.4).

The finite element method (FEM) is one of the most valuable numerical tool especially in the solution of many engineering problems. For the case of analytical solution is difficult to find or impossible, the finite element method gives a numerical solution of the problem in terms of weighted residual formulation.

The principle ingredients of the finite element method for constructing approximate solutions of problems are [58]

1. The formulation of the problem in a variational framework in which the appropriate space V of admissible functions is identified.
2. The construction of a finite element mesh and piecewise polynomial basis functions defined on the mesh, which generate a finite-dimensional subspace of V .
3. The construction of an approximation of the variational boundary-value problem on a finite element subspace V_h of V . This entails the calculation of element matrices and the generation of a sparse system of linear algebraic equations in the values of the approximate solution at nodal points in the mesh.
4. The solution of the algebraic system.

We first consider the second order boundary value problem

$$\begin{cases} -\nabla \cdot (\epsilon \nabla u(x, y)) + b(x, y)u(x, y) = f(x, y) & \text{in } \Omega \\ u(s) = \bar{u}(s) & \text{on } \partial\Omega_1 \\ -\epsilon \frac{\partial u(s)}{\partial n} = \ell(s) [u(s) - \bar{u}(s)] & \text{on } \partial\Omega_2 \end{cases} \quad (2.1)$$

where $\Omega \subset R^2$ with boundary $\partial\Omega$, u is the unknown scalar or vector valued function and f is a given source function. Dirichlet and mixed type boundary conditions are specified on $\partial\Omega_1$ and $\partial\Omega_2$ respectively, where $\partial\Omega = \partial\Omega_1 \cup \partial\Omega_2$, $\ell(s)$ and $\bar{u}(s)$ are known functions on the boundary, and ϵ is a constant, ∇ is the gradient operator.

The problem (2.1) can be transformed into a variational (weighted residual) form by multiplying the residual by a set of test functions from the space of admissible functions (that satisfy the homogeneous Dirichlet boundary conditions and are smooth enough for the integrals appearing in the variational problem to be well defined) and integrating over the domain. The resulting weighted average is set equal to zero,

$$\int_{\Omega} [-\nabla \cdot (\epsilon \nabla u) + bu - f]v \, dx dy = 0, \quad \forall v \in V. \quad (2.2)$$

Applying Green's theorem one can obtain

$$\int_{\Omega} (\epsilon \nabla u \cdot \nabla v + buv - fv) \, dx dy - \int_{\partial\Omega} \epsilon \frac{\partial u}{\partial n} v \, ds = 0, \quad \forall v \in V. \quad (2.3)$$

Boundary conditions in (2.1) give

$$\int_{\Omega} (\epsilon \nabla u \cdot \nabla v + buv - fv) \, dx dy + \int_{\partial\Omega_2} \ell(u - \bar{u})v \, ds = 0, \quad \forall v \in V. \quad (2.4)$$

Hence, our problem becomes one of finding a function $u \in V$ such that $u = \bar{u}$ on $\partial\Omega_1$ and (2.4) holds for all admissible test functions v .

The Galerkin finite element method enforces the weighted integral of the residual to be zero over the domain of the problem. To specify a Galerkin FEM for (2.1) out of the variational problem, we partition Ω as Ω_h into elements K in a standard way (e.g. no overlapping, no vertex on the edge of a neighboring elements, etc.) then we choose a finite-dimensional space V_h which is related to the choice of partition and which satisfies $V_h \subset V$, where V is the space of functions in which we seek a solution of the continuous variational problem. We define $h = \max_K \{\text{diam}(K)\}$ as the mesh diameter. Then, the Galerkin finite element method reads, [58]: Find $u_h \in V_h$ such that

$$a(u_h, v_h) = (f, v_h) + (g, v_h) \quad \forall v_h \in V_h \quad (2.5)$$

where (u, v) is the inner product of u and v as $\int_{\Omega} uv \, d\Omega$. Therefore, left hand side term in (2.5) is given explicitly as

$$a(u_h, v_h) = \int_{\Omega_h} (\epsilon \nabla u_h \cdot \nabla v_h + bu_h v_h) \, d\Omega_h$$

and the right hand side terms are

$$(f, v_h) = \int_{\Omega_h} f v_h \, d\Omega_h \quad , \quad (g, v_h) = \int_{\partial\Omega_h} \epsilon \frac{\partial u_h}{\partial n} v_h \, ds .$$

Now, we concentrate on the finite element solution of Navier-Stokes equations and the application of the finite element method is going to be given in details.

The steady, laminar flow of a viscous and incompressible fluid in an open bounded domain $\Omega \subset \mathbb{R}^2$ with the boundary $\partial\Omega$ is defined by the Navier-Stokes equations (in dimensionless form) with Dirichlet type boundary conditions as [57]

$$\begin{cases} \mathbf{u} \cdot \nabla \mathbf{u} - \epsilon \nabla^2 \mathbf{u} + \nabla p = \mathbf{f} & \text{in } \Omega, \\ \nabla \cdot \mathbf{u} = 0 & \text{in } \Omega, \\ \mathbf{u} = \mathbf{u}_0 & \text{on } \partial\Omega, \end{cases} \quad (2.6)$$

where \mathbf{u} is the unknown velocity field, p is the unknown scalar pressure function, \mathbf{f} is a given force vector, ϵ is the viscosity parameter related to the Reynolds number ($Re = 1/\epsilon$), and ∇^2 is the Laplace operator.

Thus, in two-dimension (2-D), using $\mathbf{u} = \begin{Bmatrix} u \\ v \end{Bmatrix}$ and $\mathbf{f} = \begin{Bmatrix} f_1 \\ f_2 \end{Bmatrix}$, Navier-Stokes equations can be written componentwise as

$$u \frac{\partial u}{\partial x} + v \frac{\partial u}{\partial y} - \frac{1}{Re} \left(\frac{\partial^2 u}{\partial x^2} + \frac{\partial^2 v}{\partial y^2} \right) + \frac{\partial p}{\partial x} = f_1 \quad (2.7)$$

$$u \frac{\partial v}{\partial x} + v \frac{\partial v}{\partial y} - \frac{1}{Re} \left(\frac{\partial^2 v}{\partial x^2} + \frac{\partial^2 v}{\partial y^2} \right) + \frac{\partial p}{\partial y} = f_2 \quad (2.8)$$

$$\frac{\partial u}{\partial x} + \frac{\partial v}{\partial y} = 0. \quad (2.9)$$

We use standard notation for function spaces: $C^0(\bar{\Omega})$ is the space of continuous functions on the closure of Ω , $L^2(\Omega)$ is the space of square integrable functions over the domain Ω , $H^1(\Omega)$ is the Sobolev space of $L^2(\Omega)$ functions whose derivatives are square integrable functions in Ω , and $H_0^1(\Omega)$ is the Sobolev subspace of $H^1(\Omega)$ functions in Ω with zero value on the boundary $\partial\Omega$. The weak formulation of the problem (2.6) is obtained by employing the pair of function spaces $V = (H_0^1(\Omega))^2$ and $P = L_0^2(\Omega)$, and it reads [52]: Find $\mathbf{u} \in V$, $p \in P$ such that

$$B(\mathbf{u}; \mathbf{u}, p; \mathbf{v}, q) = F(\mathbf{v}, q) \quad \text{for all } \mathbf{v} \in V, q \in P, \quad (2.10)$$

where the forms are given by

$$\begin{aligned} B(\mathbf{u}; \mathbf{u}, p; \mathbf{v}, q) &= (\mathbf{u} \cdot \nabla \mathbf{u}, \mathbf{v}) + \epsilon (\nabla \mathbf{u}, \nabla \mathbf{v}) - (\nabla \mathbf{v}, p) + (\nabla \cdot \mathbf{u}, q), \\ F(\mathbf{v}, q) &= (\mathbf{f}, \mathbf{v}). \end{aligned}$$

A mixed finite element approximation of the problem (2.10) is determined by the choice of finite dimensional subspaces $V_h \subset V$, $P_1 \subset P$ defined on a family of discretizations Ω_h of the

domain Ω . We assume that Ω_h is made of triangles or quadrangles $\{K\}$ and that Ω_h is regular as explained in [14](e.g. no overlapping, no vertex on the edge of a neighboring elements, etc.). Denoting the space of piecewise linear functions on a typical element K by $P_1(K)$, we choose the following finite dimensional subspaces on Ω_h before we specify finite element method:

$$\begin{aligned} V_h &= \{\mathbf{v} \in C^0(\bar{\Omega}) \cap (H_0^1(\Omega))^2 \mid \mathbf{v}|_K \in P_1(K)^2, K \in \Omega_h\}, \\ P_h &= \{p \in C^0(\bar{\Omega}) \cap L_0^2(\Omega) \mid p|_K \in P_1(K), K \in \Omega_h\}. \end{aligned}$$

Test and trial spaces consist of the continuous basis functions ϕ_i 's with the property that $\phi_i = 1$ at the node i and zero at the other nodes of an element. The standard Galerkin finite element method is based on employing the same function space for both test and trial spaces and it is equivalent to finding the pair $\{\mathbf{u}_h, p_h\}$ from $V_h \times P_h$ such that

$$B(\mathbf{u}_h; \mathbf{u}_h, p_h; \mathbf{v}_h, q_h) = (\mathbf{f}, \mathbf{v}_h) \quad \forall \{\mathbf{v}_h, q_h\} \in V_h \times P_h, \quad (2.11)$$

where

$$B(\mathbf{u}_h; \mathbf{u}_h, p_h; \mathbf{v}_h, q_h) = (\mathbf{u}_h \cdot \nabla \mathbf{u}_h, \mathbf{v}_h) + \epsilon(\nabla \mathbf{u}_h, \nabla \mathbf{v}_h) - (\nabla \mathbf{v}_h, p_h) + (\nabla \cdot \mathbf{u}_h, q_h). \quad (2.12)$$

If linear shape functions are used in the standard Galerkin FEM formulation, \mathbf{u}_h and \mathbf{v}_h are taken as \mathbf{u}_1 and \mathbf{v}_1 respectively, which are approximated by using linear polynomial basis functions in the finite element method.

To overcome the non-linearity in the equations, the unknowns can be written in iterative form as

$$\begin{aligned} \mathbf{u}_h^{n+1} &= \mathbf{u}_h^n + \hat{\mathbf{u}}_h \\ p_h^{n+1} &= p_h^n + \hat{p}_h \end{aligned}$$

where \mathbf{u}_h^n and p_h^n are the previous step known values and $\hat{\mathbf{u}}_h$ and \hat{p}_h are the correction values. Then, the nonlinear term is linearized as follows

$$\mathbf{u}_h^{n+1} \cdot \nabla \mathbf{u}_h^{n+1} \approx \mathbf{u}_h^n \cdot \nabla \mathbf{u}_h^n + \hat{\mathbf{u}}_h \cdot \nabla \mathbf{u}_h^n + \mathbf{u}_h^n \cdot \nabla \hat{\mathbf{u}}_h.$$

Since the pressure is determined up to a constant through the formulation, we also append the condition

$$\int_{\Omega_h} p_h = 0$$

to the formulation to fix the constant. For this purpose, we will normalize the continuity equation as

$$\kappa p_h - \nabla \cdot \mathbf{u}_h = 0$$

where κ is very small real number $\approx 10^{-5}$.

Thus, using $\mathbf{u}_h = \begin{Bmatrix} u_h \\ v_h \end{Bmatrix}$, explicit form of the Navier-Stokes equations can be written iteratively in 2-D as

$$\begin{aligned}
& u_h^n \frac{\partial \hat{u}_h}{\partial x} + v_h^n \frac{\partial \hat{u}_h}{\partial y} + \hat{u}_h \frac{\partial u_h^n}{\partial x} + \hat{v}_h \frac{\partial u_h^n}{\partial y} - \epsilon \left(\frac{\partial^2 \hat{u}_h}{\partial x^2} + \frac{\partial^2 \hat{u}_h}{\partial y^2} \right) + \frac{\partial \hat{p}_h}{\partial x} \\
& \quad = f_1 - u_h^n \frac{\partial u_h^n}{\partial x} + v_h^n \frac{\partial u_h^n}{\partial y} + \epsilon \left(\frac{\partial^2 u_h^n}{\partial x^2} + \frac{\partial^2 u_h^n}{\partial y^2} \right) - \frac{\partial p_h^n}{\partial x} \\
& u_h^n \frac{\partial \hat{v}_h}{\partial x} + v_h^n \frac{\partial \hat{v}_h}{\partial y} + \hat{u}_h \frac{\partial v_h^n}{\partial x} + \hat{v}_h \frac{\partial v_h^n}{\partial y} - \epsilon \left(\frac{\partial^2 \hat{v}_h}{\partial x^2} + \frac{\partial^2 \hat{v}_h}{\partial y^2} \right) + \frac{\partial \hat{p}_h}{\partial y} \\
& \quad = f_2 - u_h^n \frac{\partial v_h^n}{\partial x} + v_h^n \frac{\partial v_h^n}{\partial y} - \epsilon \left(\frac{\partial^2 v_h^n}{\partial x^2} + \frac{\partial^2 v_h^n}{\partial y^2} \right) - \frac{\partial p_h^n}{\partial y} \\
& \kappa \hat{p}_h + \frac{\partial \hat{u}_h}{\partial x} + \frac{\partial \hat{v}_h}{\partial y} = -\kappa p_h^n - \frac{\partial u_h^n}{\partial x} - \frac{\partial v_h^n}{\partial y}.
\end{aligned} \tag{2.13}$$

Computational Remarks

The unknowns can be expressed in terms of the basis functions of V_h and P_h in a simplified notation

$$u_h = \sum_{i=1}^{ndof_u} u_i \phi_i \quad v_h = \sum_{i=1}^{ndof_v} v_i \phi_i \quad p_h = \sum_{i=1}^{ndof_p} p_i \Phi_i$$

where ϕ_i 's are the shape functions of the velocity components and Φ_i 's are the shape functions for the pressure taken from the bases $\{\phi_1, \phi_2, \dots\}$ and $\{\Phi_1, \Phi_2, \dots\}$ of the space V_h and P_h , respectively. The shape functions are polynomials defined over an element and u_i , v_i and p_i 's are the nodal values of u_h , v_h and p_h respectively at the nodes of the element. $ndof$ denotes the degree of freedom for each approximation. We will also need the following two identities in the variational formulation

Green's Second Identity (for $\nabla^2 \mathbf{u}_h$)

$$\int_{\Omega} \left(\frac{\partial^2 \phi_i}{\partial x^2} + \frac{\partial^2 \phi_i}{\partial y^2} \right) \phi_j d\Omega = \int_{\partial\Omega} \frac{\partial \phi_i}{\partial n} \phi_j d\Omega - \int_{\Omega} \left(\frac{\partial \phi_i}{\partial x} \frac{\partial \phi_j}{\partial x} + \frac{\partial \phi_i}{\partial y} \frac{\partial \phi_j}{\partial y} \right) d\Omega.$$

If the boundary conditions (BC) are given as Dirichlet type, the boundary integral becomes zero since the shape functions vanish on $\partial\Omega$.

Integration by parts (for ∇p_h) (Divergence theorem)

Since the pressure shape functions $\Phi_i \in P_h \subset C^0(\bar{\Omega}) \cap L_0^2(\Omega)$, they are not differentiable. Therefore we will carry the differentiation to the shape functions of the velocity components (ϕ_i) by using the following equations:

$$\int_{\Omega} \frac{\partial \Phi_i}{\partial x} \phi_j d\Omega = \int_{\partial\Omega} \Phi_i \phi_j \cdot n_x d\sigma - \int_{\Omega} \Phi_i \frac{\partial \phi_j}{\partial x} d\Omega$$

$$\int_{\Omega} \frac{\partial \Phi_i}{\partial y} \phi_j d\Omega = \int_{\partial\Omega} \Phi_i \phi_j \cdot n_y d\sigma - \int_{\Omega} \Phi_i \frac{\partial \phi_j}{\partial y} d\Omega$$

where n is the outward unit surface normal to $\partial\Omega$ with $n = \begin{Bmatrix} n_x \\ n_y \end{Bmatrix}$.

Also, the following notations are made use of

$$\begin{aligned} Su &= \sum u_i \phi_i & Su_x &= \sum u_i \frac{\partial \phi_i}{\partial x} & Su_y &= \sum u_i \frac{\partial \phi_i}{\partial y} \\ Sv &= \sum v_i \phi_i & Sv_x &= \sum v_i \frac{\partial \phi_i}{\partial x} & Sv_y &= \sum v_i \frac{\partial \phi_i}{\partial y} \\ Sp &= \sum p_i \Phi_i & Sp_x &= \sum p_i \frac{\partial \Phi_i}{\partial x} & Sp_y &= \sum p_i \frac{\partial \Phi_i}{\partial y} \end{aligned}$$

for writing the variational form of the equations(2.7)-(2.9) in the matrix-vector form

$$\begin{bmatrix} E_{1\hat{u}} & E_{1\hat{v}} & E_{1\hat{p}} \\ E_{2\hat{u}} & E_{2\hat{v}} & E_{2\hat{p}} \\ E_{3\hat{u}} & E_{3\hat{v}} & E_{3\hat{p}} \end{bmatrix} \begin{pmatrix} \hat{u}_h \\ \hat{v}_h \\ \hat{p}_h \end{pmatrix} = \begin{pmatrix} R_1 \\ R_2 \\ R_3 \end{pmatrix} \quad (2.14)$$

where the entries are given as

$$\begin{aligned} E_{1\hat{u}} &= \int_{\Omega} \left\{ \left(Su_x \phi_i + Su \frac{\partial \phi_i}{\partial x} + Sv \frac{\partial \phi_i}{\partial y} \right) \phi_j + \epsilon \left(\frac{\partial \phi_i}{\partial x} \frac{\partial \phi_j}{\partial x} + \frac{\partial \phi_i}{\partial y} \frac{\partial \phi_j}{\partial y} \right) \right\} d\Omega \\ E_{1\hat{v}} &= \int_{\Omega} Su_y \phi_i \phi_j d\Omega & E_{1\hat{p}} &= \int_{\Omega} -\Phi_i \frac{\partial \phi_i}{\partial x} d\Omega & E_{2\hat{u}} &= \int_{\Omega} Sv_x \phi_i \phi_j d\Omega \\ E_{2\hat{v}} &= \int_{\Omega} \left\{ \left(Sv_y \phi_i + Su \frac{\partial \phi_i}{\partial x} + Sv \frac{\partial \phi_i}{\partial y} \right) \phi_j + \epsilon \left(\frac{\partial \phi_i}{\partial x} \frac{\partial \phi_j}{\partial x} + \frac{\partial \phi_i}{\partial y} \frac{\partial \phi_j}{\partial y} \right) \right\} d\Omega \\ E_{2\hat{p}} &= \int_{\Omega} -\Phi_i \frac{\partial \phi_i}{\partial y} d\Omega & E_{3\hat{u}} &= \int_{\Omega} \frac{\partial \phi_i}{\partial x} \Phi_j d\Omega & E_{3\hat{v}} &= \int_{\Omega} \frac{\partial \phi_i}{\partial y} \Phi_j d\Omega & E_{3\hat{p}} &= \int_{\Omega} \kappa \Phi_i \Phi_j d\Omega \\ R_1 &= \int_{\Omega} \left[- (Su.Su_x + Sv.Su_y - f_1) \phi_j - \epsilon \left(Su_x \frac{\partial \phi_j}{\partial x} + Su_y \frac{\partial \phi_j}{\partial y} \right) \phi_j + Sp \frac{\partial \phi_j}{\partial x} \right] d\Omega \\ R_2 &= \int_{\Omega} \left[- (Su.Sv_x + Sv.Sv_y - f_2) \phi_j - \epsilon \left(Sv_x \frac{\partial \phi_j}{\partial x} + Sv_y \frac{\partial \phi_j}{\partial y} \right) \phi_j + Sp \frac{\partial \phi_j}{\partial y} \right] d\Omega \\ R_3 &= \int_{\Omega} [-\kappa Sp - Su_x - Sv_y] \Phi_j d\Omega. \end{aligned}$$

The insertion of the boundary conditions in the iteration process is employed such that if Dirichlet type boundary conditions are given, u_h^n and v_h^n are equal to given boundary values and \hat{u}_h and \hat{v}_h are equal to zero on the boundary points. Starting values of u_h and v_h for the iteration process are specified as the given boundary values and zero at the other points. The pressure is set to zero initially everywhere.

The solution process of the Galerkin finite element method is based on the 'best approximation' property. That is, the difference between the exact solution and the finite element solution is minimized with respect to certain norm. Therefore, Galerkin FEM generally gives successful numerical solutions. However, solutions of the Navier-Stokes equations obtained from the standard Galerkin finite element method produce some spurious oscillations (see Figure (2.12)). The

coupled form of the problem which limits the choice of the shape functions is the first reason of these oscillations. The second one is the convective-diffusive character of the equations together with the existence of the coefficient Reynolds number(Re) which makes the problem convection dominated for high values of Re .

The special choice of the approximate functions satisfying inf-sup condition, which is defined for $\mathbf{u}_h \in V_h$ and $p_h \in P_h$ as

$$\inf_{p_h \neq 0} \sup_{\mathbf{u}_h \neq 0} \frac{|a(\mathbf{u}_h, p_h)|}{\|\mathbf{u}_h\| \|p_h\|} > 0$$

or Babuska-Brezzi condition which implies that the order of the pressure shape function is less than the order of velocity shape function (e.g. Taylor-Hood elements or $Q2 - Q1$ elements are the combination of quadratic shape functions for velocity and linear for pressure), will remove the oscillations and produces stable solutions. However, selecting higher order shape functions for velocity increases the size of the resulting matrix-vector system which is limited by computer resources. Therefore, such a selection does not allow to obtain fine meshes for the domain of the problem. In order to overcome this difficulty, stabilized methods which permit the use of equal order shape functions are proposed.

2.1 Stabilized Finite Element Methods

Stabilized finite element methods are based on adding mesh dependent terms to the standard Galerkin finite element formulation of the problem which stabilize the system. The first stabilized method proposed by Hughes [13, 38] is called as Streamline Upwind Petrov-Galerkin (SUPG) method . There are many studies with stabilized finite element methods for convection-diffusion equations [22, 25, 29, 30, 40] and incompressible Navier-Stokes equations [24, 36]. Analysis and more references can be found in the book [59].

Since the convection-diffusion terms exist in the Navier-Stokes equations, we first demonstrate the stabilized methods for the convection-diffusion equation.

2.1.1 Convection-diffusion equation

Consider the convection-diffusion equation given with the Dirichlet type boundary conditions as

$$\begin{cases} -\epsilon \nabla^2 u + \mathbf{a} \cdot \nabla u = f & \text{in } \Omega \\ u = u_0 & \text{on } \partial\Omega \end{cases} \quad (2.15)$$

where ϵ is a small parameter and $\mathbf{a} = \begin{Bmatrix} a_x \\ a_y \end{Bmatrix}$ is the flow vector. The Galerkin finite element formulation of the problem (2.15) is as; find $u_h \in V_h$ such that

$$a(u_h, v_h) = (f, v_h), \quad \forall v_h \in V_h \quad (2.16)$$

where

$$a(u_h, v_h) = \epsilon \int_{\Omega_h} \nabla u_h \cdot \nabla v_h d\Omega_h + \int_{\Omega_h} (\mathbf{a} \cdot \nabla u_h) v_h d\Omega_h.$$

Stabilized form of the convection-diffusion equation over the element K is defined in [31] as

$$a(u_h, v_h) + \sum \tau_K \int_{\Omega_K} (-\epsilon \nabla^2 u_h + \mathbf{a} \cdot \nabla u_h - f)(\gamma \epsilon \nabla^2 v_h + \mathbf{a} \cdot \nabla v_h) d\Omega_K = (f, v_h) \quad (2.17)$$

where τ_K is the stabilization parameter depending on the local character of the discretization, Ω_K is the area of the K^{th} element, and $a(u_h, v_h)$ corresponds to the standard Galerkin finite element terms. The stabilization method changes with the value of γ as

- $\gamma = -1 \Rightarrow$ Douglas-Wang method (DWG)
- $\gamma = 0 \Rightarrow$ Streamline Upwind Petrov Galerkin (SUPG)
- $\gamma = 1 \Rightarrow$ Galerkin Least Square (GLS) .

If linear elements are used, all three methods coincide since $\nabla^2 u_h = \nabla^2 v_h = 0$.

The stabilization parameter τ_K is defined in [9] as

$$\tau_K = \begin{cases} \frac{h_K}{2|\mathbf{a}|_K} & \text{if } Pe_K \geq 1 \\ \frac{h_K^2}{12\epsilon} & \text{if } Pe_K < 1 \end{cases} \quad (2.18)$$

where, h_K is the diameter of the element, Pe_K is the Peclet number, $Pe_K = \frac{|\mathbf{a}|_K h_K}{6\epsilon}$ and $|\mathbf{a}|_K = \sqrt{a_x^2 + a_y^2}$.

2.1.2 SUPG formulation of the Navier-Stokes equations

Streamline Upwind Petrov Galerkin (SUPG) formulation of the Navier-Stokes equations (2.6) for linear elements is given in [24] as; find $\{\mathbf{u}_h, p_h\}$ from $V_h \times P_h$

$$\begin{aligned} & (\mathbf{u}_h \cdot \nabla \mathbf{u}_h, \mathbf{v}_h) + \epsilon (\nabla \mathbf{u}_h, \nabla \mathbf{v}_h) - (\nabla \mathbf{v}_h, p_h) - (\nabla \cdot \mathbf{u}_h, q_h) \\ & + \sum \tau_K \int_{\Omega_K} ((\mathbf{u}_h \cdot \nabla \mathbf{u}_h + \nabla p_h - \mathbf{f}) \cdot (\mathbf{u}_h \cdot \nabla \mathbf{v}_h - \nabla q_h)) d\Omega_K = (\mathbf{f}, \mathbf{v}_h) \end{aligned} \quad (2.19)$$

$\forall \{\mathbf{v}_h, q_h\} \in V_h \times P_h$ with the stabilization parameter τ_K such that

$$\tau_K = \frac{h_K}{2|\mathbf{u}_h^n|_K} \varepsilon(Pe_K) \quad (2.20)$$

where

$$\varepsilon(Pe_K) = \begin{cases} Pe_k & \text{if } Pe_k < 1 \\ 1 & \text{if } Pe_k \geq 1 \end{cases}$$

and

$$Pe_K = \frac{|\mathbf{u}_h^n|_K h_K}{6\epsilon}.$$

Therefore the following terms will be added to the standard Galekin formulation respectively

$$\begin{aligned} & \int_{\Omega_K} \tau_K \left(\frac{\partial u_h^n}{\partial x} \hat{u}_h + \frac{\partial u_h^n}{\partial y} \hat{v}_h + u_h^n \frac{\partial \hat{u}_h}{\partial x} + v_h^n \frac{\partial \hat{u}_h}{\partial y} + u_h^n \frac{\partial u_h^n}{\partial x} + v_h^n \frac{\partial u_h^n}{\partial y} + \frac{\partial p_h^n}{\partial x} + \frac{\partial \hat{p}_h}{\partial x} - f_1 \right) \\ & \quad \left(u_h^n \frac{\partial v_1}{\partial x} + v_h^n \frac{\partial v_1}{\partial y} \right) d\Omega_K \\ & \int_{\Omega_K} \tau_K \left(\frac{\partial v_h^n}{\partial x} \hat{u}_h + \frac{\partial v_h^n}{\partial y} \hat{v}_h + u_h^n \frac{\partial \hat{v}_h}{\partial x} + v_h^n \frac{\partial \hat{v}_h}{\partial y} + u_h^n \frac{\partial v_h^n}{\partial x} + v_h^n \frac{\partial v_h^n}{\partial y} + \frac{\partial p_h^n}{\partial y} + \frac{\partial \hat{p}_h}{\partial y} - f_2 \right) \\ & \quad \left(u_h^n \frac{\partial v_2}{\partial x} + v_h^n \frac{\partial v_2}{\partial y} \right) d\Omega_K \\ & \int_{\Omega_K} -\tau_K \left\{ \left(\frac{\partial u_h^n}{\partial x} \hat{u}_h + \frac{\partial u_h^n}{\partial y} \hat{v}_h + u_h^n \frac{\partial \hat{u}_h}{\partial x} + v_h^n \frac{\partial \hat{u}_h}{\partial y} + u_h^n \frac{\partial u_h^n}{\partial x} + v_h^n \frac{\partial u_h^n}{\partial y} + \frac{\partial p_h^n}{\partial x} + \frac{\partial \hat{p}_h}{\partial x} - f_1 \right) \frac{\partial q}{\partial x} \right. \\ & \quad \left. + \left(\frac{\partial v_h^n}{\partial x} \hat{u}_h + \frac{\partial v_h^n}{\partial y} \hat{v}_h + u_h^n \frac{\partial \hat{v}_h}{\partial x} + v_h^n \frac{\partial \hat{v}_h}{\partial y} + u_h^n \frac{\partial v_h^n}{\partial x} + v_h^n \frac{\partial v_h^n}{\partial y} + \frac{\partial p_h^n}{\partial y} + \frac{\partial \hat{p}_h}{\partial y} - f_2 \right) \frac{\partial q}{\partial y} \right\} d\Omega_K. \end{aligned} \quad (2.21)$$

Then, the equation (2.19) becomes in the matrix-vector form

$$\left(\begin{bmatrix} E_{1\hat{u}} & E_{1\hat{v}} & E_{1\hat{p}} \\ E_{2\hat{u}} & E_{2\hat{v}} & E_{2\hat{p}} \\ E_{3\hat{u}} & E_{3\hat{v}} & E_{3\hat{p}} \end{bmatrix} + \tau_K \begin{bmatrix} e_{1\hat{u}} & e_{1\hat{v}} & e_{1\hat{p}} \\ e_{2\hat{u}} & e_{2\hat{v}} & e_{2\hat{p}} \\ e_{3\hat{u}} & e_{3\hat{v}} & e_{3\hat{p}} \end{bmatrix} \right) \begin{pmatrix} \hat{u} \\ \hat{v} \\ \hat{p} \end{pmatrix} = \begin{pmatrix} R_1 \\ R_2 \\ R_3 \end{pmatrix} + \tau_K \begin{pmatrix} r_1 \\ r_2 \\ r_3 \end{pmatrix} \quad (2.22)$$

with the entries in stabilized terms

$$\begin{aligned} e_{1\hat{u}} &= \int_{\Omega_K} (Su_x \phi_i + ct_1) ct_3 d\Omega_K & e_{2\hat{u}} &= \int_{\Omega_K} Sv_x \phi_i ct_3 d\Omega_K \\ e_{3\hat{u}} &= \int_{\Omega_K} \left\{ -(Su_x \phi_i + ct_1) \frac{\partial \phi_j}{\partial x} - Sv_x \phi_i \frac{\partial \phi_j}{\partial y} \right\} d\Omega_K \\ e_{1\hat{v}} &= \int_{\Omega_K} Su_y \phi_i ct_3 d\Omega_K & e_{2\hat{v}} &= \int_{\Omega_K} (Sv_y \phi_i + ct_1) ct_3 d\Omega_K \\ e_{3\hat{v}} &= \int_{\Omega_K} \left\{ -Su_y \phi_i \frac{\partial \phi_j}{\partial x} - (Sv_y \phi_i + ct_1) \frac{\partial \phi_j}{\partial y} \right\} d\Omega_K \\ e_{1\hat{p}} &= \int_{\Omega_K} \frac{\partial \phi_i}{\partial x} ct_3 d\Omega_K & e_{2\hat{p}} &= \int_{\Omega_K} \frac{\partial \phi_i}{\partial y} ct_3 d\Omega_K & e_{3\hat{p}} &= \int_{\Omega_K} -ct_2 d\Omega_K \end{aligned}$$

$$\begin{aligned}
r_1 &= \int_{\Omega_K} -(Su_x Su + Su_y Sv + Sp_x - f_1) ct_3 d\Omega_K \\
r_2 &= \int_{\Omega_K} -(Sv_x Su + Sv_y Sv + Sp_y - f_2) ct_3 d\Omega_K \\
r_3 &= \int_{\Omega_K} \left[(Su_x Su + Su_y Sv + Sp_x - f_1) \frac{\partial \phi_j}{\partial x} + (Sv_x Su + Sv_y Sv + Sp_y - f_2) \frac{\partial \phi_j}{\partial y} \right] d\Omega_K
\end{aligned}$$

where

$$ct_1 = Su \frac{\partial \phi_i}{\partial x} + Sv \frac{\partial \phi_i}{\partial y} \quad ct_2 = \frac{\partial \phi_i}{\partial x} \frac{\partial \phi_j}{\partial x} + \frac{\partial \phi_i}{\partial y} \frac{\partial \phi_j}{\partial y} \quad ct_3 = Su \frac{\partial \phi_j}{\partial x} + Sv \frac{\partial \phi_j}{\partial y}.$$

2.2 Stabilizing Subgrid Method (SSM)

Another stabilization method called as stabilizing subgrid method (**SSM**) has been developed for convection-diffusion type equations [10, 53] using triangular elements. SSM is related to the combination of the methods SUPG and residual-free-bubble functions. The method is based on the selection of a single subgrid point whose location has a role in the stabilization of the convection dominated flows. The SSM on convection-diffusion equations will be extended to the solution of the Navier-Stokes equations for the first time in this study [56].

The **SSM** and the **SUPG** formulations of the Navier-Stokes equations have identical structure except for the value of the stabilization parameter τ_K . In SSM, the stabilization parameter τ_K is explicitly given by [56]

$$\tau_K = \frac{1}{|K|} \int_K b_K dK \tag{2.23}$$

where b_K is the unique solution of the following boundary value problem in an element K

$$\begin{cases} Lb_K = -\epsilon \nabla^2 b_K + \mathbf{u}_1^n \cdot \nabla b_K = 1 & \text{in } K \\ b_K = 0 & \text{on } \partial K. \end{cases} \tag{2.24}$$

Note that, finding the exact solution b_K using (2.24) may not be an easy task in an arbitrary triangular domain. Therefore a cheap efficient approximation to b_K that generates qualitatively the same behavior with the exact function b_K is required.

Since the equation (2.24) can be viewed as a linear convection-diffusion equation, a stabilized subgrid numerical algorithm can be employed to compute the approximate solution. Specify a subgrid which consists of three vertices of the triangle plus a single additional node in the interior of each element and approximate b_K over the specified subgrid by choosing the location of the additional node such that it gives the best approximation in L_1 norm defined by

$$\|f\|_1 = \int_{\Omega} |f| d\Omega$$

for $f : \Omega \rightarrow R$.

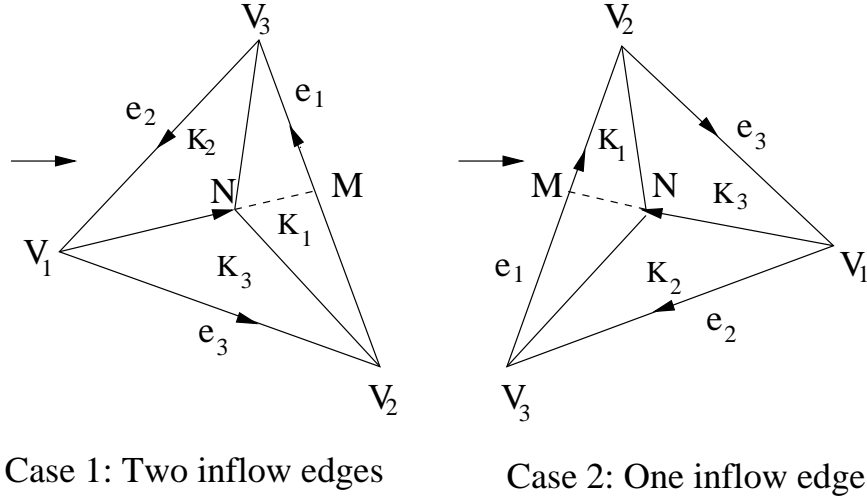


Figure 2.1: Types of inflow boundary

To describe the algorithm of the stabilizing subgrid method (SSM) [10, 53]; take a fixed element K and consider a subgrid that contains just one additional node $N = \phi_K$ in the interior of each triangular element. We drop the subscript K since the argument is similar for other elements. The node N is joined to the three vertices denoted by V_i splitting the triangle K into three sub-triangles. We will choose the point N along one of the three medians of K . Let us denote the approximate solution on K by b_N which is defined as

$$b_N(N) = 1, \quad b_N(V_i) = 0 \quad i = 1, 2, 3. \quad (2.25)$$

Thus the function b_N attached to the point N has support contained in K . We further denote the edge of K opposite to V_i by \mathbf{e}_i , the length of \mathbf{e}_i by $|\mathbf{e}_i|$, the outward unit normal to \mathbf{e}_i by \mathbf{n}_i and $\nu_i = |\mathbf{e}_i|\mathbf{n}_i$. The choice of the median on which the point N is located will depend on the number of inflow edges in the triangle and the precise location of N will be chosen such that the value of the residual in the sense of L_1 is minimum. That is

$$J(N) = \int_K |-\epsilon \nabla^2 b_N^* + \mathbf{u}_1^n \cdot \nabla b_N^* - 1| dK \quad (2.26)$$

is minimum where $b_N^*(\mathbf{x}) = \alpha(N)b_N(\mathbf{x})$ is the unique solution of

$$a_K(b_N^*, b_N) = (1, b_N) \quad \forall b_N. \quad (2.27)$$

Using the integration by parts, we observe that

$$\alpha(N) = \frac{\int_K b_N dK}{\epsilon \int_K |\nabla b_N|^2 dK}. \quad (2.28)$$

The set of points on the median V_1M can be described as a function depending on a single parameter t : $N = (1-t)V_1 + tM$ where $0 < t < 1$. In order to choose the position of N , we have

to distinguish among two cases with respect to the number of inflow edges. Define the average velocity $\tilde{\mathbf{u}}_1^n$ by arithmetic mean of the velocity components at the vertices of the triangle; i.e., $\tilde{\mathbf{u}}_1^n = (\mathbf{u}_1^n(V_1) + \mathbf{u}_1^n(V_2) + \mathbf{u}_1^n(V_3))/3$. We use $\tilde{\mathbf{u}}_1^n$ to characterize the type of the edges of the triangle: If $\tilde{\mathbf{u}}_1^n \cdot \mathbf{n}_i > 0$ then \mathbf{e}_i is an outflow edge, otherwise it is an inflow edge.

In the first case where the inflow boundary makes up of two edges, let \mathbf{e}_2 and \mathbf{e}_3 be two inflow edges (Figure (2.1)). Then for the value of t , we take

$$\begin{cases} t = 1 + \frac{\epsilon(|\mathbf{e}_1|^2)}{\epsilon(|\mathbf{e}_2 - \mathbf{e}_3|^2 - \frac{2}{3}|K|(\tilde{\mathbf{u}}_1^n, \nu_1))} & \text{if } \epsilon \leq \frac{2|K|(\tilde{\mathbf{u}}_1^n, \nu_1)/3}{3|\mathbf{e}_1|^2 + |\mathbf{e}_2 - \mathbf{e}_3|^2} \\ t = 2/3 & \text{otherwise} \end{cases} \quad (2.29)$$

where t lies in the interval $[\frac{2}{3}, 1)$. In the other case where the inflow boundary makes up of a single edge, let \mathbf{e}_1 be the inflow edge (Figure (2.1)). We use again the condition (2.26) to determine the location of N and the integral $J(N)$ becomes minimum if t is taken as

$$\begin{cases} t = \frac{\epsilon(|\mathbf{e}_2|^2 + |\mathbf{e}_3|^2)}{\epsilon(|\mathbf{e}_2 - \mathbf{e}_3|^2/2 - |K|(\tilde{\mathbf{u}}_1^n, \nu_1)/3)} & \text{if } \epsilon \leq \frac{-2|K|(\tilde{\mathbf{u}}_1^n, \nu_1)/3}{3(|\mathbf{e}_2|^2 + |\mathbf{e}_3|^2) - |\mathbf{e}_2 - \mathbf{e}_3|^2} \\ t = 2/3 & \text{otherwise.} \end{cases} \quad (2.30)$$

In this case, $0 < t \leq 2/3$. We refer to [9, 53] for the derivation of the values of t in (2.29) and (2.30). Two articles use two different criteria for choosing the subgrid node, however they reach the similar results.

Once the location of the point N is determined through the relation $N = (1-t)V_1 + tM$ with the value of t given in (2.29) or (2.30) depending on the number of inflow edges, a reasonably good approximation to the stabilization parameter τ_K can be obtained: The approximate value of τ_K is given by

$$\tilde{\tau}_K = \frac{1}{|K|} \int_K b_N^* d\Omega_K = \frac{1}{|K|} \frac{(\int_{\Omega_K} b_N d\Omega_K)^2}{\epsilon \int_{\Omega_K} |\nabla b_N|^2 d\Omega_K} = \frac{4|K|}{9\epsilon \sum_i |e_i|^2 / |K_i|} \quad (2.31)$$

where $|K_i|$ is the area of i^{th} sub-triangle. The values of $\tilde{\tau}_K$ s are then used in the global formulation (2.19) in place of τ_K .

The SSM formulations of the convection-diffusion and the Navier-Stokes equations are exactly the same with the formulations given in SUPG (Subsections 2.1.2 and 2.1.2). Here the value of stabilization parameter is obtained in a different way.

2.3 Two-Level Finite Element Method (TLFEM)

Another stabilized method which uses equal order shape functions for both the velocity and the pressure is called a two level finite element method (**TLFEM**) [26]. TLFEM is based on to enrich the finite element space appending bubble functions. Then, the finite element space V_h is decomposed as

$$V_h = V_1 \oplus V_B$$

where V_1 is the linear space, V_B is the bubble space and \oplus is the direct sum operator for the finite element spaces.

We will decompose the approximate solution as $u_h = u_1 + u_b \in V_1 \oplus V_B$ where u_1 is the linear part and u_b is the bubble part of the solution. Bubble functions have a special property being zero outside of the specific element.

For simplicity, **TLFEM** is introduced first for the convection-diffusion equation [7, 8, 9, 11, 28, 63].

2.3.1 TLFEM for the convection-diffusion equation

Residual-free bubble functions are used now in a two-level finite element method for convection-diffusion equation [7]. The variational formulation of the convection-diffusion equation is already defined in (2.16) as

$$a(u_h, v_h) = (f, v_h).$$

If the approximate solution u_h of the equation (2.15) is taken as $u_h = u_1 + u_b$, the original differential equation can be written as

$$L(u_h) = L(u_1 + u_b) = f \quad \text{in } K. \quad (2.32)$$

Using the linear property of the operator L and the property of the bubble functions that they vanish on the boundary ∂K of each element K , equation (2.32) can be written as

$$\begin{cases} L(u_b) = -L(u_1) + f & \text{in } K \\ u_b = 0 & \text{on } \partial K. \end{cases} \quad (2.33)$$

For the Galerkin finite element method that uses bubbles, each $v_h \in V_h$ is the sum of a standard piecewise polynomial and a bubble function that is selected later to be residual-free. Thus, we write

$$v_h = v_1 + v_b \quad \forall v_h \in V_h \quad (2.34)$$

where v_1 is the polynomial component of v_h and v_b is the bubble component.

We require the bubble functions to vanish on the boundary ∂K of each element K . For the particular case of residual-free-bubbles, we further define the bubble components v_b for each v_h to satisfy the original differential equation on the interior of each K , i.e,

$$Lv_h = L(v_1 + v_b) = f \quad \text{in } K.$$

For general bubble functions including the residual-free ones, the vanishing of the bubble functions on each ∂K allows us to take $v_h = v_b$ on K and $v_h = 0$ elsewhere. Therefore, variational formulation of the problem with TLFEM takes the form

$$a(u_1, v_1) + a(u_b, v_1) = (f, v_1) \quad \forall v_1 \in V_1.$$

In order to find the bubble part of the solution, we can write the two parts of the solution in terms of shape functions as

$$u_1 = \sum_{i=1}^{\#nds} u_i \phi_i, \quad u_b = \sum_{i=1}^{\#nds} u_i \varphi_i^u + \varphi^f$$

where $\#nds$ is the number of nodes over the boundary of the element, ϕ_i 's are linear shape functions, φ_i^u, φ^f are bubble functions and u_i 's are approximate solutions at the nodes. Then, variational formulation becomes

$$\sum u_i [a(\phi_i, \phi_j) + a(\varphi_i^u, \phi_j)] = (f, \phi_j) - a(\varphi^f, \phi_j). \quad (2.35)$$

Calculation of Bubble Functions φ_i^u 's and φ^f

Bubble functions will be obtained from the solutions of the following problems which are defined on the sub-mesh level for each element K

$$\begin{cases} L\varphi_i^u = -L\phi_i & \text{on } K, & L\varphi^f = f & \text{on } K \\ \varphi_i^u = 0 & \text{on } \partial K, & \varphi^f = 0 & \text{on } \partial K. \end{cases} \quad (2.36)$$

Since the sub-mesh level problems are in the same behaviour with the global problem, they should be solved with a suitable non-standard method such as stabilized method (SUPG, GLS). Stabilized form of these equations are

$$\begin{cases} \int_{\Omega_{K^*}} \{\epsilon(\nabla\phi_l^* \cdot \nabla\phi_m^*) + (\mathbf{a} \cdot \nabla\phi_l^*)\phi_m^* + \tau_{K^*}(\mathbf{a} \cdot \nabla\phi_l^*)(\mathbf{a} \cdot \nabla\phi_m^*)\} d\Omega_{K^*} = \\ \int_{\Omega_{K^*}} \{-(\mathbf{a} \cdot \nabla\phi_i)\phi_m^* - \tau_{K^*}(\mathbf{a} \cdot \nabla\phi_i)(\mathbf{a} \cdot \nabla\phi_m^*)\} d\Omega_{K^*}, & i = 1, \dots, \#nds \\ \int_{\Omega_{K^*}} \{\epsilon(\nabla\phi_l^* \cdot \nabla\phi_m^*) + (\mathbf{a} \cdot \nabla\phi_l^*)\phi_m^* + \tau_{K^*}(\mathbf{a} \cdot \nabla\phi_l^*)(\mathbf{a} \cdot \nabla\phi_m^*)\} d\Omega_{K^*} = & l, m = 1, \dots, \#nds \\ \int_{\Omega_{K^*}} \{f\phi_m^* + \tau_{K^*}f(\mathbf{a} \cdot \nabla\phi_m^*)\} d\Omega_{K^*} \end{cases} \quad (2.37)$$

where the stabilization parameter τ_{K^*} is already defined in (2.18) and ϕ^* are the basis functions defined on the submesh.

Equations (2.37) can be written in matrix-vector form as $[A]\{\varphi_i^u\} = \{F_i^u\}$ and $[A]\{\varphi^f\} = \{F^f\}$. Since the left hand side stiffness matrix is common in all the problems and the boundary conditions are homogeneous Dirichlet type, it is calculated and assembled once and used in all the problems.

Computational Algorithm

Equation (2.35) is calculated in two parts. Linear part terms $a(\phi_i, \phi_j)$ and (f, ϕ_j) are calculated on each element in global mesh directly. However, bubble functions φ_i^u and φ^f are defined on a sub-mesh in a discrete way by

$$\varphi_i^u = \sum_l^{\#nds} c_l^{u_i} \phi_l^*, \quad \varphi^f = \sum_l^{\#nds} c_l^f \phi_l^*,$$

where $c_l^{u_i}$ and c_l^f are the discrete values of the bubble functions φ_i^u and φ^f , respectively and ϕ_l^* 's are the basis functions on the submesh. Therefore, the bubble part terms $a(\varphi_i^u, \phi_j)$ and $a(\varphi^f, \phi_j)$ must be calculated as summation of sub-integrals

$$\begin{cases} \int_{\Omega_K} a(\varphi_i^u, \phi_j) d\Omega_K = \sum_l^{\#K^*} \int_{\Omega_{K^*}} c_l^{u_i} a(\phi_l^*, \phi_j) d\Omega_{K^*} \\ \int_{\Omega_K} a(\varphi^f, \phi_j) d\Omega_K = \sum_l^{\#K^*} \int_{\Omega_{K^*}} c_l^f a(\phi_l^*, \phi_j) d\Omega_{K^*} \end{cases}$$

where K^* is an element in the submesh and $\#K^*$ indicates the number of elements on the submesh. This process will be repeated for each global element separately.

2.3.2 TLFEM for the Navier-Stokes equations

Two-level finite element method is going to be used now for approximating residual-free bubble functions for the Navier-Stokes equations. The variational formulation of the Navier-Stokes equations has already been given in (2.12) as; find $\mathbf{u}_h \in V_h$ and $p_h \in P_h$ such that

$$(\mathbf{u}_h \cdot \nabla \mathbf{u}_h, \mathbf{v}_h) + \epsilon(\nabla \mathbf{u}_h, \nabla \mathbf{v}_h) - (\nabla \mathbf{v}_h, p_h) - (\nabla \cdot \mathbf{u}_h, q_h) = (f, \mathbf{v}_h) \quad \forall \mathbf{v}_h \in V_h, q_h \in P_h.$$

If we set $\mathbf{u}_h = \mathbf{u}_1 + \mathbf{u}_b$, $\mathbf{v}_h = \mathbf{v}_1$, $p_h = p_1$ and $q_h = q_1$ we will get the equation

$$(\mathbf{u}_1 \cdot \nabla(\mathbf{u}_1 + \mathbf{u}_b), \mathbf{v}_1) + \epsilon(\nabla(\mathbf{u}_1 + \mathbf{u}_b), \nabla \mathbf{v}_1) - (\nabla \mathbf{v}_1, p_1) - (\nabla \cdot (\mathbf{u}_1 + \mathbf{u}_b), q_1) = (f, \mathbf{v}_1) \quad (2.38)$$

For the Navier-Stokes equations, bubble part of the solution \mathbf{u}_b can be obtained from the solution of the following equation [52]

$$\begin{aligned} \mathbf{u}_1^n \cdot \nabla \mathbf{u}_b^{n+1} - \epsilon \nabla^2 \mathbf{u}_b^{n+1} &= \mathbf{f} - \mathbf{u}_1^n \cdot \nabla \mathbf{u}_1^{n+1} + \epsilon \nabla^2 \mathbf{u}_1^{n+1} - \nabla p_1^{n+1} && \text{in } K \\ \mathbf{u}_b &= 0 && \text{on } \partial K. \end{aligned} \quad (2.39)$$

In 2-D, explicit form of the bubble functions are

$$\begin{aligned}
u_b &= \sum_{i=1}^{\#nds} u_i \varphi_i^u + \sum_{i=1}^{\#nds} p_i \varphi_i^{p1} + \varphi^{f1} \\
v_b &= \sum_{i=1}^{\#nds} v_i \varphi_i^v + \sum_{i=1}^{\#nds} p_i \varphi_i^{p2} + \varphi^{f2}
\end{aligned} \tag{2.40}$$

where φ_i^u ; φ_i^{p1} , φ_i^{p2} ; φ^{f1} and φ^{f2} are the basis functions for the bubble components of the velocity bubble, pressure bubble and external force bubble, respectively.

Therefore, sub-mesh problems are written separately. For the velocity components u and v , the same sub-mesh problem will be solved

$$\begin{cases} L\varphi_i^u = -(u_1^n \frac{\partial \phi_i}{\partial x} + v_1^n \frac{\partial \phi_i}{\partial y}) & \text{in } K \\ \varphi_i^u = 0 & \text{on } \partial K \end{cases} \tag{2.41}$$

where u_1^n and v_1^n are the known values of the velocity component from the previous iteration.

For the pressure part of the bubble functions there are two different sub-mesh problems

$$\begin{cases} L\varphi_i^{p1} = -\frac{\partial \phi_i}{\partial x} & \text{in } K \\ \varphi_i^{p1} = 0 & \text{on } \partial K \end{cases}, \begin{cases} L\varphi_i^{p2} = -\frac{\partial \phi_i}{\partial y} & \text{in } K \\ \varphi_i^{p2} = 0 & \text{on } \partial K. \end{cases} \tag{2.42}$$

Finally, for the body force part of the bubbles, we have the following sub-mesh problems

$$\begin{cases} L\varphi^{f1} = f_1 & \text{in } K \\ \varphi^{f1} = 0 & \text{on } \partial K \end{cases}, \begin{cases} L\varphi^{f2} = f_2 & \text{in } K \\ \varphi^{f2} = 0 & \text{on } \partial K. \end{cases} \tag{2.43}$$

Equations (2.41)-(2.43) again should be solved on a sub-mesh with a non-standard method (such as SUPG). In all of the sub-mesh level problems, left hand side is common for each element. Therefore, it can be calculated only once and used for all the problems on element level. Explicit form of the left hand side of the sub-mesh problems is given as

$$\int_{\Omega_{K^*}} \left\{ \epsilon(\nabla \phi_l^* \cdot \nabla \phi_m^*) + (u_1^n \frac{\partial \phi_l^*}{\partial x} + v_1^n \frac{\partial \phi_l^*}{\partial y}) \phi_m^* + \tau_{K^*} (u_1^n \frac{\partial \phi_l^*}{\partial x} + v_1^n \frac{\partial \phi_l^*}{\partial y}) (u_1^n \frac{\partial \phi_m^*}{\partial x} + v_1^n \frac{\partial \phi_m^*}{\partial y}) \right\} d\Omega_{K^*} \tag{2.44}$$

where $l, m = 1, \dots, \#nds$.

Right hand sides of the equations (2.41)-(2.43) are respectively

velocity bubble:

$$\int_{\Omega_{K^*}} \left\{ -(u_1^n \frac{\partial \phi_i}{\partial x} + v_1^n \frac{\partial \phi_i}{\partial y}) \phi_m^* - \tau_{K^*} (u_1^n \frac{\partial \phi_i}{\partial x} + v_1^n \frac{\partial \phi_i}{\partial y}) (u_1^n \frac{\partial \phi_m^*}{\partial x} + v_1^n \frac{\partial \phi_m^*}{\partial y}) \right\} d\Omega_{K^*} \tag{2.45}$$

pressure bubble:

$$\int_{\Omega_{K^*}} \left\{ -\frac{\partial \phi_i}{\partial x} \phi_m^* - \tau_{K^*} \frac{\partial \phi_i}{\partial x} (u_1^n \frac{\partial \phi_m^*}{\partial x} + v_1^n \frac{\partial \phi_m^*}{\partial y}) \right\} d\Omega_{K^*} \tag{2.46}$$

$$\int_{\Omega_{K^*}} \left\{ -\frac{\partial \phi_i}{\partial y} \phi_m^* - \tau_{K^*} \frac{\partial \phi_i}{\partial y} \left(u_1^n \frac{\partial \phi_m^*}{\partial x} + v_1^n \frac{\partial \phi_m^*}{\partial y} \right) \right\} d\Omega_{K^*} \quad (2.47)$$

body force bubble:

$$\int_{\Omega_{K^*}} \left\{ f_1 \phi_m^* + \tau_{K^*} f_1 \left(u_1^n \frac{\partial \phi_m^*}{\partial x} + v_1^n \frac{\partial \phi_m^*}{\partial y} \right) \right\} d\Omega_{K^*} \quad (2.48)$$

$$\int_{\Omega_{K^*}} \left\{ f_2 \phi_m^* + \tau_{K^*} f_2 \left(u_1^n \frac{\partial \phi_m^*}{\partial x} + v_1^n \frac{\partial \phi_m^*}{\partial y} \right) \right\} d\Omega_{K^*} \quad (2.49)$$

with previously defined stabilization parameter τ_{K^*} .

Once all the bubble parts of the solutions are calculated, they will be substituted in the equation (2.38) which is solved over global mesh.

2.4 Numerical Results

In this section, we present some numerical results with the stabilizing methods presented above and compare these methods. We work on two test problems for the convection-diffusion equations: (1) L-Shape flow problem, (2) Rotating flow field, and on three test problems for the steady incompressible Navier-Stokes equations: (1) 2D laminar flow inside a lid-driven cavity, (2) Backward facing step flow and (3) 2D flow past a cylinder. We use the tool VIGIE (Visualization Generale Interactive d'Écoulements) to visualize the numerical results. The iteration cycle that resolve the nonlinearity of the problems stops when the maximum norm of the error is less than 10^{-6} .

Before we present numerical results we briefly mention our convention in labels. The upper case letters at the beginning of each label refers to the method we employ at : **BB** refers to the method which uses Q2-Q1 elements (the combination of quadratic shape functions for velocity and linear shape functions for pressure approximations) and satisfies the inf-sup or Babuska-Brezzi condition, **SSM** refers to the stabilizing subgrid method, **GP** refers to the method selecting subgrid point at the gravity center of each element, **BE** refers to the TLFEM in which subgrid is generated using equally spaced \mathbf{s} points on each side of the element and, **BG** refers to the TLFEM in which subgrid is the finest and generated by repeating the subgrid strategy in **GP** to subtriangles \mathbf{s} times. Numerical experiments show that the optimum value for \mathbf{s} is 5. So, we keep the value of \mathbf{s} fixed and take $\mathbf{s} = 5$ throughout the calculations. What follows the part of the label referring to the method employed is Reynolds number tag which we denote it by \mathbf{re} . The number of elements on the global mesh follows \mathbf{e} . Thus, for example, the label **SSMre26e6800** means that, for the problem of interest, we test the SSM at Reynolds number 26 over a global mesh with 6800 elements. We remark that all three methods use the same formulation at the global scale.

First, we will concentrate on the details of the TLFEM. The TLFEM was applied to the

solution of the convection-diffusion equations [28] and Navier-Stokes equations [27] by using quadrangle elements. In the solution of the submesh level problem, submesh should be generated for each element. As mentioned before, bubble functions are defined for each element separately and they vanish on the boundary of the element. In Figure (2.2) submesh for rectangular and quadrangle elements are displayed. Figures (2.3) and (2.4) show the 2-D and 3-D behaviour of the bubble functions on rectangular elements.

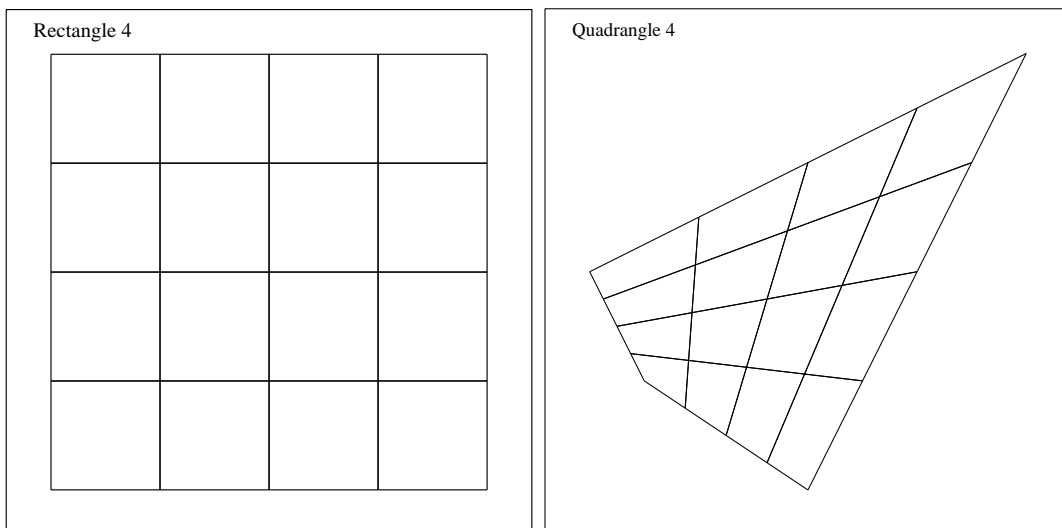


Figure 2.2: Submesh for rectangle and quadrangle elements

For a triangular element, two different types of submesh generation are tested. First one, labeled **BE**, generates the submesh from equally spaced points on the edges of the triangle. The second one, labeled **BG**, generates the submesh using the point on the body center of each newly obtained triangle sequentially. In Figure (2.5) these two types of submeshes for two different levels and corresponding bubble functions are displayed. From the experiments, it is seen that 5 times repeated **BG** submesh captures all the behaviour of the flow for the Navier-Stokes equations.

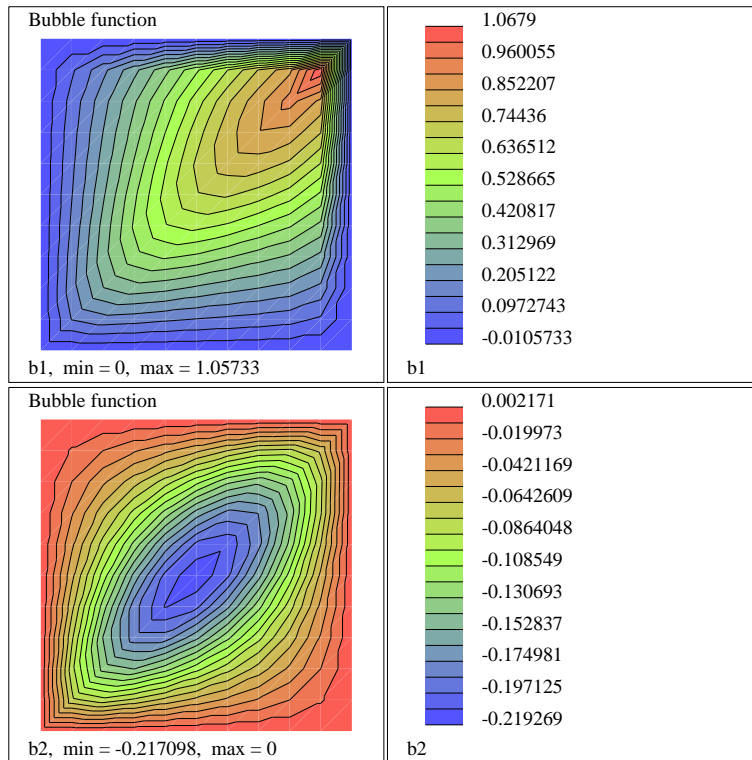


Figure 2.3: Bubble functions for rectangular elements

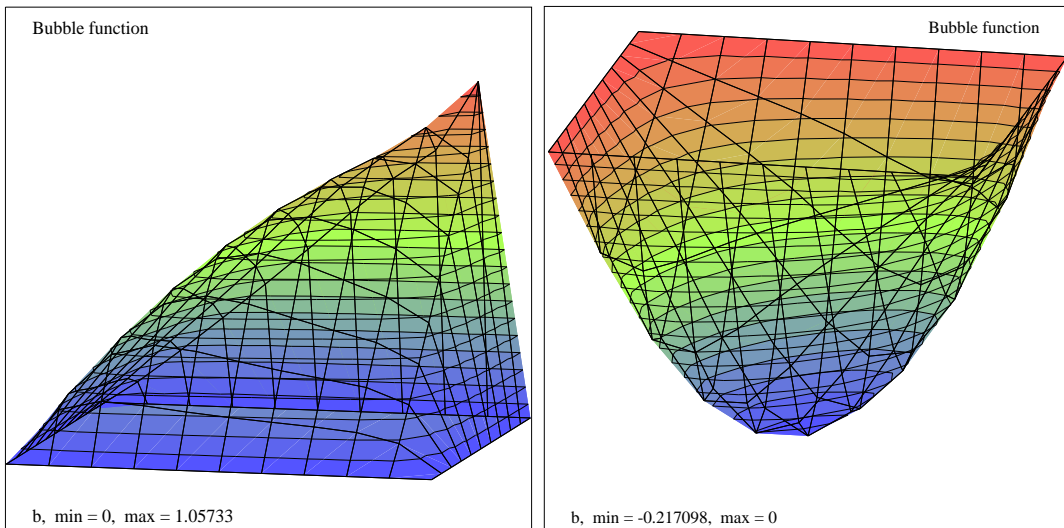


Figure 2.4: 3-D view of bubble function for rectangular elements

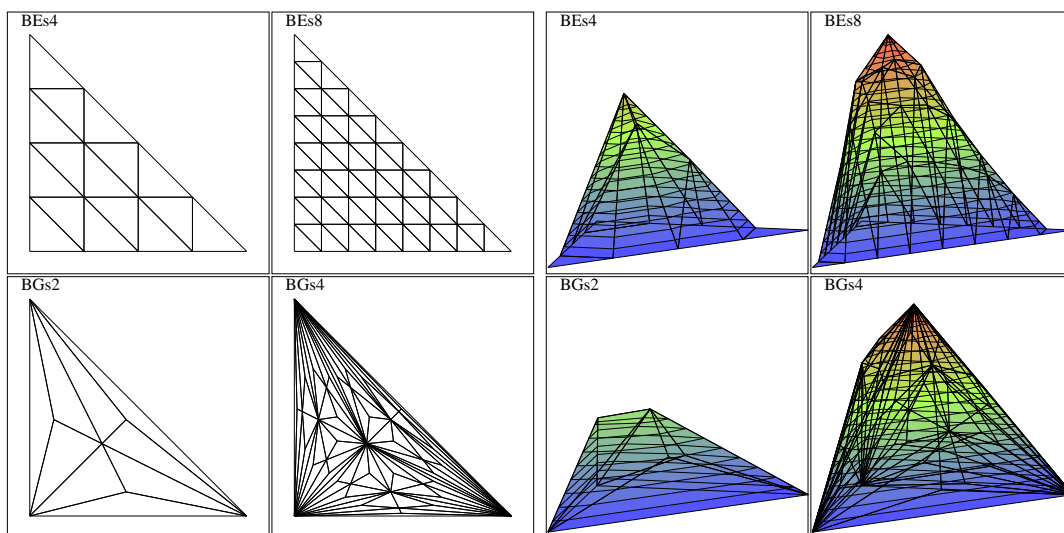


Figure 2.5: Two different types of submesh generations and corresponding bubble functions for triangular elements

2.4.1 L-Shape flow

The stabilization effect on the finite element method is shown first on the convection-diffusion problem (2.15) which is convection dominated. The SUPG method is tested on L-Shape flow problem [9] with the domain and boundary conditions described in Figure (2.6).

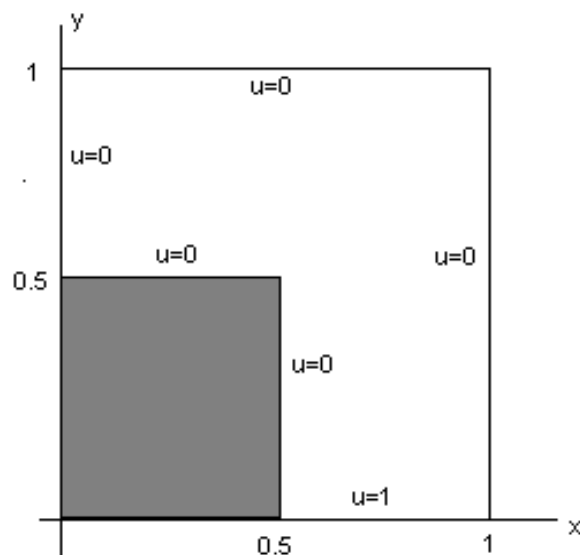


Figure 2.6: Definition of L-shape flow problem

For the convection dominated case ($\epsilon = 5 \times 10^{-4}$, $a(x, y) = (-y, x)$), boundary layers occur close to the upper left corner and L-shaped corner. Solution with standard Galerkin finite element method ($\tau_K = 0$) exhibits deformations as ϵ gets smaller in these parts whereas the stabilized FEM eliminates these disturbances. Figure (2.7) presents solution contours of convection-diffusion problem for $\epsilon = 5 \times 10^{-2}$, $\epsilon = 5 \times 10^{-3}$, $\epsilon = 5 \times 10^{-4}$ respectively.

In Figure (2.8), the disturbances close to the L-shape corner and upper left corner can be seen clearly when the standard FEM is used especially for small values of ϵ .

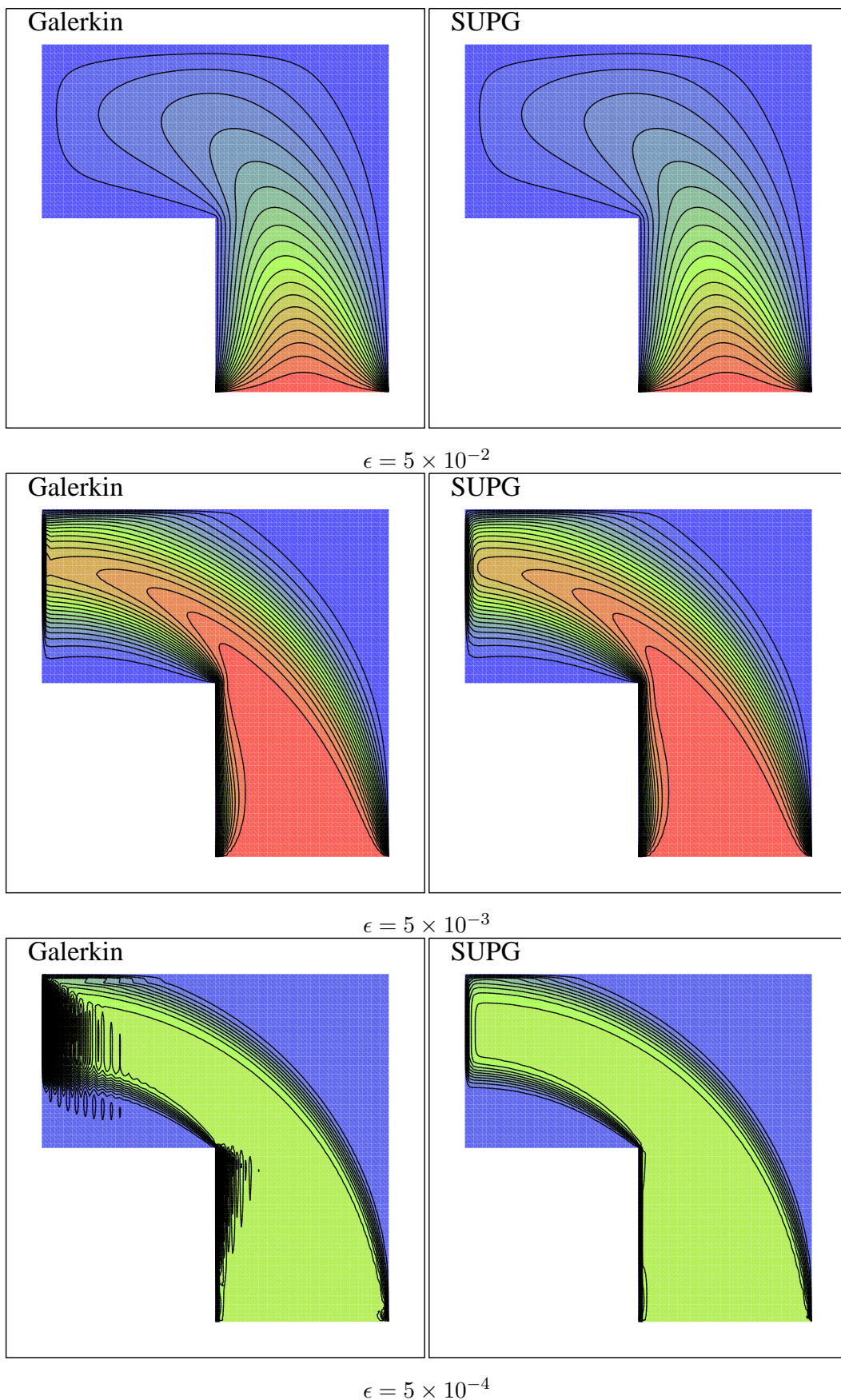
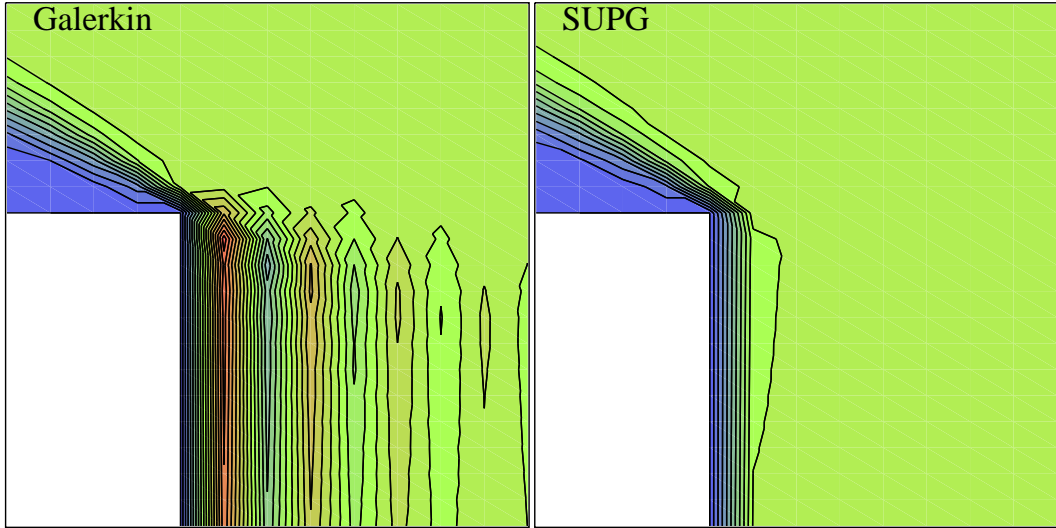
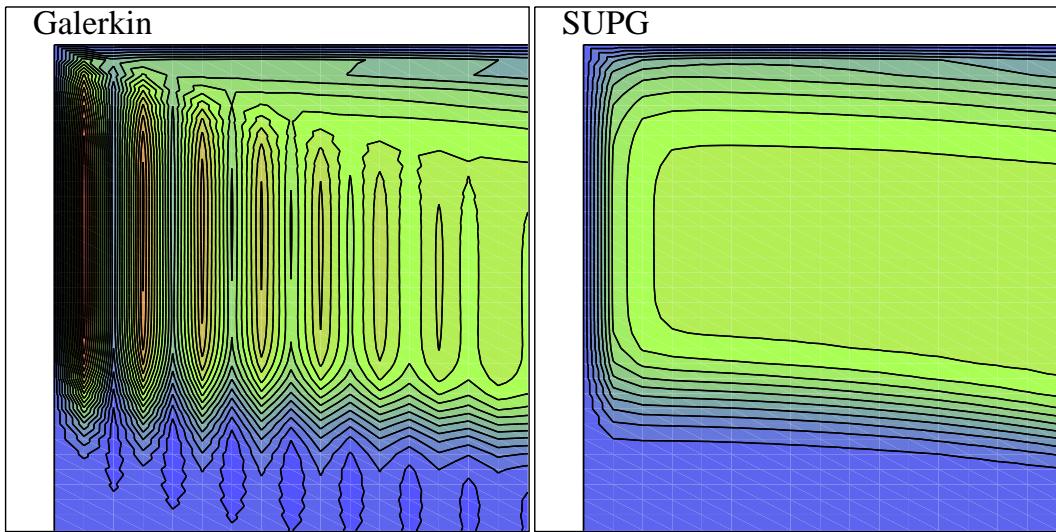


Figure 2.7: Standard Galerkin FEM and SUPG solutions of L-Shape flow



(a) Zoom: corner at $x = 0.5, y = 0.5$



(b) Zoom: left upper boundary at $x = 0, y = 1$

Figure 2.8: Stabilization effect in L-shape flow near boundary layers for $\epsilon = 5 \times 10^{-4}$

2.4.2 Rotating flow field

The TLFEM method is tested on a rotating flow field problem which is defined by the convection-diffusion equation (2.15). The same problem is also solved with SUPG method which is more faster than TLFEM in the sense of computational time.

The problem is defined on a unit square $0 \leq x, y \leq 1$ with the parameters $\epsilon = 10^{-6}$, $\mathbf{a} = (0.5 - y, x - 0.5)$. The boundary conditions are; $u = 0$ along the external boundary and in the internal boundary on $x = 0.5$ and $0 \leq y \leq 0.5$, $u = \frac{1}{2}(\cos(4\pi y - \pi) + 1)$, [28].

The problem is solved by using both SUPG and TLFEM methods with almost the same accuracy. In the solution 30×30 global mesh elements and for each element 7×7 subelements are used. Solutions are compared in Figure (2.9).

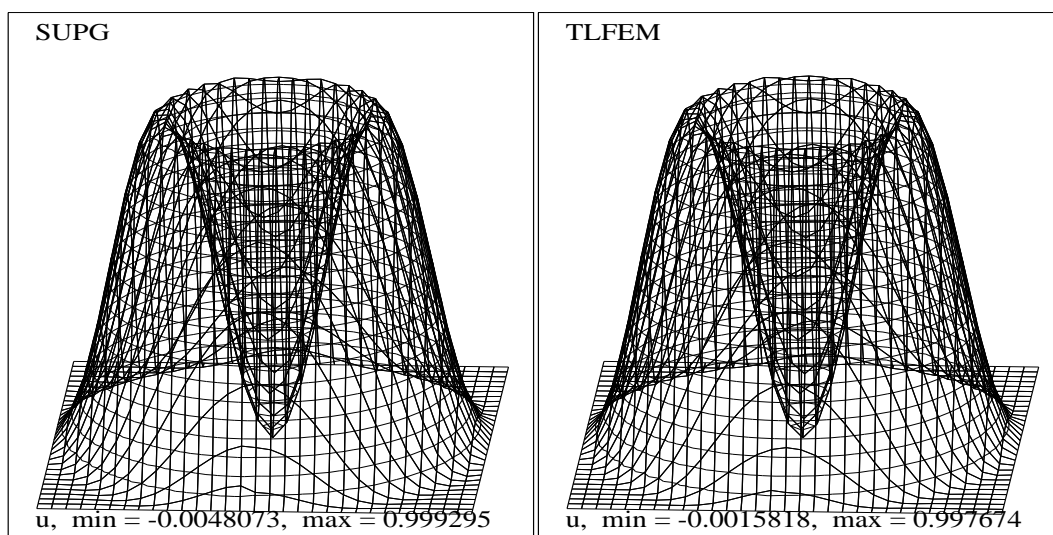


Figure 2.9: Comparison of SUPG and TLFEM solutions of rotating flow field

2.4.3 Lid-Driven Cavity flow

This is a standard benchmark problem defined by the Navier-Stokes equations (2.6) [52]. The problem specifications are given in Figure (2.10). We impose continuous boundary conditions by means of a linear transition from the level $y = 0.9$ to $y = 1.0$ on the upper corners of the boundary, and this is used in all the meshes. The Reynolds number is based on the characteristic velocity \mathbf{U}_0 and the characteristic length L and given by

$$Re = \frac{\mathbf{U}_0 L \rho}{\mu}.$$

For problems having high Reynolds number, the convergence of the iteration is only attained under a good initial guess. For higher Reynolds number we use the converged results obtained with smaller Re as starting values for the iteration.

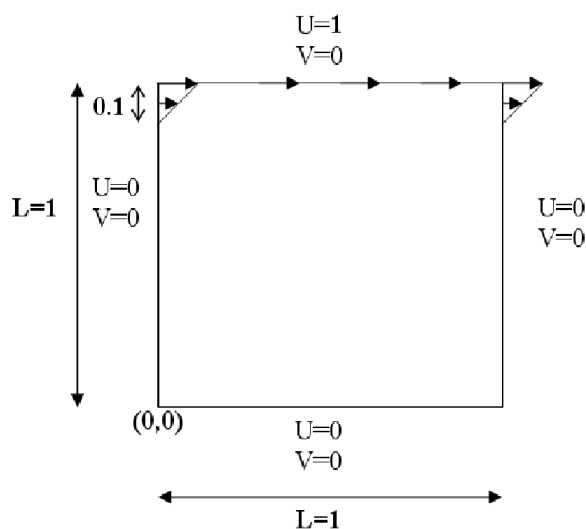


Figure 2.10: The problem statement of the lid-driven cavity flow

We present the numerical results for $Re = 400$ and $Re = 5200$ on a pair of successively refined uniform meshes (see Figure (2.11)).

Solution of the Navier-Stokes equations with equal order shape functions

Cavity flow problem has been solved first, by using linear shape functions for both the velocity components and the pressure of the Navier-Stokes equations. Results obtained from this selection show periodic behaviour in pressure (Figure (2.12)) even for small Reynolds numbers. Although velocity components are suitable, there are some oscillations in the streamlines which are seen more clearly especially at the right bottom vortex. As mentioned before, convective-diffusive character of the Navier-Stokes equations and mixed formulation ($u-v-p$ form) cause

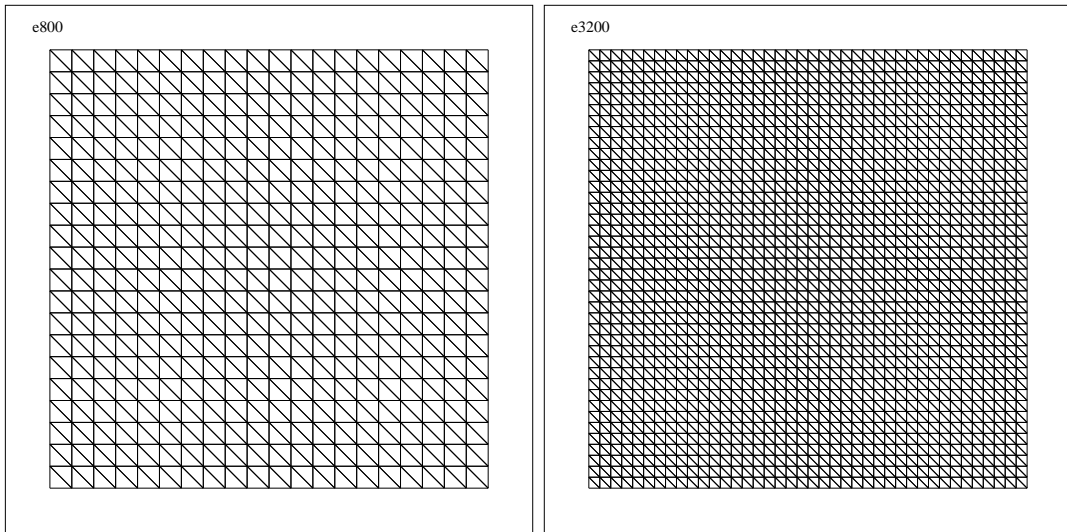


Figure 2.11: The problem meshes tested for the cavity flow: 800 and 3200 elements

these oscillations for the choice of equal order shape functions.

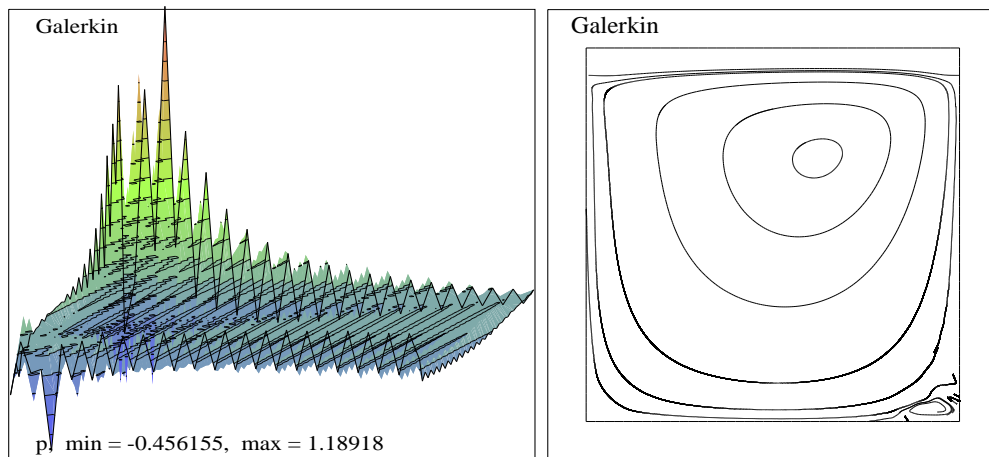


Figure 2.12: Pressure elevation and streamlines for the cavity flow, $Re = 100$

Solution of the Navier-Stokes equations with Babuska-Brezzi condition

Babuska-Brezzi condition (Q_2-Q_1 elements) implies the use of linear shape functions for pressure and quadratic shape functions for the velocity components. With this solution technique, oscillations in the pressure values which occurred in the use of equal order shape functions have disappeared.

The cavity flow problem has been solved for Reynolds numbers 400 and 5200 using $Q_2 - Q_1$ elements. As Reynolds number increases new vortices will occur. The disadvantage of the

method is the need of the fine mesh for high Reynolds numbers. Since the quadratic shape functions already require extra points in an element, it is difficult to make the mesh very fine. Figure (2.13) presents pressure values and streamlines for $Re = 400$ and $Re = 5200$ in terms of contours and elevations for the flow.

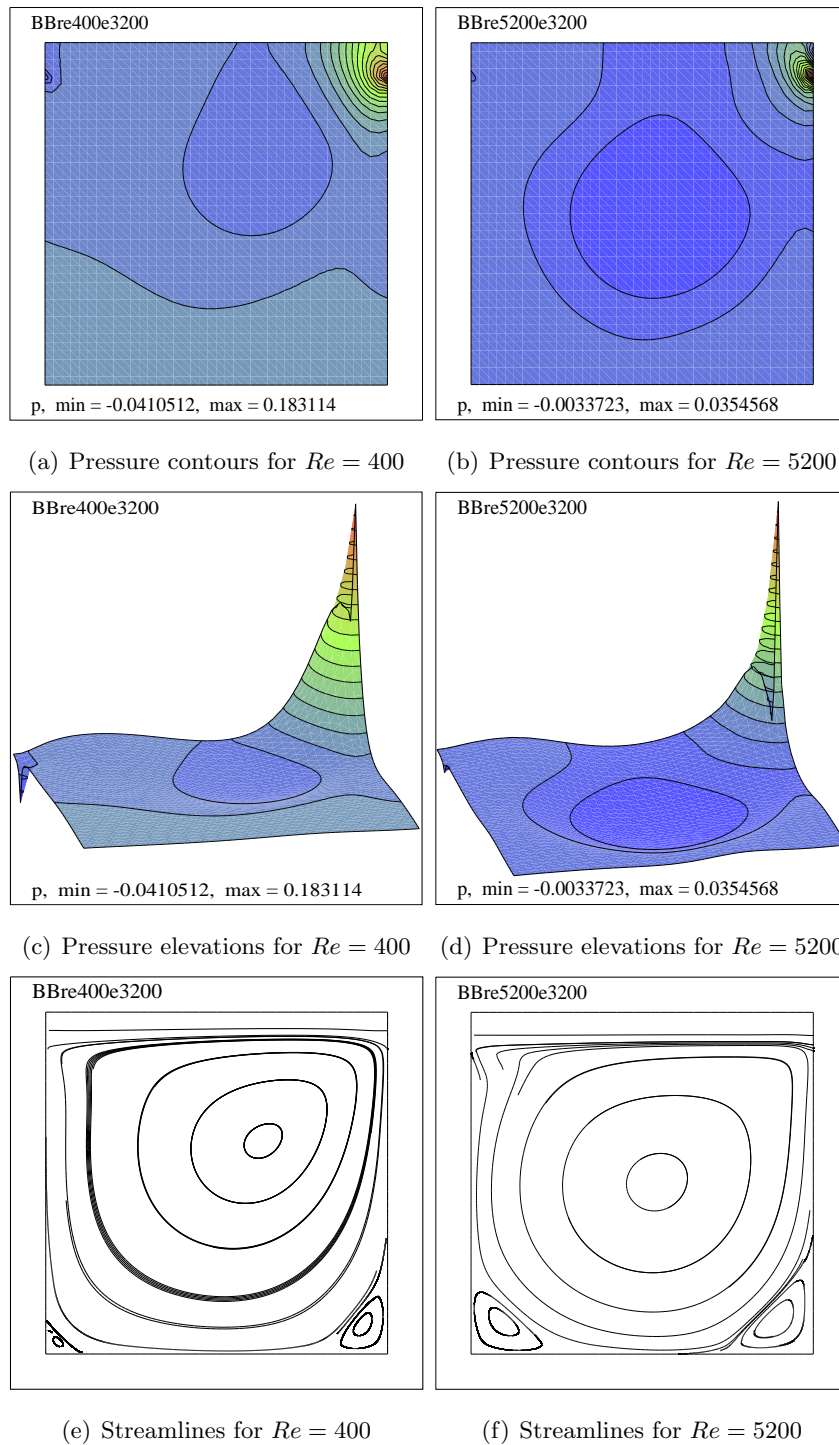


Figure 2.13: Solutions of the cavity flow with 3200 elements of Q2-Q1 type

Solutions of the Navier-Stokes equations with stabilized methods(SUPG, SSM, TLFEM)

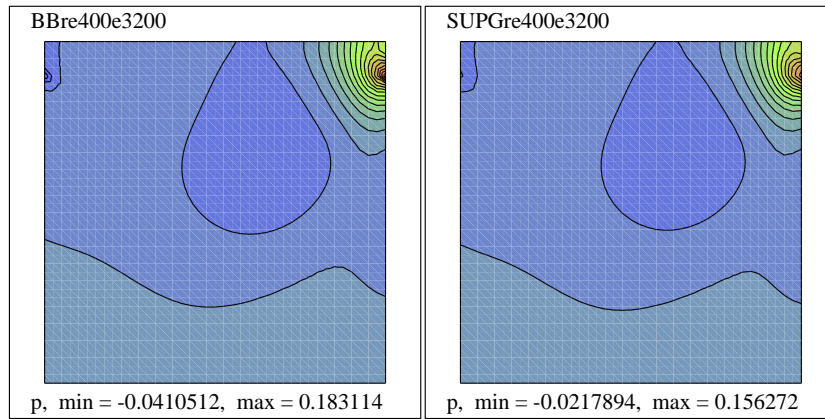
We have compared the solutions obtained from **SUPG** method with the solutions obtained by using Q2-Q1 elements on cavity flow problem for Reynolds number $Re = 400$ and $Re = 5200$ with 3200 elements . From the Figures (2.14) and (2.15), it is seen that although the behaviour of the flow is captured by **SUPG** method, maximum and minimum values are not predicted successfully compared to **BB** method. This can be seen more clearly as Reynolds number increases. However, streamlines of the flow are almost indistinguishable in the comparison of both methods.

Solutions obtained with SSM, TLFEM and Q2-Q1 elements for Reynolds number 400 and 5200 are compared in the Figures (2.16) and (2.17) from left to right, respectively. They show the characteristic features of the real solution and comparable with the results that are present in the literature [52, 73]. Unlike SUPG method, both SSM and TLFEM give accurate results even for the rough meshes.

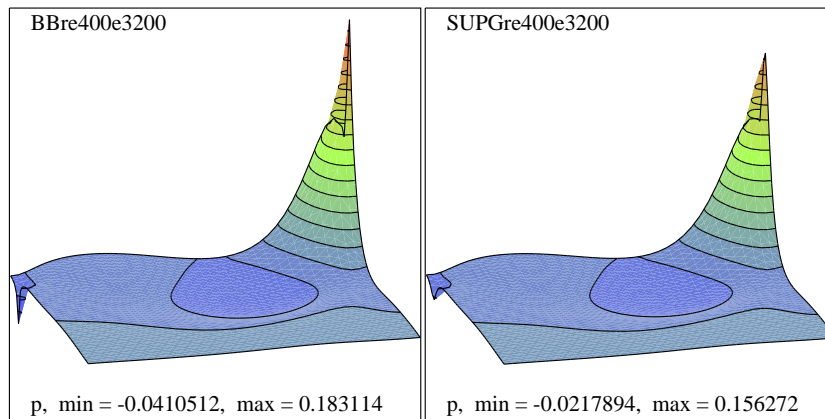
SSM, GP and Q2-Q1 element type solutions are compared for high Reynolds numbers. Figure (2.18) shows pressure contours and pressure elevations at Reynolds number $Re = 5200$. Assuming the results obtained through the TLFEM are the most accurate, we may conclude that SSM predicts the real solution better than GP at both levels of the problem meshes. This shows that the proper choice of the subgrid node may play a significant role in obtaining more accurate approximations. As the mesh gets finer, the problem becomes locally diffusive dominated in a larger portion of the domain and the need for stabilization is diminished (Figure (2.19)). The situation is apparent as the location of the subgrid point suggested by SSM moves to the gravity center of the element and all three solutions get closer to each other. However, SSM is slightly better than GP as SSM suggests a more correct location for the subgrid node over a smaller portion of the domain (Figure (2.19)).

On the other hand, Figures (2.20) shows the configuration of subgrid points in the mesh e800 for $Re = 400$ and $Re = 5200$, respectively. For $Re = 400$, the flow regime of the real solution is diffusive dominated in the most part of the domain and the role of stabilization components is not so significant. As the Reynolds number increases the problem becomes convection dominated and therefore the adaptation of the position of the subgrid point is strongly pronounced. The stabilization is now effective on a larger portion of the entire domain. Streamlines presented in Figure (2.21) for $Re = 5200$ with **SSM** method are also in agreement with the results in the literature(see [52]). As given in the reference [32], velocity values through the geometric center of the cavity are presented in terms of table and figure in Table (2.1) and Figure (2.22), respectively.

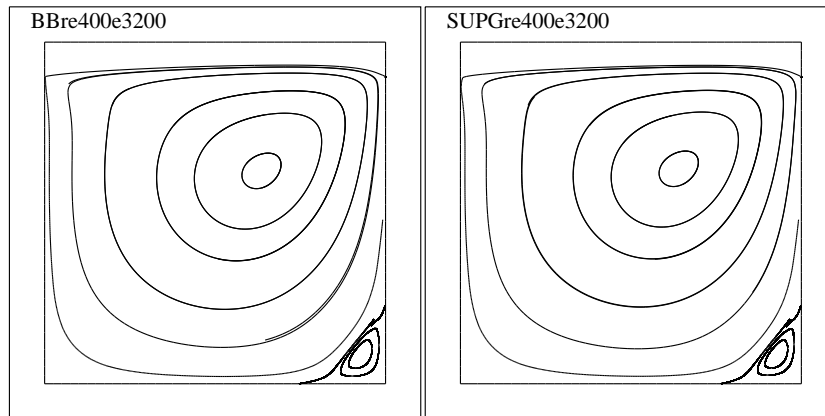
We have also tested different type of global meshes. Randomly generated non-uniform mesh



(a) Pressure contours for $Re = 400$



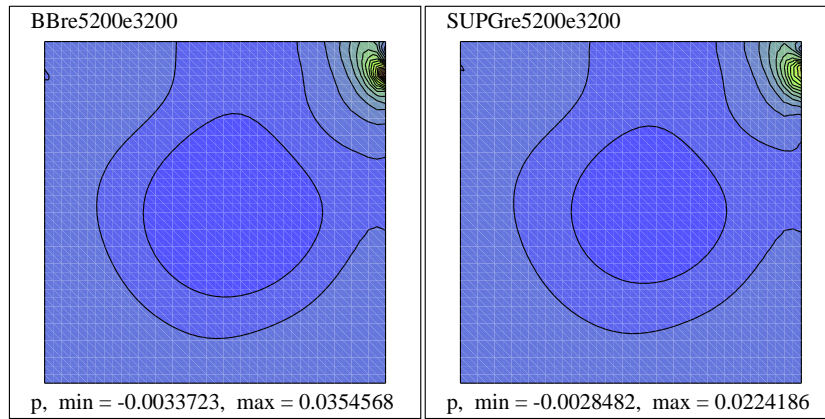
(b) Pressure elevations for $Re = 400$



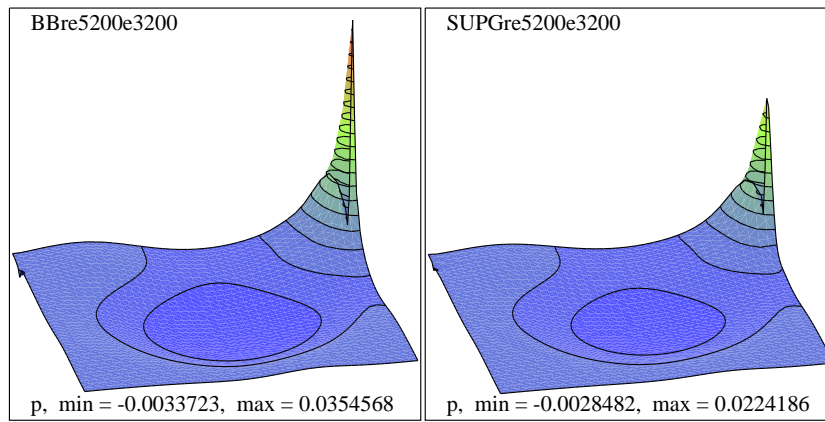
(c) Streamlines for $Re = 400$

Figure 2.14: Comparison of Q2-Q1 elements with SUPG method for the cavity flow, $Re = 400$

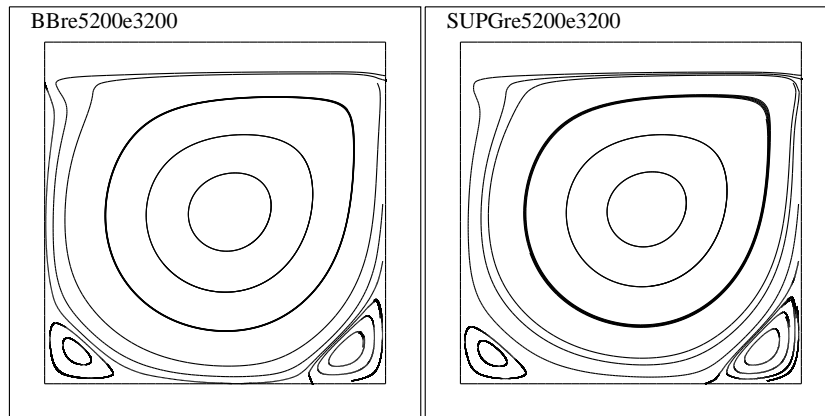
does not provide accurate results (Figure (2.23)). Since the critical changes exist at the upper lid of the cavity, a modification on the upper lid mesh produces accurate results for the pressure (Figure (2.24)). For high values of Reynolds number, vortices in the streamline graphics occur near the boundaries. Therefore selecting a refined mesh with quadratic distribution through the



(a) Pressure contours for $Re = 5200$



(b) Pressure elevations for $Re = 5200$



(c) Streamlines for $Re = 5200$

Figure 2.15: Comparison of Q2-Q1 elements with SUPG method for the cavity flow, $Re = 5200$

boundaries will capture the behaviour of the flow in terms of streamlines more clearly (Figure (2.25)).

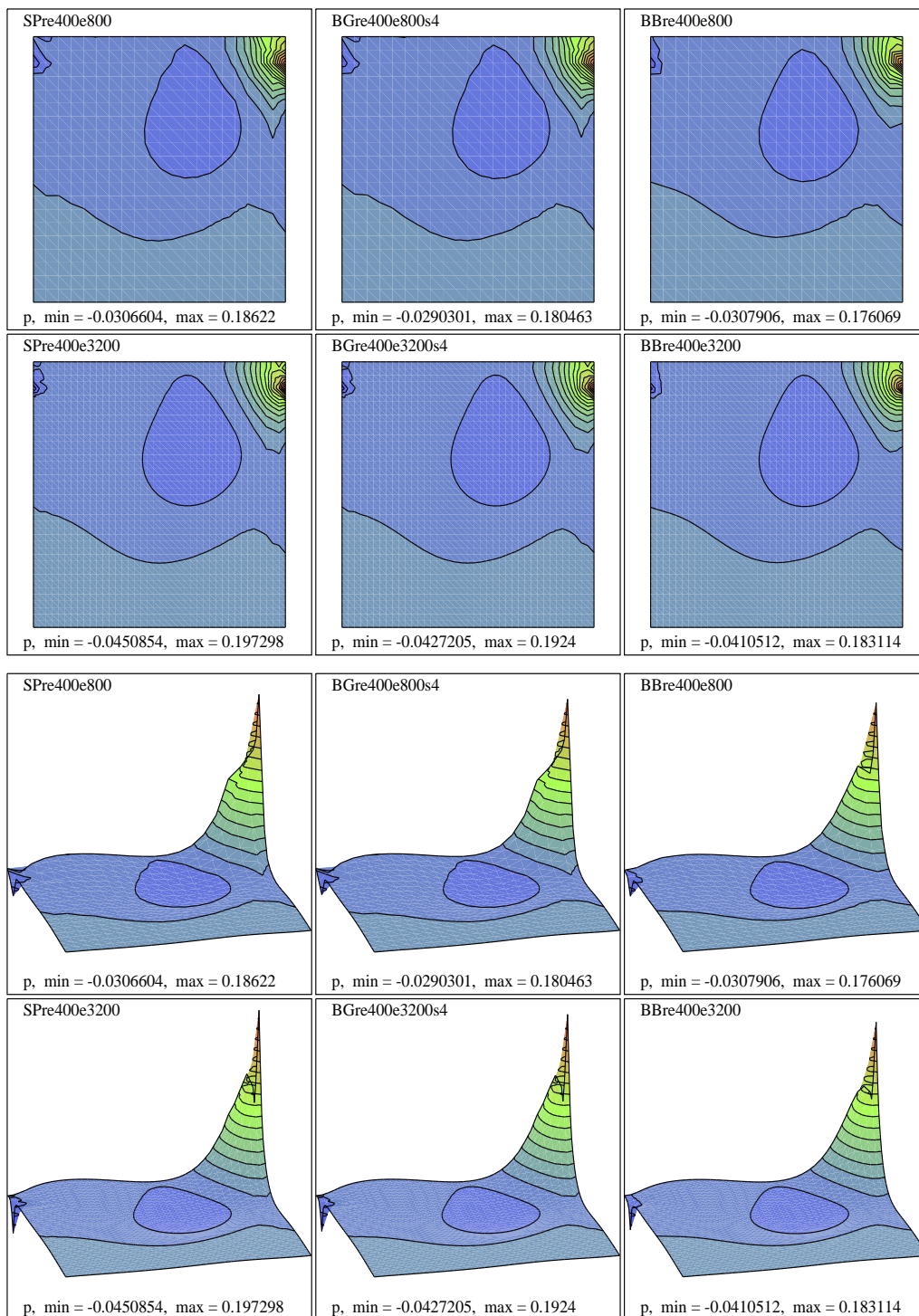


Figure 2.16: Pressure contours and elevations for the cavity flow with SSM, TLFEM and Q2-Q1, $Re = 400$

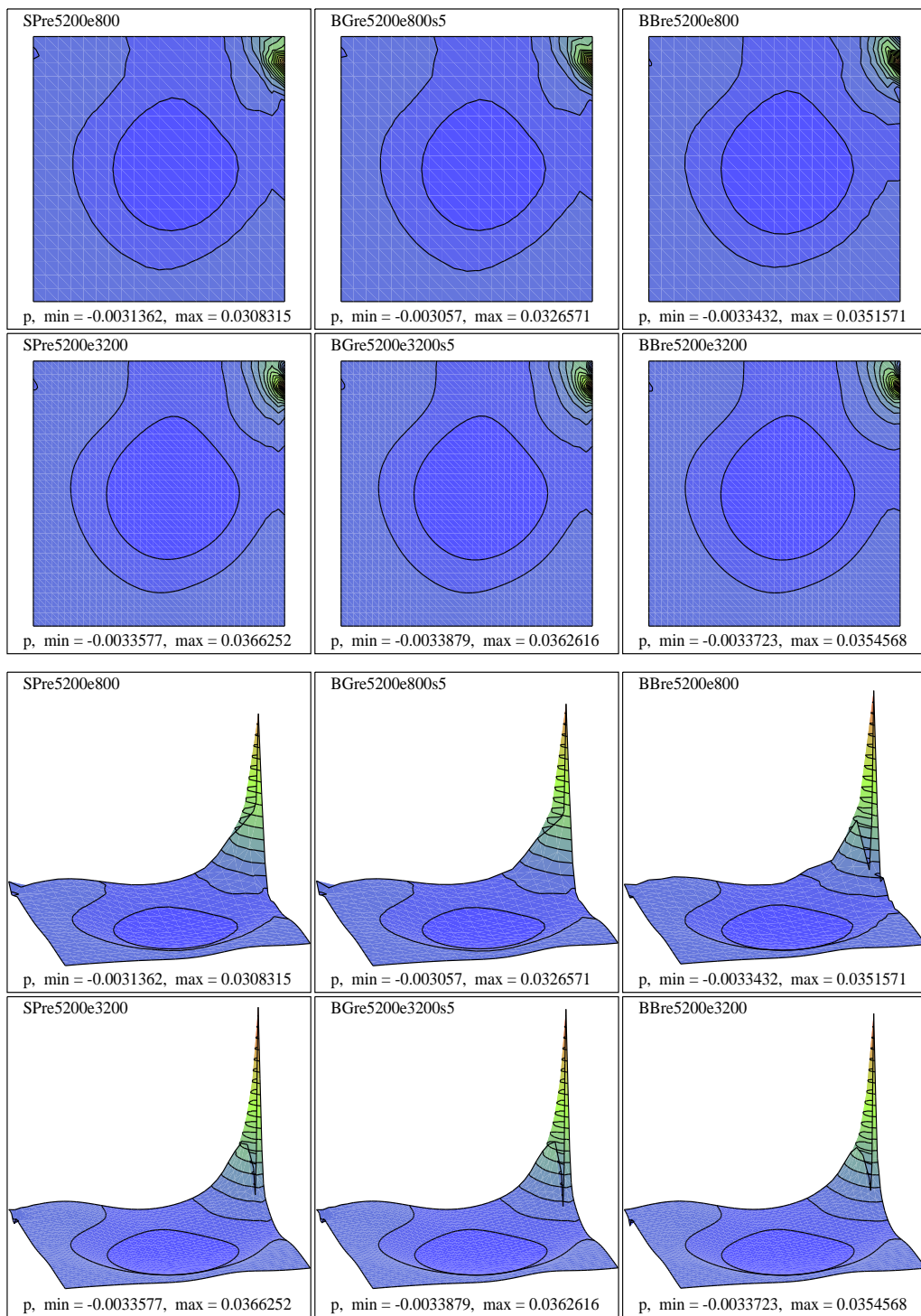


Figure 2.17: Pressure contours and elevations for the cavity flow with SSM, TLFEM and Q2-Q1, $Re = 5200$

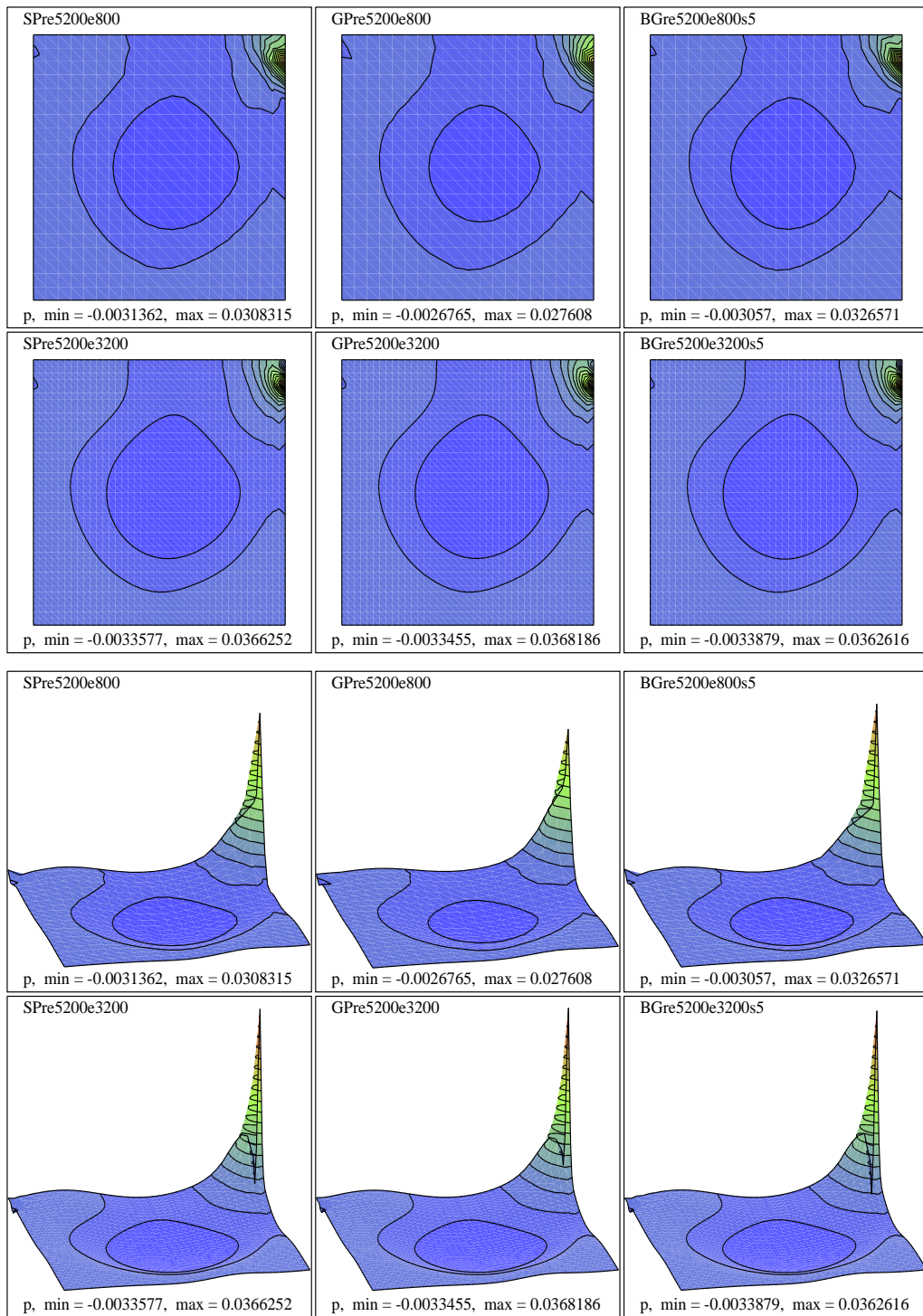


Figure 2.18: Pressure contours and elevations for the cavity flow with SP, GP and TLFEM, $Re = 5200$

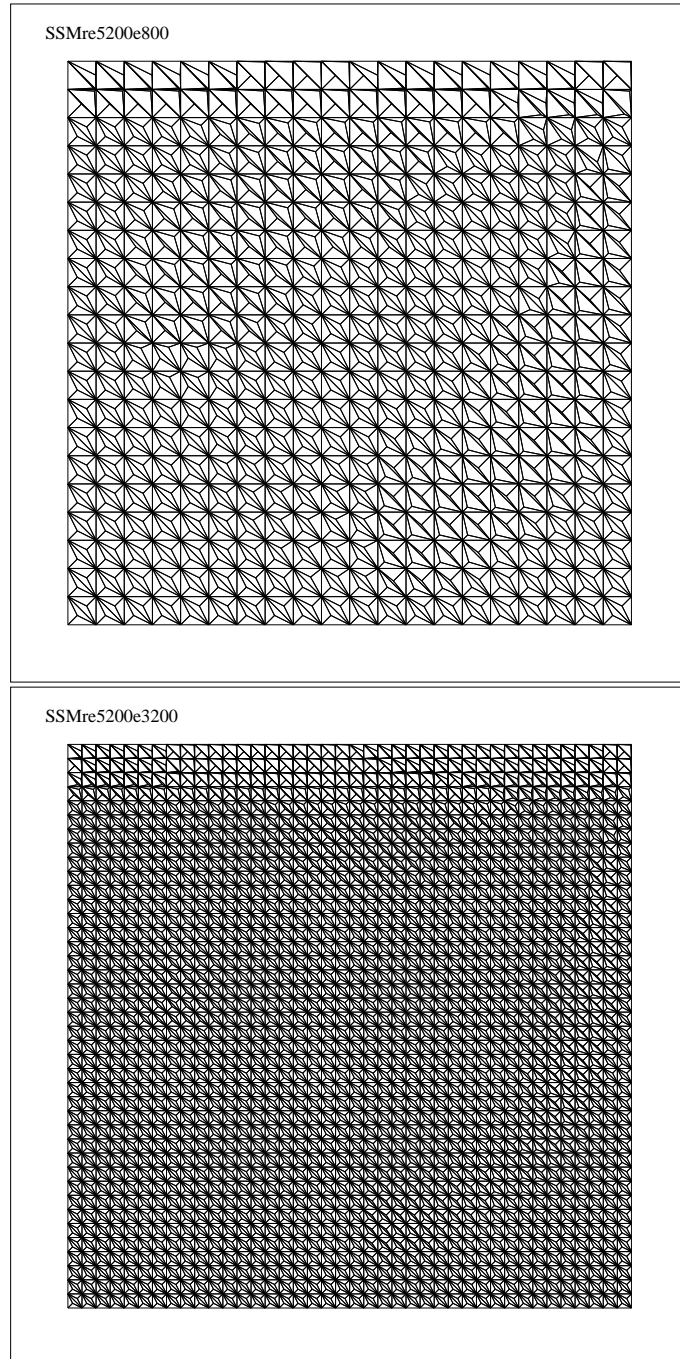


Figure 2.19: Adaptation of the subgrid points in SSM as the problem mesh is refined at $Re = 5200$: The problem meshes are **e800** and **e3200**

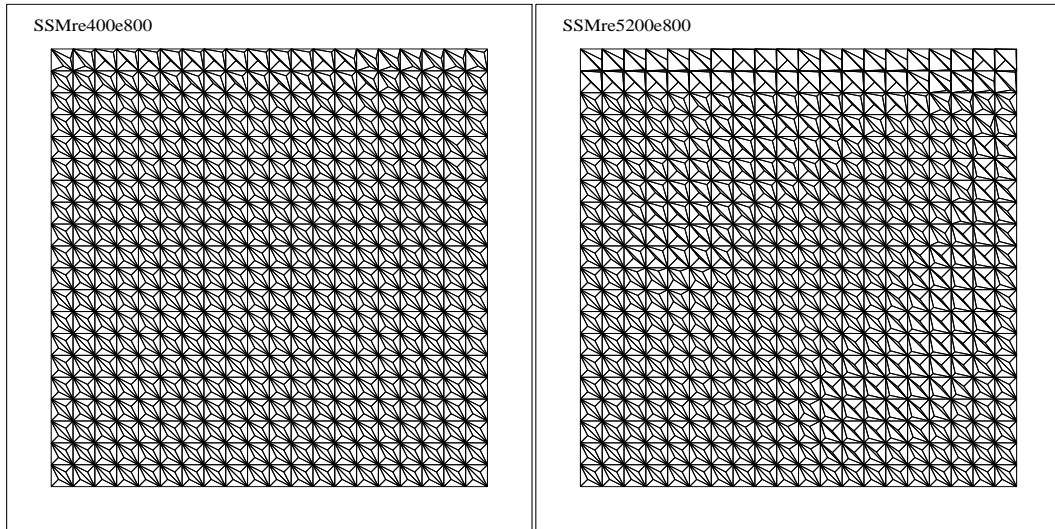


Figure 2.20: Adaptation of the subgrid points in SSM as the problem becomes convection dominated on a fixed mesh e800: $Re = 400$ and $Re = 5200$

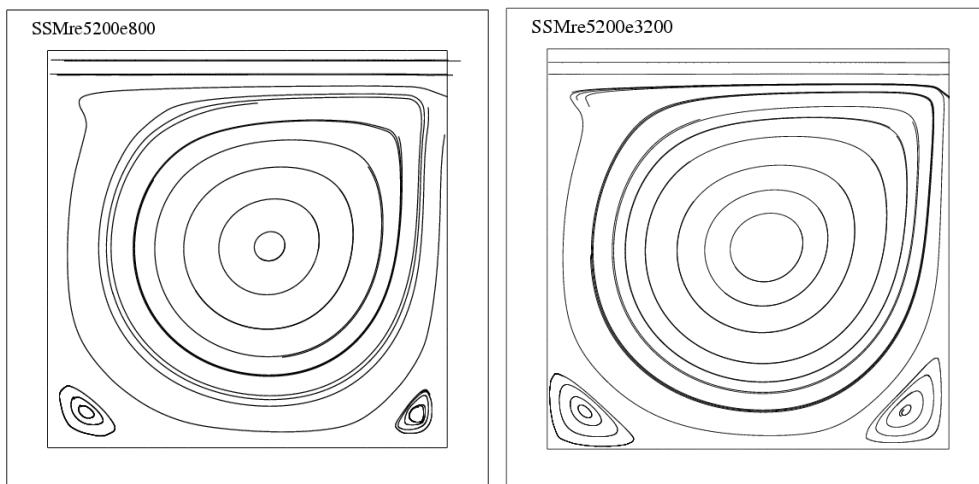


Figure 2.21: Streamlines for the cavity flow with SSM, $Re = 5200$

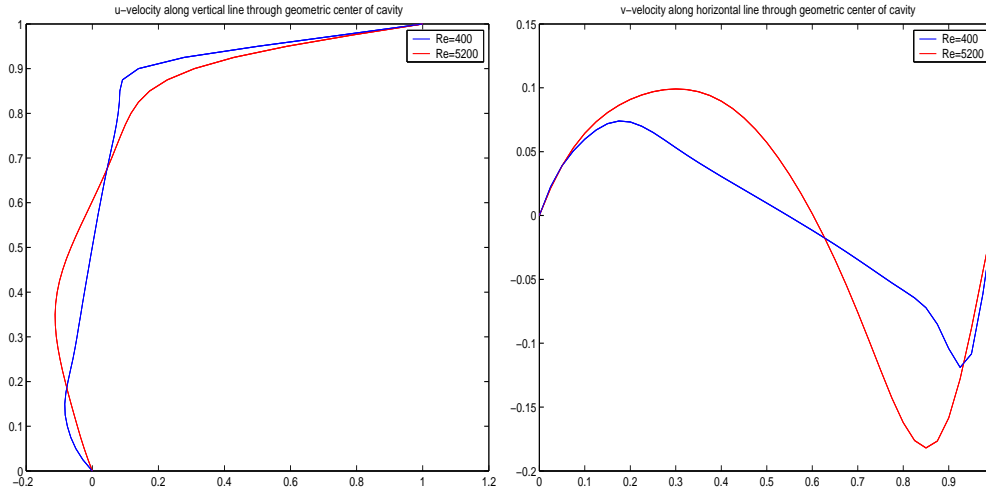


Figure 2.22: Velocity profiles for the cavity flow with SSM, $Re = 400$ and $Re = 5200$

Table 2.1: Velocity values at some selected points through the geometric center of the cavity

u -velocity along vertical line			v -velocity along horizontal line		
y	$Re=400$	$Re=5200$	x	$Re=400$	$Re=5200$
0.000000	0.000000	0.000000	0.000000	0.000000	0.000000
0.075000	-0.0350700	-0.0648715	0.075000	0.0530557	0.0506292
0.125000	-0.0548183	-0.0819039	0.125000	0.0734340	0.0669750
0.250000	-0.0977078	-0.0588283	0.250000	0.0969054	0.0650425
0.375000	-0.1107317	-0.0293358	0.375000	0.0939595	0.0359474
0.500000	-0.0645859	-0.0002669	0.500000	0.0571612	0.0097147
0.625000	0.0137531	0.0308169	0.625000	-0.0158838	-0.0171241
0.750000	0.0858983	0.0664360	0.750000	-0.1208616	-0.0467028
0.850000	0.1736514	0.0834718	0.850000	-0.1819628	-0.0721858
0.900000	0.3088252	0.1397576	0.900000	-0.1584394	-0.1042040
0.950000	0.5886718	0.5006183	0.950000	-0.0880898	-0.1083465
0.975000	0.7852072	0.7521335	0.975000	-0.0438278	-0.0614507
1.000000	1.000000	1.000000	1.000000	0.000000	0.000000

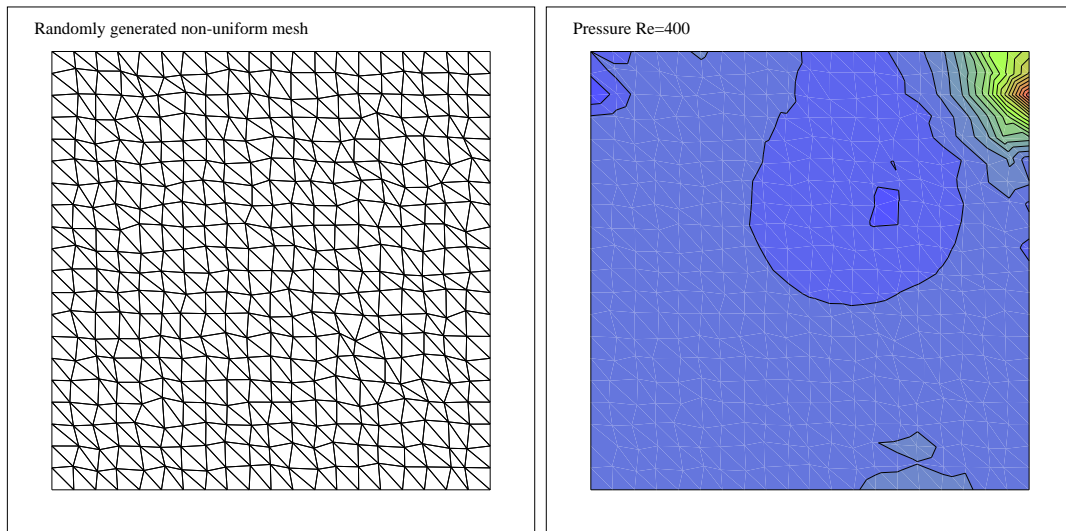


Figure 2.23: Randomly generated non-uniform mesh and pressure contours for the cavity flow

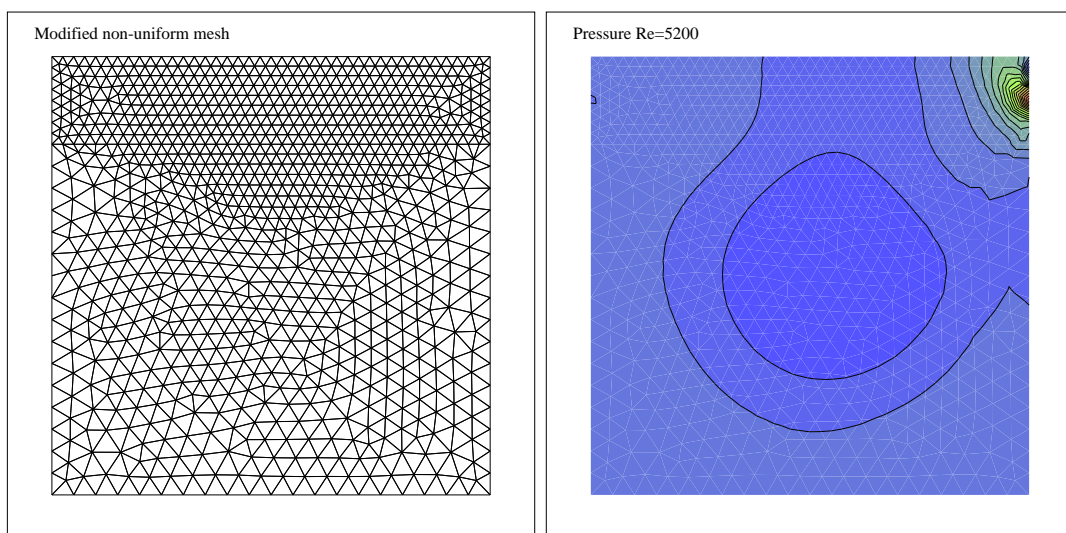


Figure 2.24: Modified non-uniform mesh and pressure contours for the cavity flow

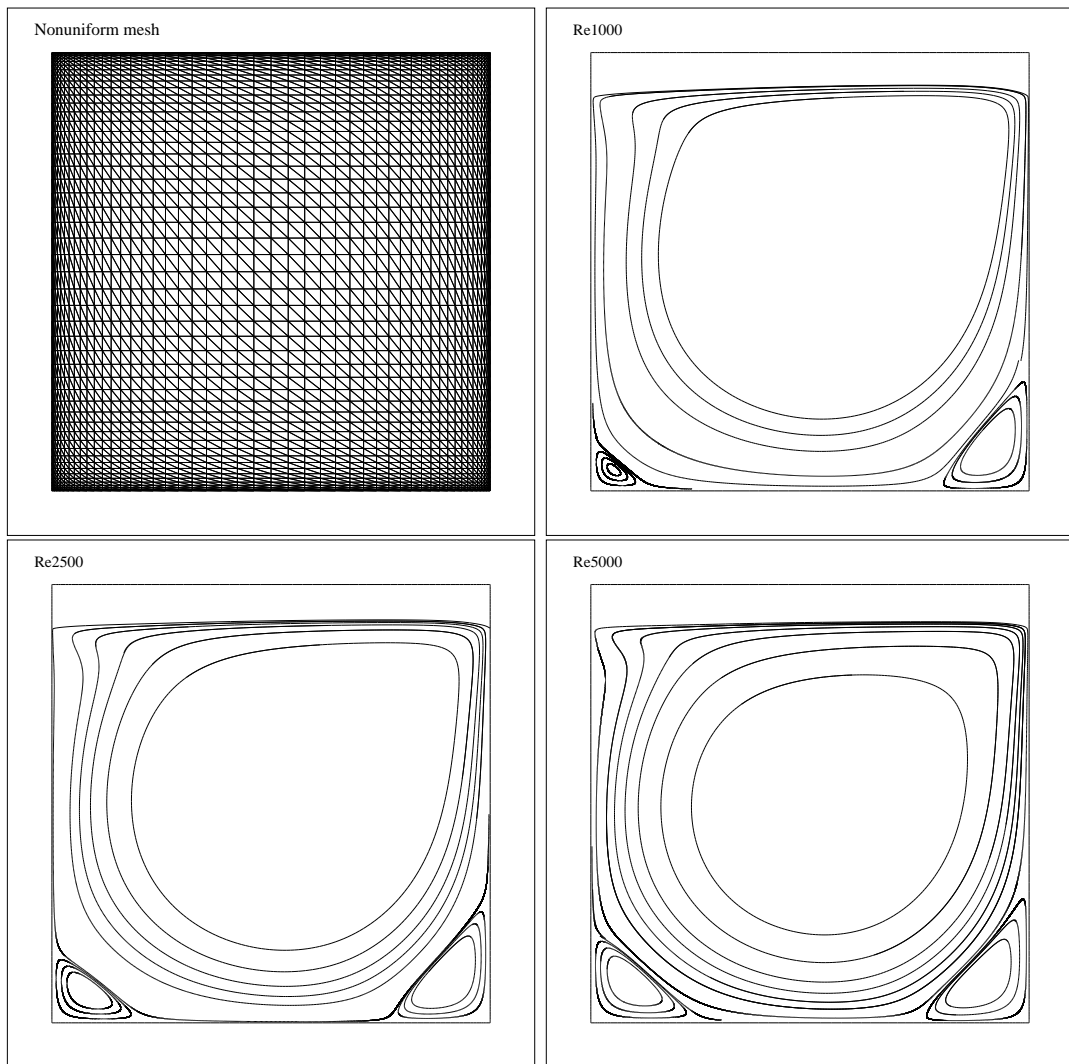


Figure 2.25: Unstructured, quadratically distributed mesh and streamlines for the cavity flow:
 $Re = 1000, 2500$ and 5000

2.4.4 Backward facing step flow

This problem is known to have a corner singularity. The geometry and the boundary conditions are shown in Figure (2.26) [52]. We choose the Reynolds number based on the maximum velocity U_{max} ($U_{max} = 1$) at the inlet boundary and the height of the step l ($l = 0.5$):

$$Re = \frac{U_{max} l}{\nu}.$$

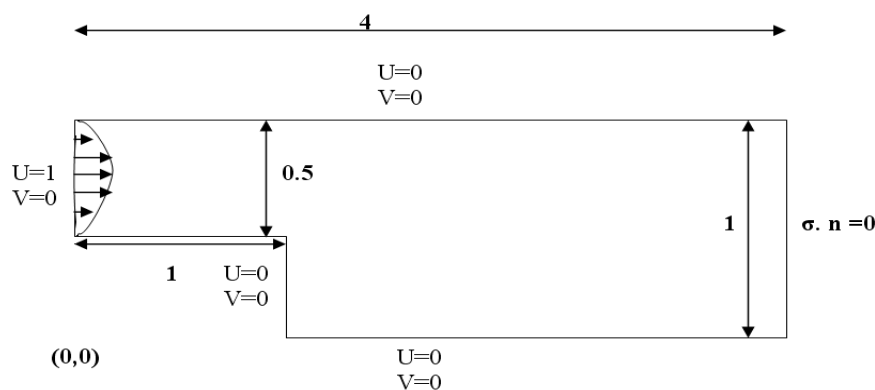


Figure 2.26: The statement of the backward facing step flow

A fully developed parabolic velocity profile is prescribed at the inlet boundary. A successively refined uniform meshes of 448, 1792 and 7168 elements, were employed (see Figure (2.27)). The Reynolds number selected is 150.

In Figures (2.28) and (2.29), pressure contours and elevations are presented for stabilizing subgrid method (SSM), GP and TLFEM (BE type) solutions. It is seen that, all the methods bring out almost similar results and as the mesh gets thinner SSM and GP solutions become the same. We give the streamline details behind the step in Figure (2.30) and note that all the results are comparable with the solutions in [52]. We have also tested the changes in the flow in terms of pressure contours and streamlines as Reynolds number increases. Figure (2.31) shows this behavior for $Re = 150$, $Re = 300$, $Re = 600$ and $Re = 900$ with the solutions obtained by SSM.

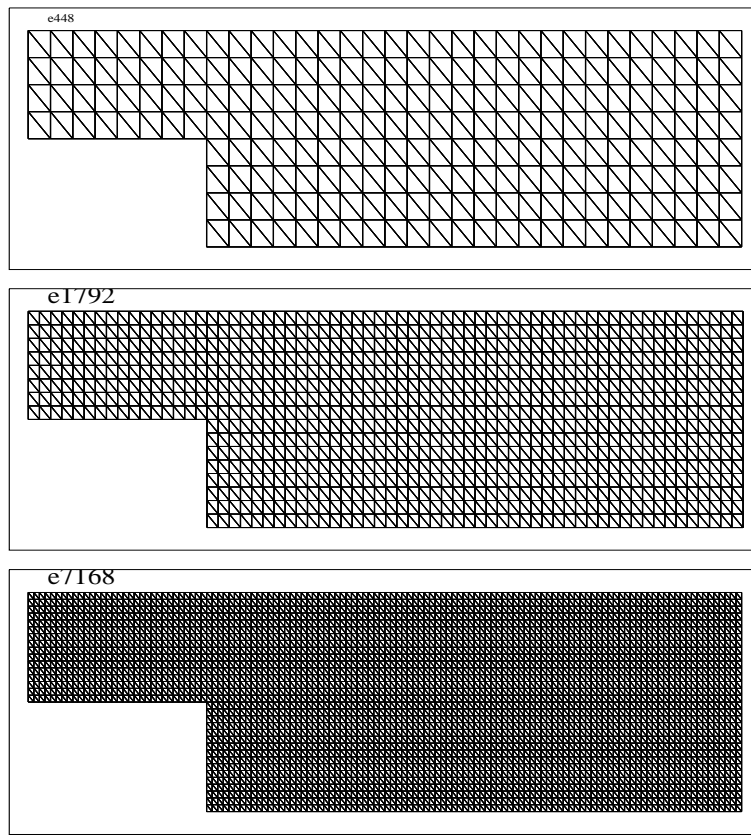


Figure 2.27: The problem meshes tested for the backward facing step flow

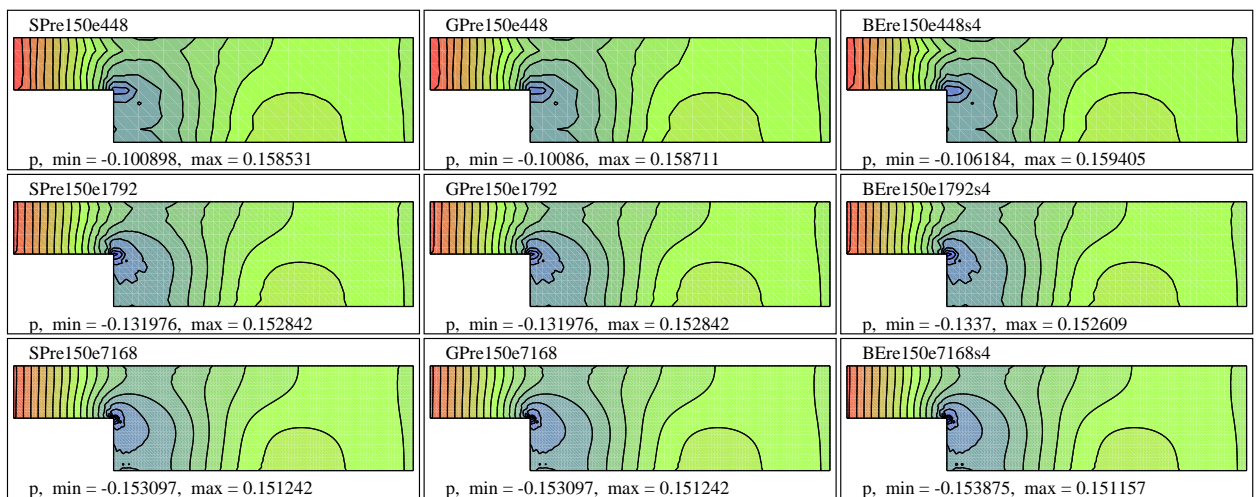


Figure 2.28: Pressure contours for the backward facing step flow with SP, GP and TLFEM, $Re = 150$

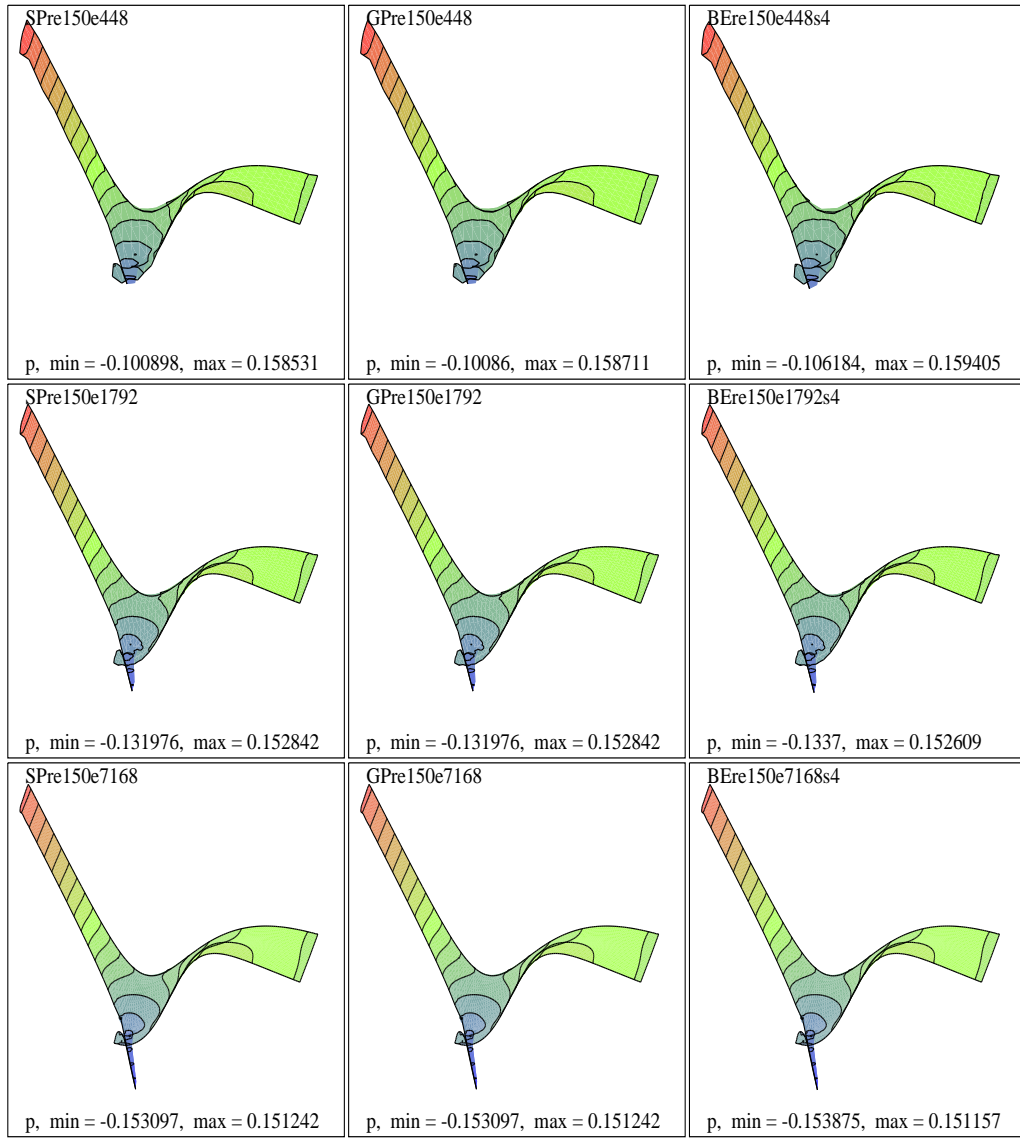


Figure 2.29: Pressure elevations for the backward facing step flow with SP, GP and TLFEM, $Re = 150$

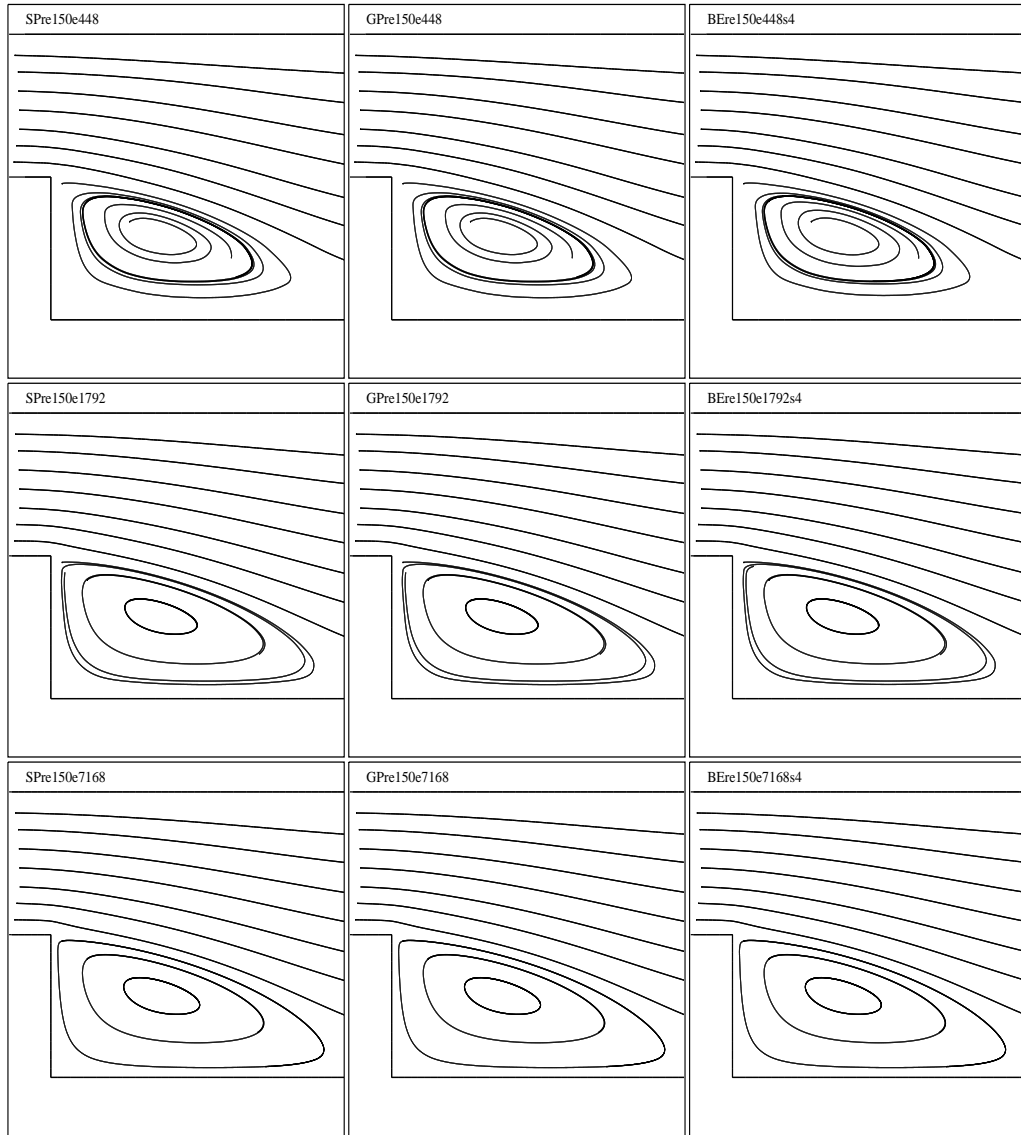
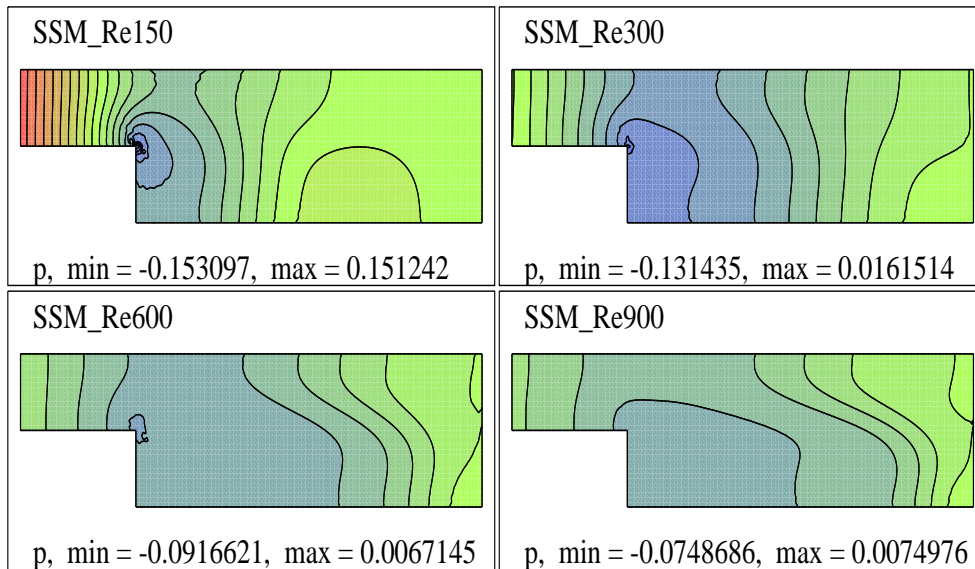
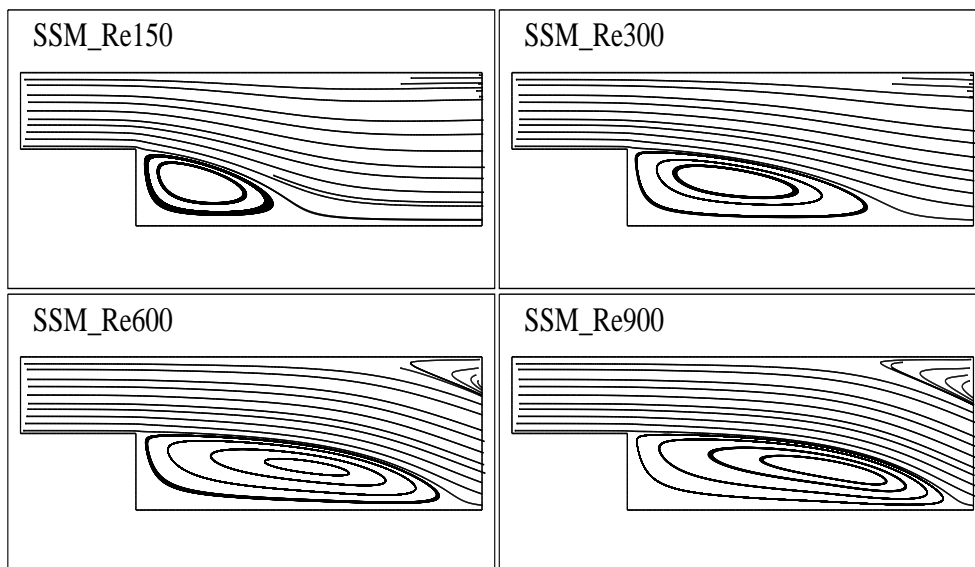


Figure 2.30: Streamline details for the backward facing step flow behind the step with SP, GP and TLFEM, $Re = 150$



(a) Pressure contours



(b) Streamlines

Figure 2.31: Changes in the flow as Reynolds number increases for the backward facing step flow with SSM

2.4.5 Flow past a cylinder

The geometry and the boundary conditions for the flow past a cylinder are shown in Figure (2.32) [52]. At the upper and lower computational boundaries and at the inflow section, a uniform free-stream velocity boundary condition is imposed. The traction-free condition is given at the outflow boundary. The steady flow past a cylinder is studied at $Re = 26$. See [21] for a historical overview of this problem.

We are interested in the performance of the **SSM** over a series of successively refined meshes (Figure (2.33)). Around the cylinder, we employ a uniform distribution of 40,80,160 nodes in angular direction and a quadratic distribution of 21,41,81 nodes in radial direction, respectively. We present the pressure contours for $Re=26$ in Figure (2.34). Although the method captures the main features of the exact solution, even at the very coarse level of the global mesh, the increase in the number of elements improves the approximation. A detailed plot of pressure contours around the cylinder in Figure (2.35) confirms this observation.

We note that the stabilizing subgrid method is more effective over coarser meshes. This can be observed in Figure (2.36), as SSM adapts the location of the subgrid node over a larger portion of the region. This adaptation is crucial in obtaining stabilized approximations. We note that the streamlines in Figure (2.37) are in good agreement with the results in [52].

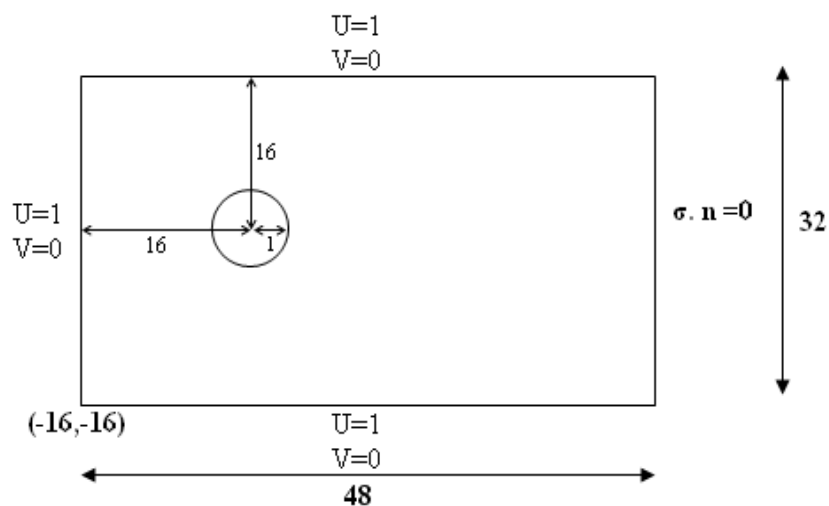


Figure 2.32: The statement of the flow past a cylinder

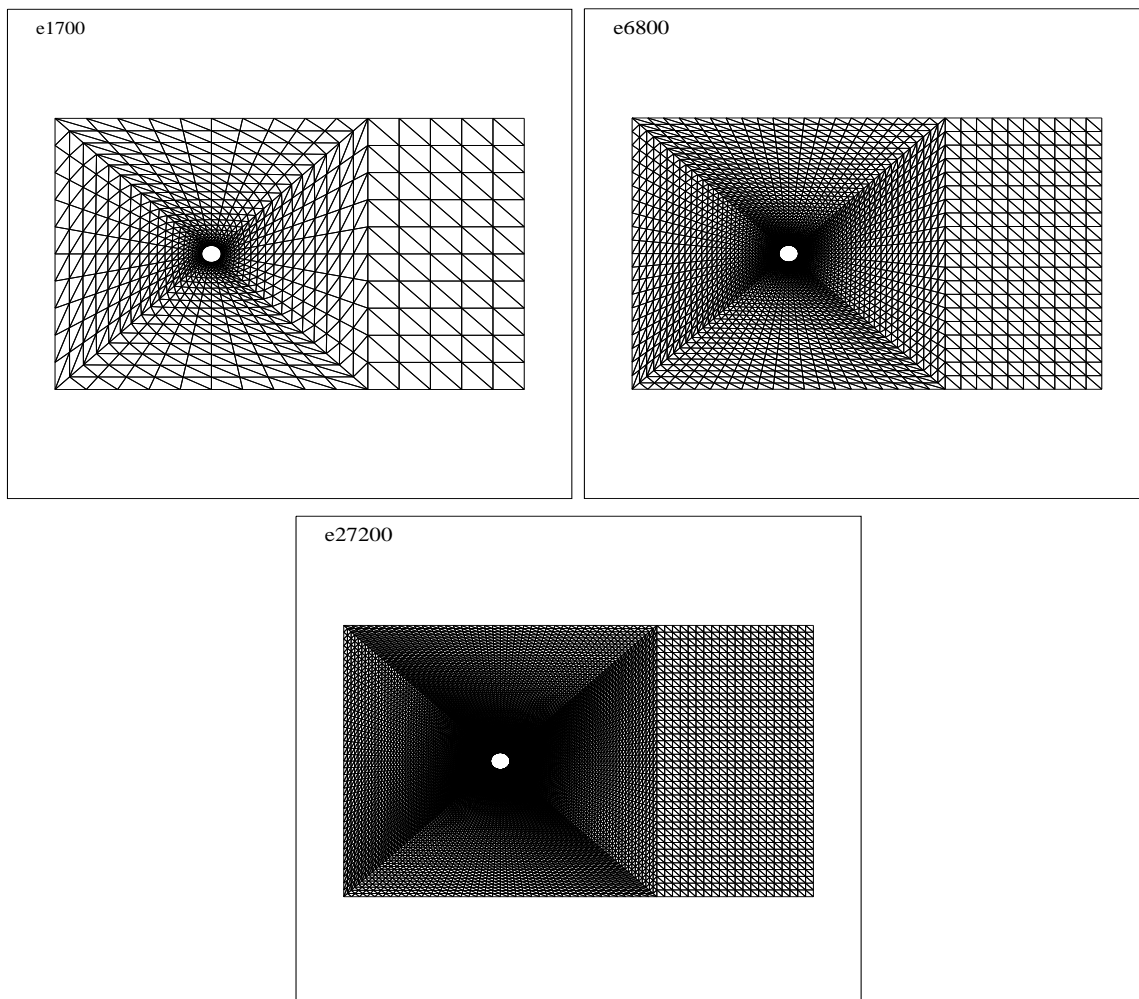


Figure 2.33: The problem meshes tested for the flow past a cylinder

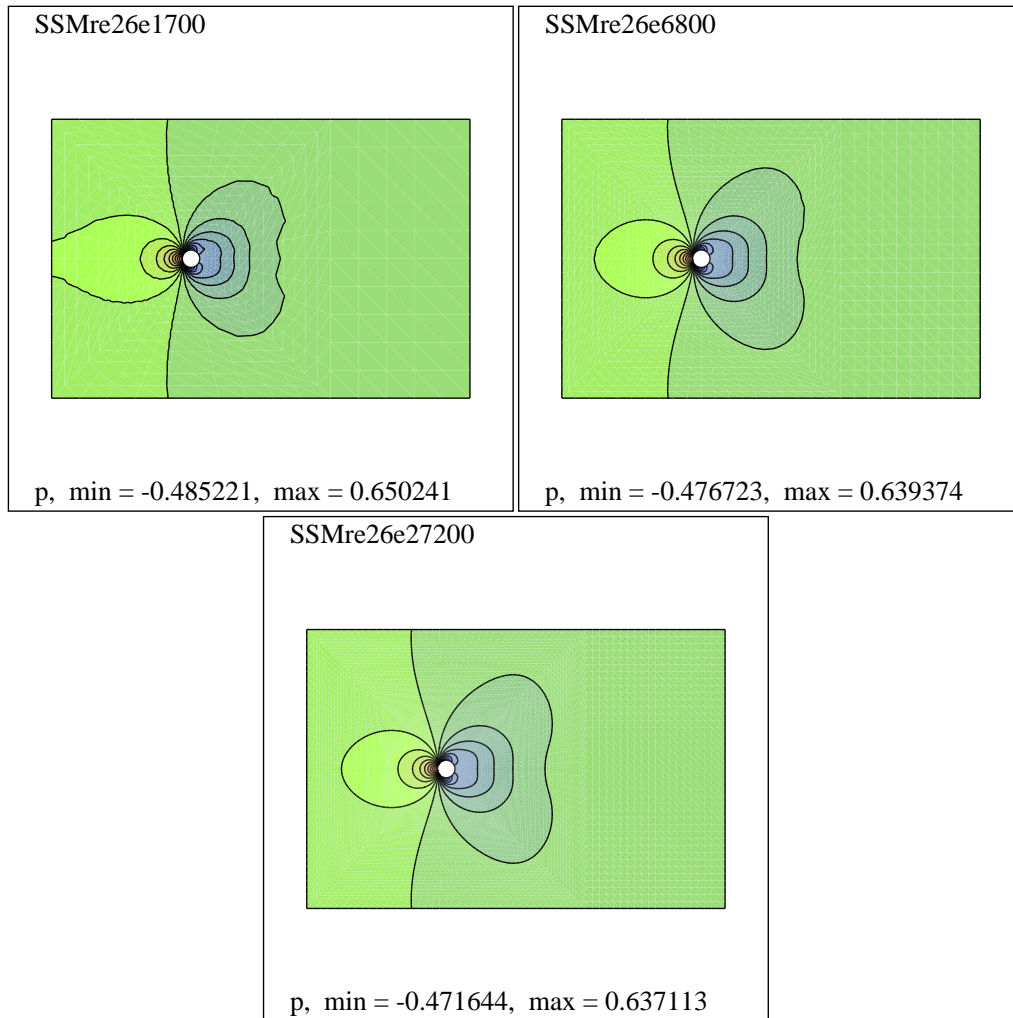


Figure 2.34: Pressure contours for the flow past a cylinder, $Re = 26$

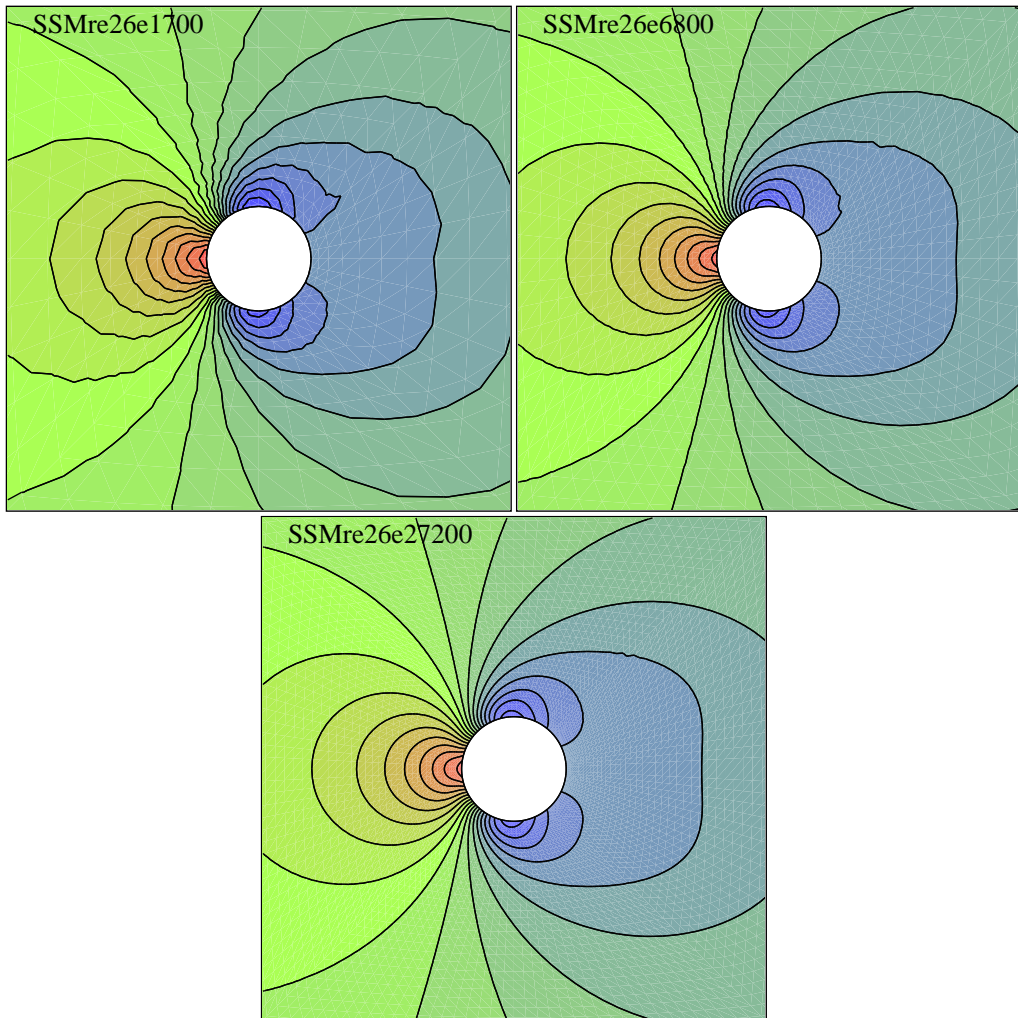


Figure 2.35: Pressure detail behind the cylinder for $Re = 26$

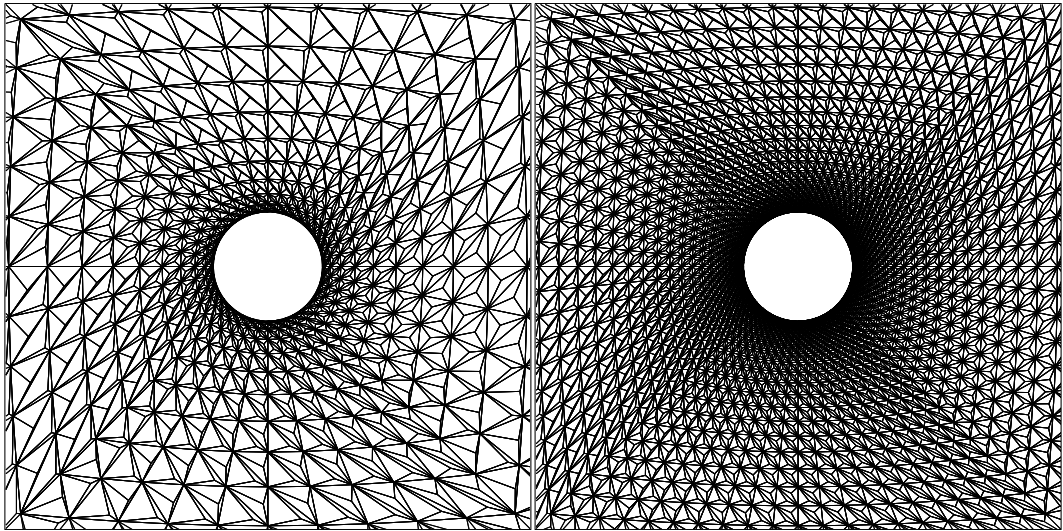


Figure 2.36: Mesh detail around the cylinder for $Re = 26$ with $e=1700$ and $e=6800$

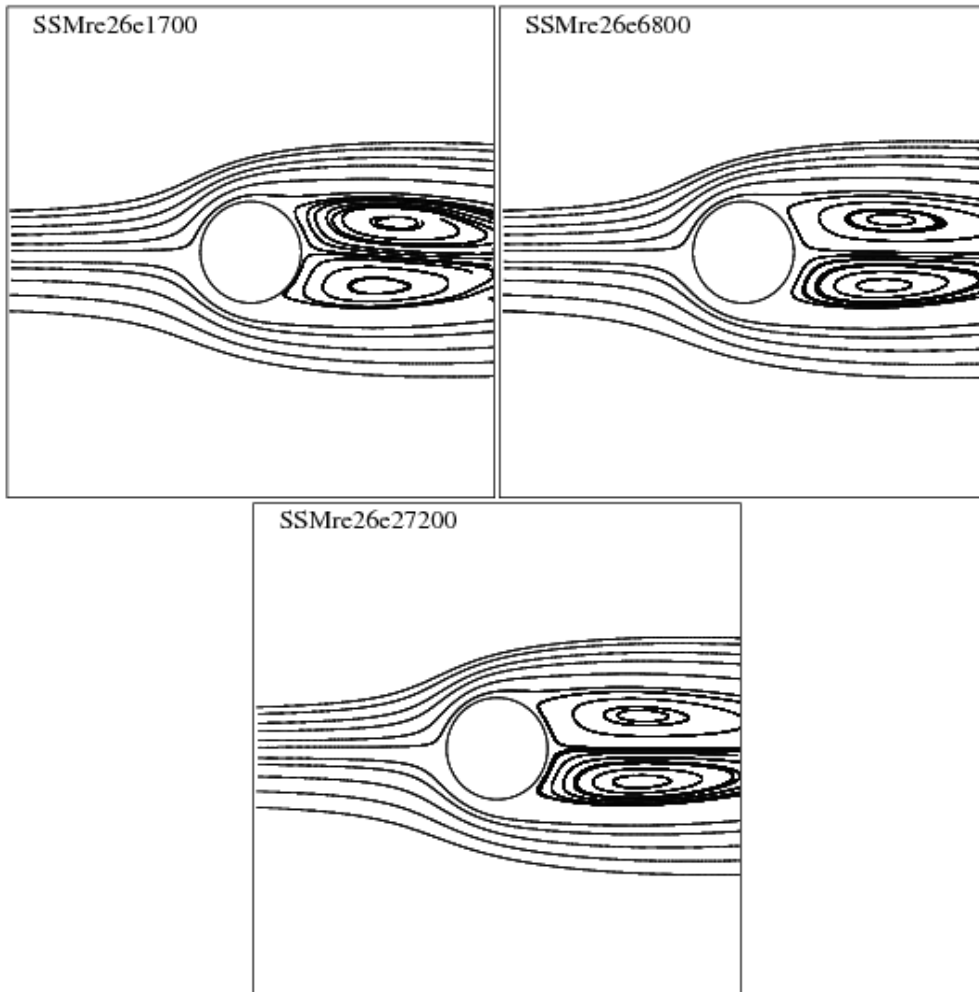


Figure 2.37: Streamlines details behind the cylinder for $Re = 26$

CHAPTER 3

SOLUTION OF THE UNSTEADY NAVIER-STOKES EQUATIONS

In this chapter, we describe the stabilized FEM in space-FEM in time domain procedure first on the diffusion and convection-diffusion equations and then on the unsteady incompressible flows governed by Navier-Stokes equations. In order to compare the methods, the finite difference method (FDM) in time domain for the unsteady convection-diffusion and Navier-Stokes equations is also given at the end of the chapter.

3.1 Finite Element Method in Time

It is already stated in Chapter 1 that, there are different solution approaches (finite difference, least squares, Runge-Kutta methods, etc.) for the transient field problems. In this study, transient field problems containing convection-diffusion terms are solved by using FEM in both space and time directions with a separation of variables idea. Thus, the temporal and space derivatives can be expressed independently in terms of the derivatives of corresponding shape functions which may be taken equal order since the SUPG stabilization is performed. In this way, we take into account the deformation due to the convection terms (spatial domain) and also protect the computations against numerical oscillations in the time domain. The resulting discretized equations are solved iteratively in the time domain without the need of very small time increments.

3.1.1 Diffusion equation

We consider first the time dependent linear diffusion equation in an open, bounded and polyhedral domain $\Omega \subset R^2$ with given initial and boundary conditions

$$\begin{cases} \frac{\partial u}{\partial t} - \epsilon \nabla^2 u = f, & \text{in } \Omega \times [0, T] \\ u(\mathbf{x}, 0) = u_0 & \text{at } t = 0 \\ u(\mathbf{x}, t) = \bar{u}(\mathbf{x}, t) & \text{on } \partial\Omega \end{cases} \quad (3.1)$$

where $u = u(\mathbf{x}, t)$ is the solution and f is a given source term, u_0, \bar{u} are given functions and ϵ is the diffusivity coefficient, $\partial\Omega$ is the boundary of Ω and $[0, T]$ is the time interval of analysis.

In order to use finite element method both in space and time domains we introduce the space

$$V = V_1 \times Q_1$$

for the transient problem where $V_1 = L^2(0, T; H_0^1(\Omega))$ and $Q_1 = L^2(0, T; Q)$. $H_0^1(\Omega)$ is the subspace of $H^1(\Omega)$ of functions with zero trace on $\partial\Omega$, $H^1(\Omega)$ being the Sobolev space of functions whose first derivatives belong to $L^2(\Omega)$ where L^2 is the space of scalar product (\cdot, \cdot) on the square integrable functions and $Q = \{q \in L^2(\Omega) \mid \int_{\Omega} q = 0\}$. Let $V_h = V_1^h \times Q_1^h$ be the discretized space with linear or bilinear finite elements for V_1 and linear elements for Q_1 .

If the solution u of diffusion equation is defined as $u = u(x, y, t)$, then it can be approximated by u_h ($u_h \in V_1^h$) as

$$u \approx u_h = \sum_{k=1}^2 \sum_{i=1}^{ndof} \phi_i(x, y) \tau_k(t) u_{ik} \quad (3.2)$$

where ϕ_i 's are the linear or bilinear shape functions in the space domain, τ_k 's are the linear shape functions in the time direction and $ndof$ is the degree of freedom for a space element.

The time interval $[0, T]$ is partitioned into subintervals $I_s = [t_s, t_{s+1}]$ where t_s and t_{s+1} are selected from the set $0 = t_0 < t_1 < \dots < t_S = T$ and S is the number of subintervals in the time direction. Linear shape functions in the time direction can be defined on an interval $[t_s, t_{s+1}]$ with the following property

$$\tau_1 = \begin{cases} 1 & \text{at } t_s \\ 0 & \text{at } t_{s+1} \end{cases} \quad \tau_2 = \begin{cases} 0 & \text{at } t_s \\ 1 & \text{at } t_{s+1} \end{cases} .$$

Thus, τ_1 and τ_2 can be selected as $\tau_1 = \frac{t - t_{s+1}}{t_s - t_{s+1}}$ and $\tau_2 = \frac{t - t_s}{t_{s+1} - t_s}$.

The weak form of problem (3.1) consists of finding $u \in V_1$ such that [58]

$$\int_{t_s}^{t_{s+1}} \int_{\Omega} [iuv + \epsilon(\nabla u \cdot \nabla v)] \, d\mathbf{x}dt = \int_{t_s}^{t_{s+1}} \int_{\Omega} f v \, d\mathbf{x}dt \quad (3.3)$$

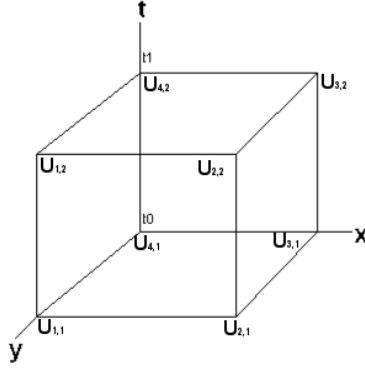


Figure 3.1: A sample bilinear-linear element in the spatial-time domain

for all $v \in H_0^1(\Omega)$ and satisfying the initial condition in a weak sense. f is assumed to be square integrable. The superimposed 'dot' implies the time derivative.

Let Ω_h denote a finite element partition of the domain Ω and construct finite element spaces $V^h = V_1^h \times Q_1^h$ as subspaces of V , V_1 and Q_1 , respectively. Then the discrete version of problem (3.1) can be defined as: Find finite element approximation $u_h \in V_1^h$ such that

$$\int_{t_s}^{t_{s+1}} \int_{\Omega_h} [\dot{u}_h v_h + \epsilon(\nabla u_h \cdot \nabla v_h)] \, d\mathbf{x} dt = \int_{t_s}^{t_{s+1}} \int_{\Omega_h} f v_h \, d\mathbf{x} dt \quad (3.4)$$

for all $v^h \in V_1^h$. \dot{u}_h corresponds to the discrete values of the derivative of u with respect to time and ∇u_h is the gradient of u_h . Equation (3.4) is written in a discrete form as

$$\int_{t_s}^{t_{s+1}} \left[\left(\frac{\partial \tau_1}{\partial t} \mathbf{M} + \epsilon \mathbf{K} \tau_1 \right) \tau_1 \mathbf{U}_s + \left(\frac{\partial \tau_2}{\partial t} \mathbf{M} + \epsilon \mathbf{K} \tau_2 \right) \tau_1 \mathbf{U}_{s+1} \right] dt = \int_{t_s}^{t_{s+1}} \tau_1 \mathbf{F} dt \quad (3.5)$$

$$\int_{t_s}^{t_{s+1}} \left[\left(\frac{\partial \tau_1}{\partial t} \mathbf{M} + \epsilon \mathbf{K} \tau_1 \right) \tau_2 \mathbf{U}_s + \left(\frac{\partial \tau_2}{\partial t} \mathbf{M} + \epsilon \mathbf{K} \tau_2 \right) \tau_2 \mathbf{U}_{s+1} \right] dt = \int_{t_s}^{t_{s+1}} \tau_2 \mathbf{F} dt \quad (3.6)$$

where the matrices \mathbf{M} and \mathbf{K} are the mass and stiffness matrices given by entrywise

$$M_{ij} = \int_{\Omega_h} \phi_i \phi_j \, d\mathbf{x} \quad (3.7)$$

$$K_{ij} = \int_{\Omega_h} (\nabla \phi_i \cdot \nabla \phi_j) \, d\mathbf{x} \quad (3.8)$$

and F_j 's are the force vectors

$$F_j = \int_{\Omega_h} f \phi_j \, d\mathbf{x}. \quad (3.9)$$

Thus, the system (3.5)-(3.6) can be solved iteratively for \mathbf{U}_{s+1} values with $\mathbf{U}_{s+1} = u_h(x, y, t_{s+1})$ by using the previously known $\mathbf{U}_s = u_h(x, y, t_s)$ values.

3.1.2 Convection-diffusion equation

The unsteady linear convection-diffusion problem with initial and Dirichlet boundary conditions is written as

$$\begin{cases} \frac{\partial u}{\partial t} - \epsilon \nabla^2 u + \mathbf{a} \cdot \nabla u = f, & \text{in } \Omega \times [0, T] \\ u(\mathbf{x}, 0) = u_0 & \text{at } t = 0 \\ u(\mathbf{x}, t) = \bar{u}(\mathbf{x}, t) & \text{on } \partial\Omega \end{cases} \quad (3.10)$$

where $\mathbf{a} \cdot \nabla u = a(x, y) \frac{\partial u}{\partial x} + b(x, y) \frac{\partial u}{\partial y}$ and $a(x, y)$, $b(x, y)$, $u_0(\mathbf{x})$, $\bar{u}(\mathbf{x}, t)$ are given functions. Thus, the standard Galerkin finite element formulation reads [58]; find $u_h \in V_1^h$ such that

$$\int_{t_s}^{t_{s+1}} \int_{\Omega_h} [u_h v_h + \epsilon(\nabla u_h \cdot \nabla v_h) + (\mathbf{a} \cdot \nabla u_h) v_h] \, d\mathbf{x} dt = \int_{t_s}^{t_{s+1}} \int_{\Omega_h} f v_h \, d\mathbf{x} dt, \quad \forall v_h \in V_1^h. \quad (3.11)$$

For convection dominated flows, one of the stabilized finite element method must be used in the spatial domain in order to obtain stable solutions.

Stabilized form of the unsteady convection-diffusion equation can be similarly written as in [31]

$$\int_{t_s}^{t_{s+1}} a(u_h, v_h) dt + \int_{t_s}^{t_{s+1}} \sum_K \tau_K \int_{\Omega_h} [u_h + (\mathbf{a} \cdot \nabla u_h) - f] [\mathbf{a} \cdot \nabla v_h] \, d\mathbf{x} dt + \int_{t_s}^{t_{s+1}} \int_{\Omega_h} f v_h \, d\mathbf{x} dt \quad (3.12)$$

where $a(u_h, v_h)$ is the bilinear operator given by

$$a(u_h, v_h) = \int_{\Omega_h} [u_h v_h + \epsilon(\nabla u_h \cdot \nabla v_h) + (\mathbf{a} \cdot \nabla u_h) v_h] \, d\mathbf{x}$$

and τ_K is the stabilization parameter given in (2.18).

3.1.3 Unsteady Navier-Stokes equations

The transient flow of an incompressible, viscous fluid is given in terms of the velocity \mathbf{u} and the pressure p as

$$\begin{cases} \frac{\partial \mathbf{u}}{\partial t} + \mathbf{u} \cdot \nabla \mathbf{u} - \epsilon \nabla^2 \mathbf{u} + \nabla p = \mathbf{f} & \text{in } [0, T] \times \Omega \\ \nabla \cdot \mathbf{u} = 0 & \text{in } [0, T] \times \Omega \\ \mathbf{u} = \mathbf{g} & \text{on } [0, T] \times \partial\Omega \\ \mathbf{u}(0, \mathbf{x}) = \mathbf{u}_0 & \text{in } \Omega \\ \int_{\Omega} p \, d\mathbf{x} = 0 & \text{in } [0, T] \times \Omega \end{cases} \quad (3.13)$$

where \mathbf{u}_0 is the initial velocity, \mathbf{f} represents the body force, \mathbf{g} is the given Dirichlet boundary condition, $[0, T]$ is a given time interval and $\Omega \subset R^2$ is the domain where the problem is defined.

The standard Galerkin finite element method in discrete form can be obtained for one time interval $[t_s, t_{s+1}]$ by employing the function space $V_h = V_1^h \times Q_1^h$ for both test and trial spaces with $\mathbf{u}_h \in V_1^h$, $p_h \in Q_1^h$ as

$$B(\mathbf{u}_h; \mathbf{u}_h, p_h; \mathbf{v}_h, q_h) = \int_{t_s}^{t_{s+1}} \int_{\Omega_h} (\mathbf{f} \cdot \mathbf{v}_h) \, d\mathbf{x}dt \quad \forall \mathbf{v}_h \in V_1^h, q_h \in Q_1^h, \quad (3.14)$$

where

$$B(\mathbf{u}_h; \mathbf{u}_h, p_h; \mathbf{v}_h, q_h) =$$

$$\int_{t_s}^{t_{s+1}} \int_{\Omega_h} [(\hat{\mathbf{u}}_h \cdot \mathbf{v}_h) + ((\mathbf{u}_h \cdot \nabla \mathbf{u}_h) \cdot \mathbf{v}_h) + \epsilon(\nabla \mathbf{u}_h \cdot \nabla \mathbf{v}_h) - \nabla \mathbf{v}_h p_h + (\nabla \cdot \mathbf{u}_h) q_h] \, d\mathbf{x}dt$$

for all $v_h \in V_1^h$ and $q_h \in Q_1^h$.

The problem (3.14) is nonlinear due to the presence of the convection terms which will be resolved by employing an iteration process: Let us decompose the approximate solutions \mathbf{u}_h and p_h as

$$\mathbf{u}_h^{s+1} = \mathbf{u}_h^s + \hat{\mathbf{u}}_h \quad (3.15)$$

$$p_h^{s+1} = p_h^s + \hat{p}_h \quad (3.16)$$

where \mathbf{u}_h^{s+1} and p_h^{s+1} are the approximations at the current iteration step, \mathbf{u}_h^s and p_h^s are the approximations at the previous iteration step and $\hat{\mathbf{u}}_h$ and \hat{p}_h are the corrections to the approximations at the previous iteration step. Therefore, the nonlinear convection term is replaced by

$$\mathbf{u}_h^{s+1} \cdot \nabla \mathbf{u}_h^{s+1} \approx \mathbf{u}_h^s \cdot \nabla \hat{\mathbf{u}}_h + \hat{\mathbf{u}}_h \cdot \nabla \mathbf{u}_h^s + \mathbf{u}_h^s \nabla \mathbf{u}_h^s.$$

Similar to the formulation of the linear diffusion equation, the unknowns are approximated as

$$\mathbf{u} \approx \mathbf{u}_h = \sum_{i=1}^{ndof} \phi_i(x, y) \tau_1(t) \mathbf{u}_{i,s} + \sum_{i=1}^{ndof} \phi_i(x, y) \tau_2(t) \mathbf{u}_{i,(s+1)}, \quad (3.17)$$

$$p \approx p_h = \sum_{i=1}^{ndof} \phi_i(x, y) \tau_1(t) p_{i,s} + \sum_{i=1}^{ndof} \phi_i(x, y) \tau_2(t) p_{i,(s+1)} \quad (3.18)$$

where $\mathbf{u}_{i,s} = \mathbf{u}_h(x_i, y_i, t_s)$ and $\mathbf{u}_{i,(s+1)} = \mathbf{u}_h(x_i, y_i, t_{s+1})$, $p_{i,s} = p_h(x_i, y_i, t_s)$ and $p_{i,(s+1)} = p_h(x_i, y_i, t_{s+1})$ and $ndof$ is the number of degrees of freedom in the space direction.

Substituting (3.17), (3.18) in (3.15), (3.16) and rewriting the equation (3.14) with the new approximations give the following representative equations in terms of shape functions

$$S(\phi_i, \tau_1; \phi_j, \tau_1) \begin{Bmatrix} \mathbf{U}_s \\ P_s \end{Bmatrix} + S(\phi_i, \tau_2; \phi_j, \tau_2) \begin{Bmatrix} \mathbf{U}_{s+1} \\ P_{s+1} \end{Bmatrix} = \int_{t_s}^{t_{s+1}} \int_{\Omega} (\mathbf{f} \cdot \phi_j \tau_1) \, d\mathbf{x}dt \quad (3.19)$$

$$S(\phi_i, \tau_1; \phi_j, \tau_2) \begin{Bmatrix} \mathbf{U}_s \\ P_s \end{Bmatrix} + S(\phi_i, \tau_2; \phi_j, \tau_2) \begin{Bmatrix} \mathbf{U}_{s+1} \\ P_{s+1} \end{Bmatrix} = \int_{t_s}^{t_{s+1}} \int_{\Omega} (\mathbf{f} \cdot \phi_j \tau_2) \, d\mathbf{x}dt \quad (3.20)$$

with

$$S(\phi_i, \tau_k; \phi_j, \tau_l) = \int_{t_s}^{t_{s+1}} \int_{\Omega_h} \left[\phi_i \phi_j \frac{\partial \tau_k}{\partial t} \tau_l + \{ \nabla \phi_i \phi_j + \epsilon (\nabla \phi_i \cdot \nabla \phi_j) - \nabla \phi_j \phi_i + \nabla \phi_i \phi_j \} \tau_k \tau_l \right] d\mathbf{x} dt$$

where $i, j = 1 \dots ndof$, ϕ_i 's are the shape functions for the approximation of unknowns and ϕ_j 's are the shape functions for the approximation of test functions.

Since $\left\{ \begin{array}{c} \mathbf{U}_s \\ P_s \end{array} \right\}$ values are known previously, the unknown values $\left\{ \begin{array}{c} \mathbf{U}_{s+1} \\ P_{s+1} \end{array} \right\}$ can be obtained iteratively from the solution of the system equation (3.19)-(3.20).

Selection of the finite element spaces V_h and Q_h has some restrictions for obtaining stable solutions. Either inf-sup or Babuska-Brezzi condition should be satisfied or one of the stabilized methods (SUPG, GLS, etc.) should be used in the space dimension. We use SUPG method for the stabilization.

SUPG formulation of the unsteady Navier-Stokes equations can be obtained from [24] as; Find $\{\mathbf{u}_h, p_h\}$ in $V_h \times P_1$ such that

$$\begin{aligned} & B(\mathbf{u}_h; \mathbf{u}_h, p_h; \mathbf{v}_h, q_h) + \\ & \int_{t_s}^{t_{s+1}} \sum_K \tau_K \int_{\Omega_K} ((\dot{\mathbf{u}}_h + \mathbf{u}_h \cdot \nabla \mathbf{u}_h + \nabla p_h - \mathbf{f}) \cdot (\mathbf{u}_h \cdot \nabla \mathbf{v}_h + \nabla q_h)) d\mathbf{x} dt \quad (3.21) \\ & = \int_{t_s}^{t_{s+1}} \int_{\Omega} (\mathbf{f} \cdot \mathbf{v}_h) d\mathbf{x} dt, \quad \forall \{\mathbf{v}_h, q_h\} \in V_1 \times P_1 \end{aligned}$$

with the stabilization parameter τ_K given in (2.20).

3.2 Finite Difference Method in Time

In this section, approximation of the time derivative term by using the finite difference method (FDM) in the unsteady flow problems is presented for the convection-diffusion and Navier-Stokes equations.

3.2.1 Convection-diffusion equation

The unsteady linear convection-diffusion equation with initial and Dirichlet boundary conditions is already given in (3.10) as

$$\begin{cases} \frac{\partial u}{\partial t} - \epsilon \nabla^2 u + \mathbf{a} \cdot \nabla u = f, & \text{in } \Omega \times [0, T] \\ u(\mathbf{x}, 0) = u_0 & \text{at } t = 0 \\ u(\mathbf{x}, t) = \bar{u}(\mathbf{x}, t) & \text{on } \partial\Omega. \end{cases} \quad (3.22)$$

We approximate the time derivative terms by using the finite difference method (FDM) as [58]

$$u^{s+1} - u^s = \Delta t [\alpha \dot{u}^{s+1} + (1 - \alpha) \dot{u}^s] \quad (3.23)$$

where $\dot{u} = \frac{\partial u}{\partial t}$, α is the relaxation parameter with $\alpha \in [0, 1]$ and $\Delta t = t_{s+1} - t_s$, the length of the time interval in a typical slab $[t_s, t_{s+1}] \times \Omega$. For special values of α , the method turns into one of the following well-known time-stepping procedures:

- $\alpha = 1$: Implicit type
- $\alpha = \frac{1}{2}$: Crank-Nicolson type
- $\alpha = 0$: Explicit type .

Stabilized form of the unsteady convection-diffusion equation is written as; Find $u_1^{s+1} \in V_1$ such that

$$\begin{aligned} & (u_1^{s+1}, v_1) + \Delta t \alpha [(\mathbf{a} \cdot \nabla u_1^{s+1}, v_1) + \epsilon (\nabla u_1^{s+1}, \nabla v_1) - (f, v_1)] \\ & + \Delta t \alpha \left[\sum_{K \in T_h} \tau_K \int_K [\dot{u}_1^{s+1} + \mathbf{a} \cdot \nabla u_1^{s+1} - f] [\mathbf{a} \cdot \nabla v_1] d\mathbf{x} \right] \\ & - (u_1^s, v_1) + \Delta t (1 - \alpha) [(\mathbf{a} \cdot \nabla u_1^s, v_1) + \epsilon (\nabla u_1^s, \nabla v_1) - (f, v_1)] \\ & + \Delta t (1 - \alpha) \left[\sum_{K \in T_h} \tau_K \int_K [\dot{u}_1^s + \mathbf{a} \cdot \nabla u_1^s - f] [\mathbf{a} \cdot \nabla v_1] d\mathbf{x} \right] = 0, \quad \forall v_1 \in V_1 \end{aligned} \quad (3.24)$$

where τ_K is the previously introduced stabilization parameter given in (2.18) and the values u_1^s are known from the previous time step.

3.2.2 Unsteady Navier-Stokes equation

The time dependent Navier-Stokes equations which are given in (3.13) together with initial and boundary conditions are written as

$$\begin{cases} \frac{\partial \mathbf{u}}{\partial t} + \mathbf{u} \cdot \nabla \mathbf{u} - \epsilon \nabla^2 \mathbf{u} + \nabla p = \mathbf{f} & \text{in } \Omega \times (0, T) \\ \nabla \cdot \mathbf{u} = 0 & \text{in } \Omega \times (0, T) \\ \mathbf{u} = \mathbf{g} & \text{on } \partial\Omega \times (0, T) \\ \mathbf{u}(0, \mathbf{x}) = \mathbf{u}_0 & \text{in } \Omega \\ \int_{\Omega} p \, d\mathbf{x} = 0 & \text{in } \Omega \times (0, T) \end{cases} \quad (3.25)$$

where \mathbf{u} is the velocity, \mathbf{u}_0 is the initial velocity, p is the pressure, \mathbf{f} represents the body force, and \mathbf{g} is a given function defined on the boundary.

The spatial discretization of the weak form of (3.25) leads to the following equation: Find $\{\mathbf{u}_h, p_1\}$ in $V_h \times P_1$ such that

$$B(\mathbf{u}_h; \mathbf{u}_h, p_1; \mathbf{v}_h, q_1) = (\mathbf{f}, \mathbf{v}_h) \quad \forall \{\mathbf{v}_h, q_1\} \in V_h \times P_1, \quad (3.26)$$

where

$$\begin{aligned} B(\mathbf{u}_h; \mathbf{u}_h, p_1; \mathbf{v}_h, q_1) &= (\dot{\mathbf{u}}_h, \mathbf{v}_h) + (\mathbf{u}_h \cdot \nabla \mathbf{u}_h, \mathbf{v}_h) + \epsilon (\nabla \mathbf{u}_h, \nabla \mathbf{v}_h) \\ &\quad - (\nabla \mathbf{v}_h, p_1) + (\nabla \cdot \mathbf{u}_h, q_1). \end{aligned}$$

If the velocity field \mathbf{u}_h is decomposed to the linear and bubble parts as

$$\mathbf{u}_h(\mathbf{x}, t) = \mathbf{u}_1(\mathbf{x}, t) + \mathbf{u}_b(\mathbf{x}) \quad (3.27)$$

in which we assume the bubble part depends on space variables only, then the RFB method applied to the time-dependent problem leaves behind a stabilized finite element formulation of the SUPG type. With a temporal discretization of type (3.23), it reads: Find $\{\mathbf{u}_1^{s+1}, p_1^{s+1}\} \in V_1 \times P_1$ such that

$$\begin{aligned} &(\mathbf{u}_1^{s+1}, \mathbf{v}_1) + \Delta t \alpha \left[(\mathbf{u}_1^{s+1} \cdot \nabla \mathbf{u}_1^{s+1}, \mathbf{v}_h) + \epsilon (\nabla \mathbf{u}_1^{s+1}, \nabla \mathbf{v}_1) - (\nabla \mathbf{v}_1, p_1^{s+1}) - (\mathbf{f}, \mathbf{v}_1) \right] \\ &+ \Delta t \alpha \left[\sum_{K \in T_h} \tau_K \int_K ([\dot{\mathbf{u}}_1^{s+1} + \mathbf{u}_1^{s+1} \cdot \nabla \mathbf{u}_1^{s+1} + \nabla p_1^{s+1} - \mathbf{f}] \cdot [\mathbf{u}_1^{s+1} \cdot \nabla \mathbf{v}_1 - \nabla q_1]) \, d\mathbf{x} \right] \\ &- (\mathbf{u}_1^s, \mathbf{v}_1) + \Delta t (1 - \alpha) \left[(\mathbf{u}_1^s \cdot \nabla \mathbf{u}_1^s, \mathbf{v}_1) + \epsilon (\nabla \mathbf{u}_1^s, \nabla \mathbf{v}_1) - (\nabla \mathbf{v}_1, p_1^s) - (\mathbf{f}, \mathbf{v}_1) \right] \\ &+ \Delta t (1 - \alpha) \left[\sum_{K \in T_h} \tau_K \int_K ([\dot{\mathbf{u}}_1^s + \mathbf{u}_1^s \cdot \nabla \mathbf{u}_1^s + \nabla p_1^s - \mathbf{f}] \cdot [\mathbf{u}_1^s \cdot \nabla \mathbf{v}_1 - \nabla q_1]) \, d\mathbf{x} \right] \\ &- \alpha (\nabla \cdot \mathbf{u}_1^{s+1}, q_1) - (1 - \alpha) (\nabla \cdot \mathbf{u}_1^s, q_1) = 0 \quad \forall \{\mathbf{v}_1, q_1\} \in V_1 \times P_1 \end{aligned} \quad (3.28)$$

where the values \mathbf{u}_1^s and p_1^s are known from the previous time step. The time-derivatives in mesh-dependent terms are approximated by backward and forward difference operators, accordingly. The non-linearity in the equation can be eliminated by a similar argument described in previous chapter.

3.3 Numerical Results

The performance of the numerical procedure proposed above which is the stabilized FEM in space - FEM in time domain is tested with four problems. The comparisons are held with the solutions obtained by using FDM time integration scheme.

3.3.1 Diffusion equation

Transient diffusion in a domain $\Omega = [0, 1] \times [0, 1]$ with constant material properties and unit diffusivity is governed by the parabolic equation [15],

$$\frac{\partial u}{\partial t} = \nabla^2 u \quad \text{in} \quad (x, y) \in \Omega \quad \text{and} \quad t \in [0, T] \quad (3.29)$$

with initial condition

$$u(x, y, 0) = \sin(\pi x) \sin(2\pi y)$$

and boundary conditions

$$u = 0 \quad \text{on} \quad \partial\Omega \times [0, T].$$

The exact solution is given as

$$u_{exact} = e^{-5\pi^2 t} \sin(\pi x) \sin(2\pi y).$$

The discretization for both the space and the time directions by using linear finite elements is obtained with the increments $\Delta x = \Delta y = 0.0625$ and time step $\Delta t = 0.01$. We have used linear finite elements with three nodes at the vertices in space domain. The problem is also solved using the same discretization by using the finite difference method for approximating the time derivative term.

From Figure (3.2), it is seen that, even using rough mesh in the spatial domain and large time increments in the time direction, the numerical results obtained by FEM and FDM agree well with the exact solution at $t = 0.05$. This shows the accuracy of the proposed methods. In this problem there was no need for the stabilization of the FEM in space domain since there is no convection term.

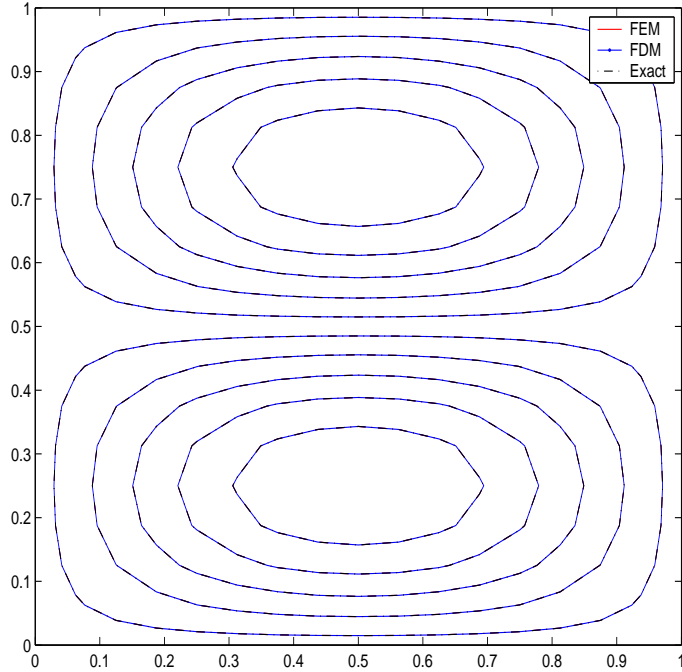


Figure 3.2: FEM, FDM and exact solutions of diffusion problem at $t = 0.05$

3.3.2 Convection-diffusion equation

Consider the rotating cylinder problem [35], which is governed by unsteady convection-diffusion equation in $\Omega = [0, 1] \times [0, 1]$ with $\epsilon = 10^{-5}$, $a = -2\pi(2y-1, 1-2x)$, $f = 0$, homogeneous boundary condition $\bar{u}(\mathbf{x}, t) = 0$ and initial condition

$$u(x, y, 0) = \begin{cases} 1 & \text{for } r \leq 1/4 \\ 0 & \text{otherwise} \end{cases}$$

where $r = \sqrt{(2x - 1/2)^2 + (2y - 1)^2}$.

Numerical calculations are performed on 80×80 grid in space discretization with 6400 rectangular elements and the time step $\Delta t = 0.01$. Since the flow is convection dominated, SUPG stabilized finite element method is carried out through the calculations. As time increases, the unknown function rotates around a circle in a periodic way. This behavior is displayed at starting position ($t = 0.0$) and the time levels $t = 0.25$ and $t = 2.0$ in Figure (3.3)

3.3.3 Taylor vortex flow

The governing equations are the homogeneous unsteady Navier-Stokes equations defined in the domain $[-\pi, \pi] \times [-\pi, \pi]$ on the time interval $[0, T]$ [2],

$$\begin{aligned} \frac{\partial \mathbf{u}}{\partial t} + \mathbf{u} \cdot \nabla \mathbf{u} - \epsilon \nabla^2 \mathbf{u} + \nabla p &= 0 \\ \nabla \cdot \mathbf{u} &= 0 \end{aligned}$$

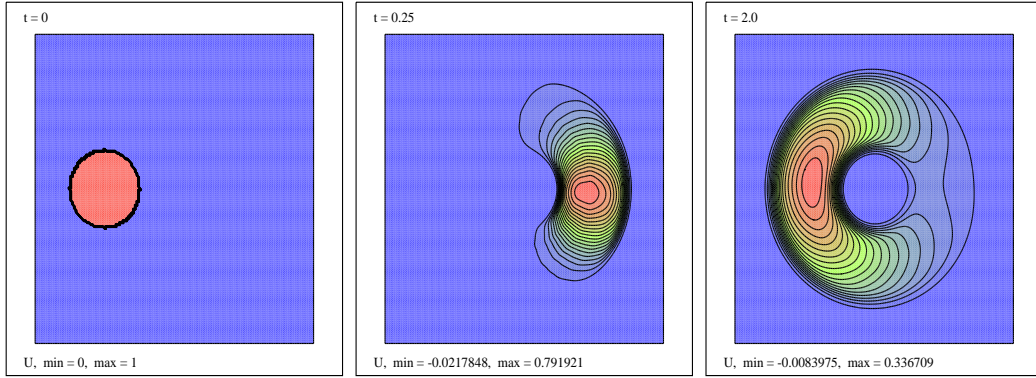


Figure 3.3: Solution of convection-diffusion problem at $t = 0, 0.25$ and $t = 2.0$

The exact solution is

$$\mathbf{u} = e^{-2t\epsilon} \begin{Bmatrix} -\cos x \sin y \\ \sin x \cos y \end{Bmatrix}, \quad p = -\frac{1}{4}e^{-4t\epsilon}(\cos 2x + \cos 2y). \quad (3.30)$$

Initial and boundary conditions are derived from the exact solution for u and v . We have used $\Delta t = 0.1$ as a time step and results obtained at $t = 1.0$ in terms of pressure-streamlines and the velocity contours are given in Figures (3.4) and (3.5).

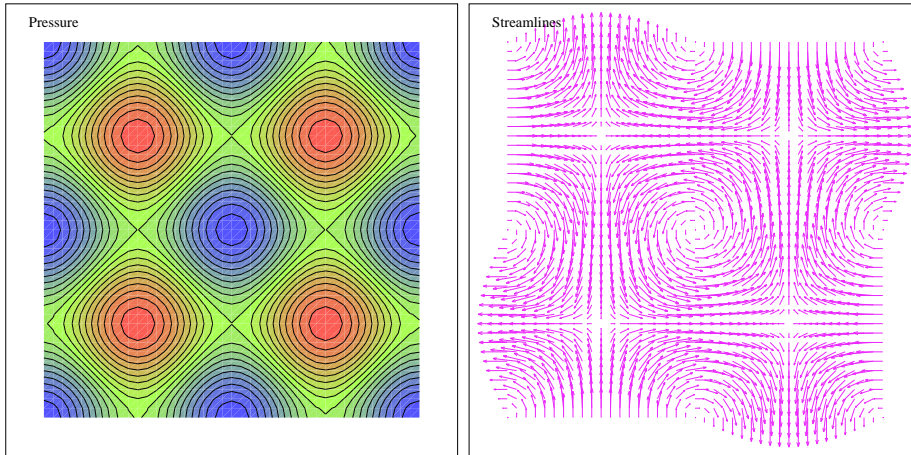


Figure 3.4: Pressure and Streamlines for Taylor vortex flow($t = 1.0$)

3.3.4 Flow around a cylinder

The problem of flow around a cylinder [41] is governed by the unsteady Navier-Stokes equations with $Re = 100$ and $\mathbf{f} = 0$. The problem is given with homogeneous initial condition, $\mathbf{u}(x, y, 0) = 0$, and boundary conditions at inflow ($x = 0$) and outflow ($x = 2.2$) boundaries are

$$\mathbf{u}(0, y, t) = \mathbf{u}(2.2, y, t) = 0.41^{-2} \sin(\pi t/8) \begin{Bmatrix} 6y(0.41 - y) \\ 0 \end{Bmatrix}, \quad 0 \leq y \leq 0.41. \quad (3.31)$$

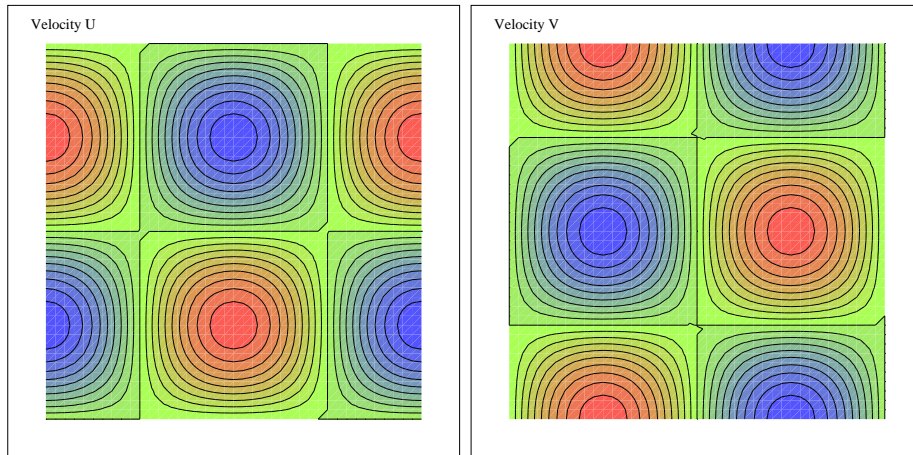


Figure 3.5: The velocity contours for Taylor vortex flow ($t = 1.0$)

No-slip boundary conditions are described at the other boundaries ($y = 0, 0.41$ and around the cylinder). It is seen from the given boundary conditions that the problem has periodic behaviour at $T = 8$. Therefore, problem is solved in the time domain for $t \in [0, 8]$ with a time step $\Delta t = 0.1$. In space dimension, the problem domain is discretized by 5404 triangular linear elements (Figure (3.6)). Pressure contours at the time levels $t = 1, 2, 4, 6, 8$ are displayed in Figure (3.7) and streamlines of the flow in Figure (3.8). Results show the development of the flow as time increases. Vortices start to develop behind the cylinder and around $t = 4.0$ and later, vortices start to separate from the cylinder. At the final time $t = 8.0$ the flow settles back to the original form.

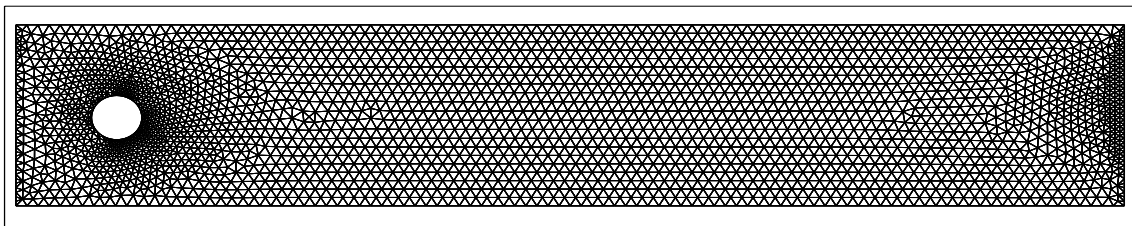


Figure 3.6: The problem mesh tested for flow around a cylinder: 5404 triangular elements

The same problem is also solved by using finite difference method for the time derivative term. Similar results are obtained and displayed for the pressure in Figure (3.9), velocity component u in Figure (3.10) and flow vectors in Figure (3.11) at $t = 1, 2, 4, 6$ and 8 , respectively.

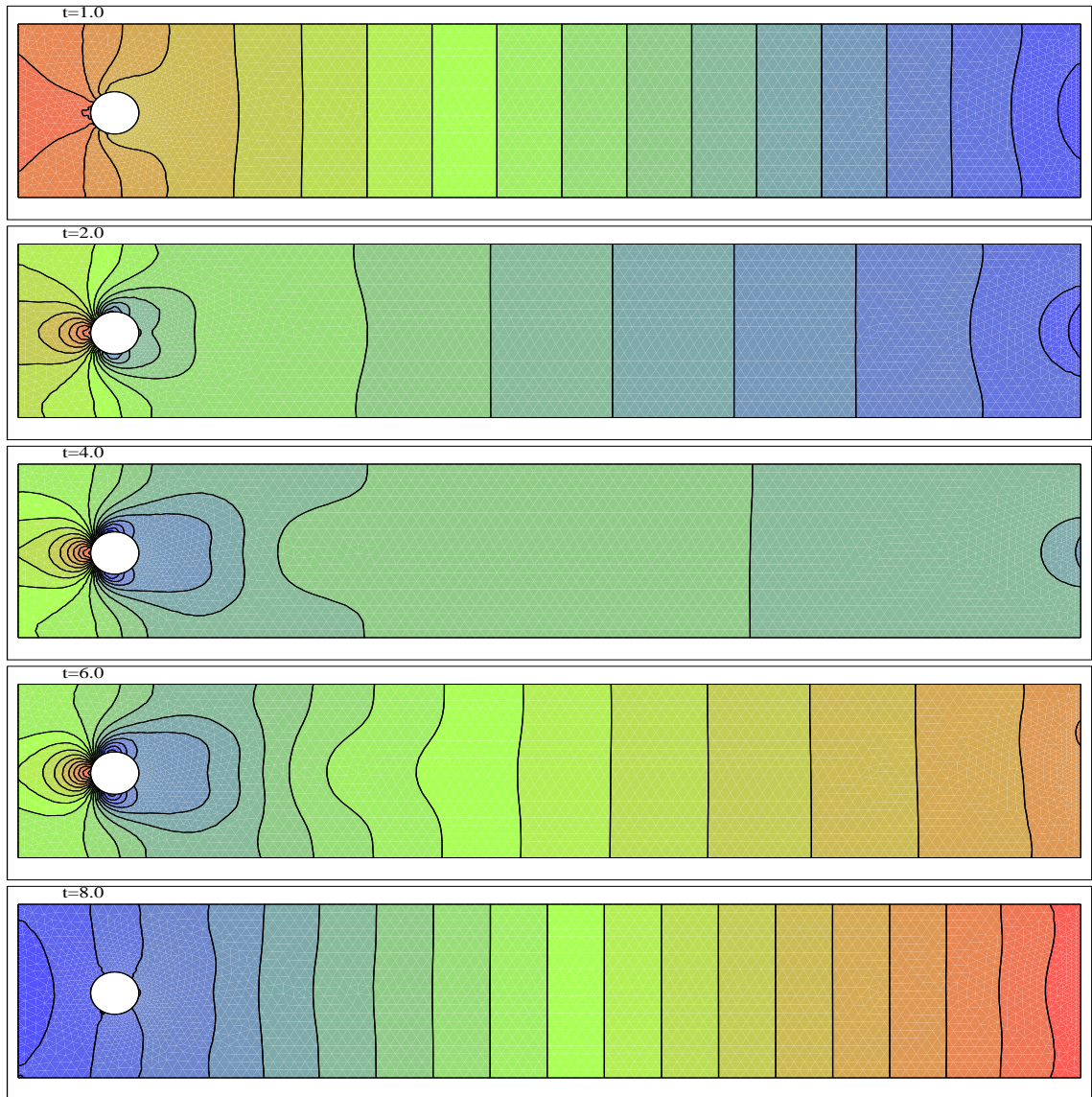


Figure 3.7: Pressure contours for flow around a cylinder

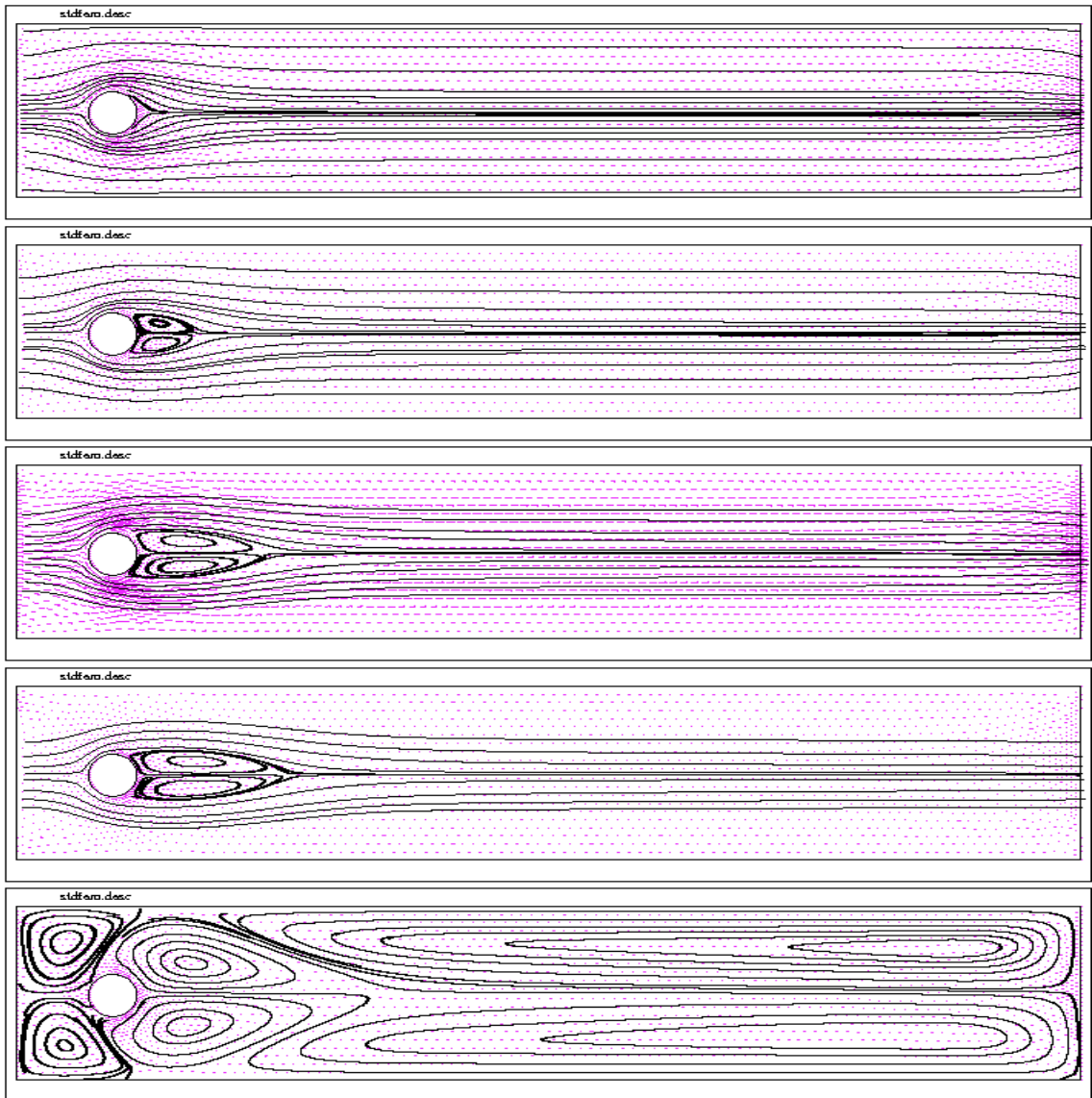


Figure 3.8: Streamlines for flow around a cylinder

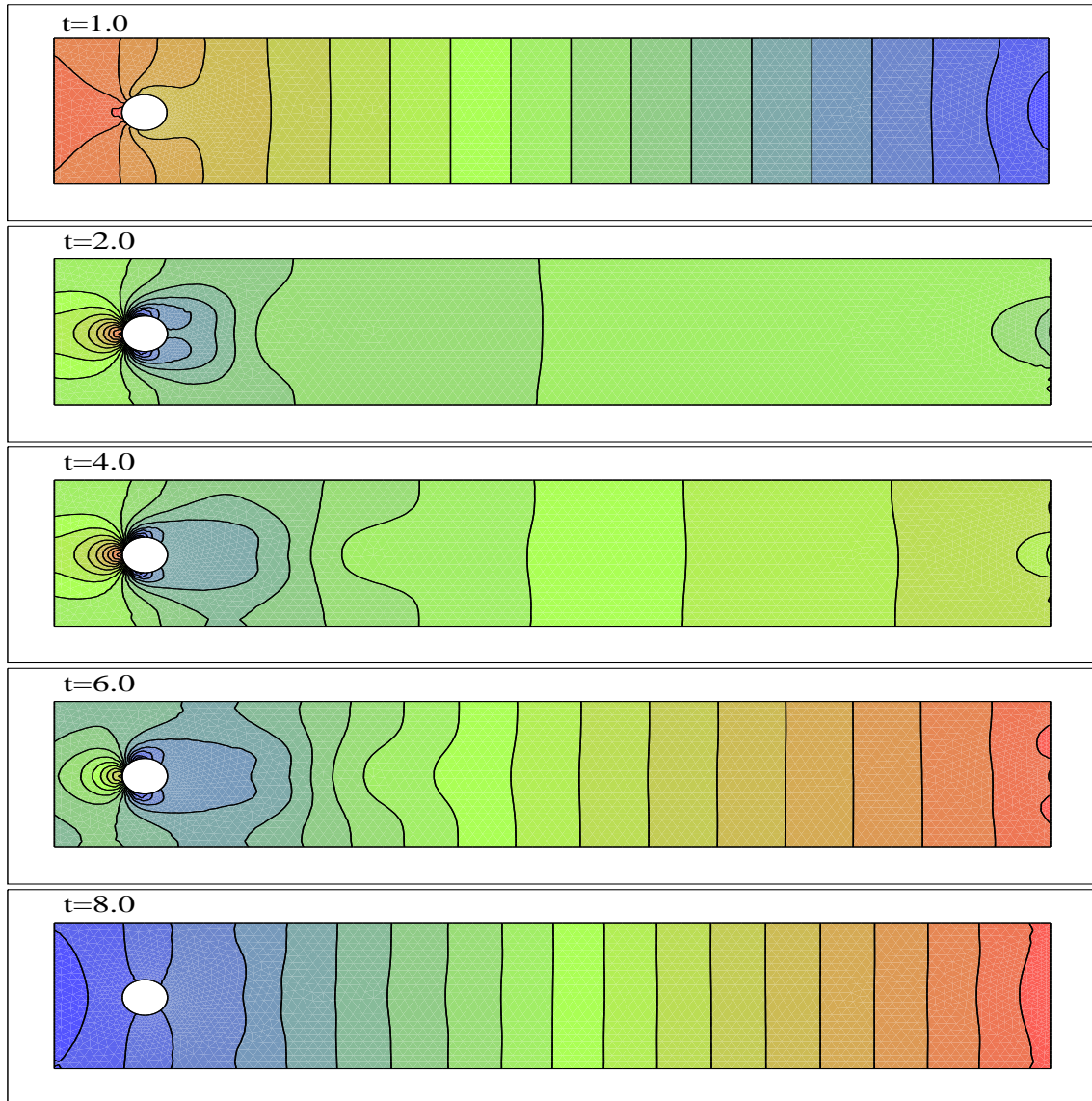


Figure 3.9: Pressure contours for unsteady flow around a cylinder using FDM in time at $t = 1, 2, 4, 6$ and 8

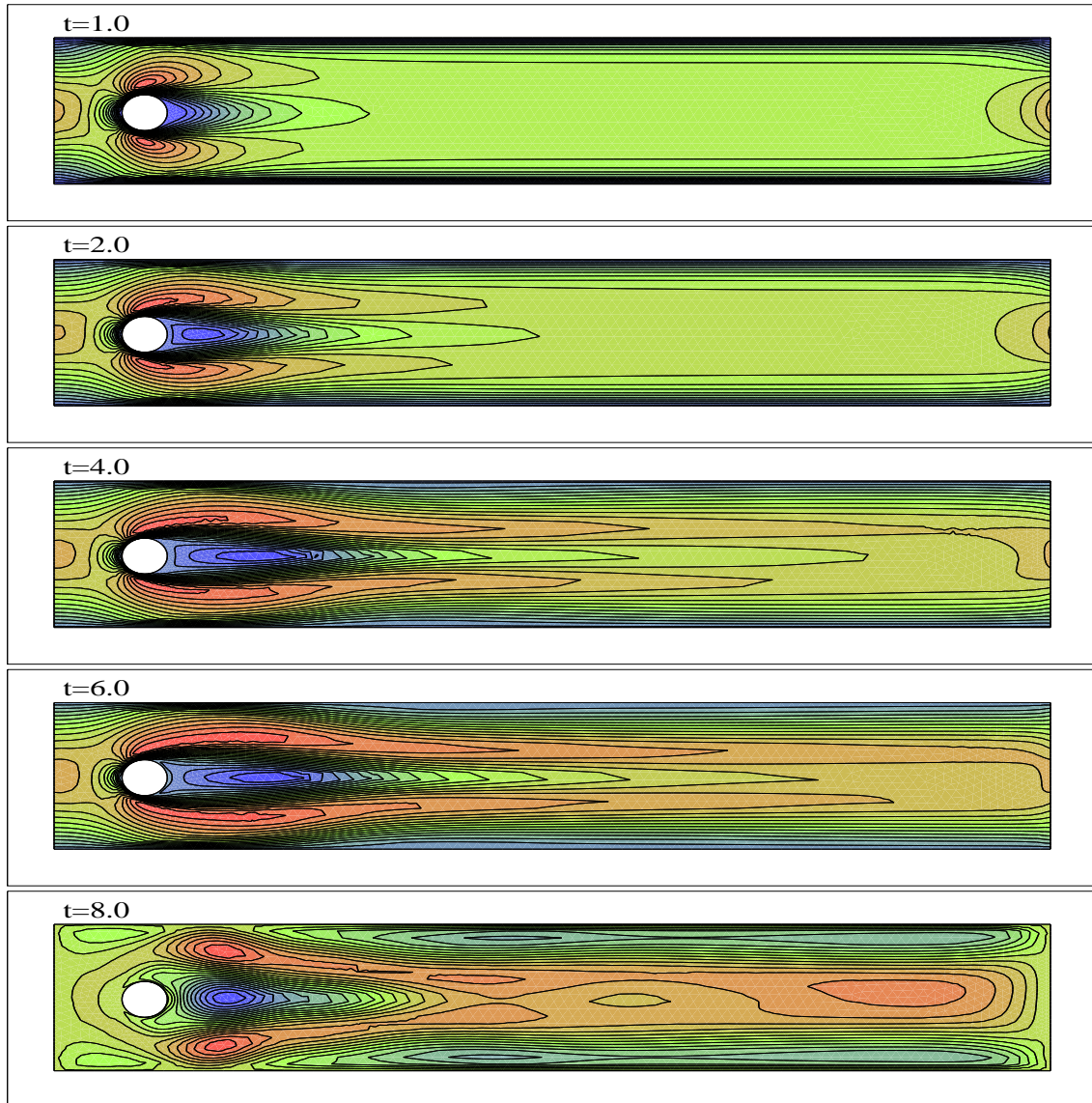


Figure 3.10: Velocity (u) component for unsteady flow around a cylinder using FDM in time at $t = 1, 2, 4, 6$ and 8

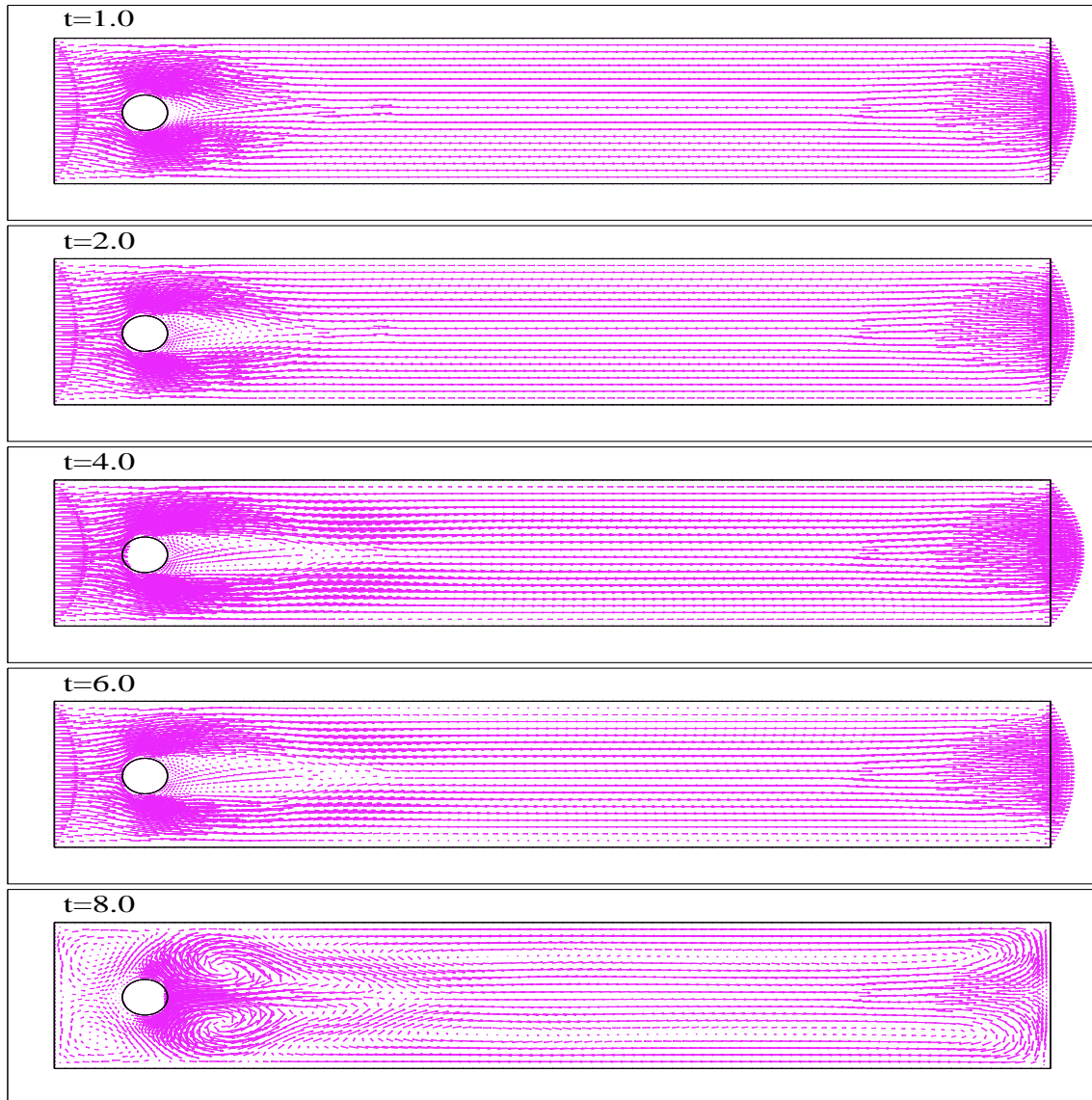


Figure 3.11: Flow vectors for unsteady flow around a cylinder using FDM in time at $t = 1, 2, 4, 6$ and 8

CHAPTER 4

SOLUTION OF THE MAGNETOHYDRODYNAMIC EQUATIONS

The two-dimensional (2-D) magnetohydrodynamic (MHD) equations are defined in terms of momentum equations (Navier-Stokes equations), Maxwell's equation with Ohm's Law and the continuity equation. In terms of the unknowns which are the velocity field \mathbf{u} , the pressure of the fluid p and the magnetic field \mathbf{B} , MHD equations are written as [31],

$$\left\{ \begin{array}{l} \rho \mathbf{u} \cdot \nabla \mathbf{u} - \mu \nabla^2 \mathbf{u} + \nabla p + \frac{1}{\mu_0} \mathbf{B} \times \text{curl } \mathbf{B} = \rho \mathbf{f} \\ \text{div } \mathbf{u} = 0 \\ \frac{1}{\mu_0 \sigma} \text{curl} (\text{curl } \mathbf{B}) - \text{curl} (\mathbf{u} \times \mathbf{B}) = 0 \\ \text{div } \mathbf{B} = 0 \end{array} \right. \quad (4.1)$$

where \mathbf{f} denotes the external force, ρ is the density of the fluid, μ is the dynamic viscosity, σ is the electrical conductivity and μ_0 is the magnetic permeability. In order to nondimensionalize the MHD equations, we introduce a characteristic value \mathbf{U}_0 for the velocity field, a characteristic value \mathbf{B}_0 for the magnetic field and a characteristic length L [31, 46, 68]. Then Re is the fluid Reynolds number, Rem is the magnetic Reynolds number, Ha is the Hartmann number and S is the Coupling number as

$$\begin{aligned} Re &= \frac{\rho \mathbf{U}_0 L}{\mu} \\ Rem &= \mu_0 \sigma \mathbf{U}_0 L \\ S &= \frac{\mathbf{B}_0^2}{\mu_0 \rho \mathbf{U}_0} \\ Ha &= \sqrt{Re Rem S}. \end{aligned}$$

Also, $\mathbf{u} = \tilde{\mathbf{u}}/\mathbf{U}_0$, $\mathbf{B} = \tilde{\mathbf{B}}/\mathbf{B}_0$, $p = \tilde{p}/\rho \mathbf{U}_0^2$ and $\mathbf{f} = \tilde{\mathbf{f}}L/\mathbf{U}_0^2$ are made use of for the physical quantities $\tilde{\mathbf{u}}$, $\tilde{\mathbf{B}}$, \tilde{p} and $\tilde{\mathbf{f}}$ in the nondimensionalizing [31, 68]. Then the MHD equations are expressed in non-dimensional form as;

$$\mathbf{u} \cdot \nabla \mathbf{u} - \frac{1}{Re} \nabla^2 \mathbf{u} + \nabla p - \frac{Ha^2}{Re \cdot Rem} (\nabla \times \mathbf{B}) \times \mathbf{B} = \mathbf{f} \quad (4.2)$$

$$\nabla \cdot \mathbf{u} = 0 \quad (4.3)$$

$$-\nabla \times (\mathbf{u} \times \mathbf{B}) + \frac{1}{Rem} \nabla \times (\nabla \times \mathbf{B}) = 0 \quad (4.4)$$

$$\nabla \cdot \mathbf{B} = 0. \quad (4.5)$$

In 2-D, if we define $\mathbf{u} = \begin{Bmatrix} u_1 \\ u_2 \end{Bmatrix}$, $\mathbf{B} = \begin{Bmatrix} B_1 \\ B_2 \end{Bmatrix}$ and $\mathbf{f} = \begin{Bmatrix} f_1 \\ f_2 \end{Bmatrix}$,

$$\nabla \times \mathbf{B} = \begin{vmatrix} i & j & k \\ \frac{\partial}{\partial x} & \frac{\partial}{\partial y} & 0 \\ B_1 & B_2 & 0 \end{vmatrix} = k \left(\frac{\partial B_2}{\partial x} - \frac{\partial B_1}{\partial y} \right), \quad \mathbf{u} \times \mathbf{B} = \begin{vmatrix} i & j & k \\ u_1 & u_2 & 0 \\ B_1 & B_2 & 0 \end{vmatrix} = k(u_1 B_2 - u_2 B_1)$$

then

$$(\nabla \times \mathbf{B}) \times \mathbf{B} = \begin{vmatrix} i & j & k \\ 0 & 0 & \frac{\partial B_2}{\partial x} - \frac{\partial B_1}{\partial y} \\ B_1 & B_2 & 0 \end{vmatrix} = i \left(B_2 \frac{\partial B_1}{\partial y} - B_2 \frac{\partial B_2}{\partial x} \right) + j \left(B_1 \frac{\partial B_2}{\partial x} - B_1 \frac{\partial B_1}{\partial y} \right)$$

and

$$-\nabla \times (\mathbf{u} \times \mathbf{B}) = - \begin{vmatrix} i & j & k \\ \frac{\partial}{\partial x} & \frac{\partial}{\partial y} & 0 \\ 0 & 0 & u_1 B_2 - u_2 B_1 \end{vmatrix} = i \left(-u_1 \frac{\partial B_2}{\partial y} + u_2 \frac{\partial B_1}{\partial y} - B_2 \frac{\partial u_1}{\partial y} + B_1 \frac{\partial u_2}{\partial y} \right) + j \left(u_1 \frac{\partial B_2}{\partial x} - u_2 \frac{\partial B_1}{\partial x} + B_2 \frac{\partial u_1}{\partial x} - B_1 \frac{\partial u_2}{\partial x} \right).$$

We will also make us of the following properties

$$\nabla \times (\nabla \times \mathbf{B}) = -\nabla^2 \mathbf{B} + \nabla(\nabla \cdot \mathbf{B})$$

$$\nabla \cdot \mathbf{B} = 0 \quad \Rightarrow \quad \frac{\partial B_1}{\partial x} = -\frac{\partial B_2}{\partial y}.$$

The 2-D MHD equations (4.2) - (4.5) are written in open form as

$$u_1 \frac{\partial u_1}{\partial x} + u_2 \frac{\partial u_1}{\partial y} - \frac{1}{Re} \left(\frac{\partial^2 u_1}{\partial x^2} + \frac{\partial^2 u_1}{\partial y^2} \right) + \frac{\partial p}{\partial x} - S B_2 \left(\frac{\partial B_1}{\partial y} - \frac{\partial B_2}{\partial x} \right) = f_1 \quad (4.6)$$

$$u_1 \frac{\partial u_2}{\partial x} + u_2 \frac{\partial u_2}{\partial y} - \frac{1}{Re} \left(\frac{\partial^2 u_2}{\partial x^2} + \frac{\partial^2 u_2}{\partial y^2} \right) + \frac{\partial p}{\partial y} + S B_1 \left(\frac{\partial B_1}{\partial y} - \frac{\partial B_2}{\partial x} \right) = f_2 \quad (4.7)$$

$$u_1 \frac{\partial B_1}{\partial x} + u_2 \frac{\partial B_1}{\partial y} + \frac{\partial u_2}{\partial y} B_1 - \frac{\partial u_1}{\partial y} B_2 - \frac{1}{Rem} \left(\frac{\partial^2 B_1}{\partial x^2} + \frac{\partial^2 B_1}{\partial y^2} \right) = 0 \quad (4.8)$$

$$u_1 \frac{\partial B_2}{\partial x} + u_2 \frac{\partial B_2}{\partial y} + \frac{\partial u_1}{\partial x} B_2 - \frac{\partial u_2}{\partial x} B_1 - \frac{1}{Rem} \left(\frac{\partial^2 B_2}{\partial x^2} + \frac{\partial^2 B_2}{\partial y^2} \right) = 0 \quad (4.9)$$

$$\frac{\partial u_1}{\partial x} + \frac{\partial u_2}{\partial y} = 0. \quad (4.10)$$

4.1 FEM formulation of the MHD equations

Consider the incompressible MHD problem (4.2)-(4.5) in the domain $\Omega \in \mathbb{R}^2$

$$\left\{ \begin{array}{l} \mathbf{u} \cdot \nabla \mathbf{u} - \frac{1}{Re} \nabla^2 \mathbf{u} + \nabla p - \frac{Ha^2}{Re \cdot Rem} (\nabla \times \mathbf{B}) \times \mathbf{B} = \mathbf{f} \\ -\nabla \times (\mathbf{u} \times \mathbf{B}) - \frac{1}{Rem} \nabla^2 \mathbf{B} = 0 \\ \nabla \cdot \mathbf{u} = 0 \end{array} \right. \quad (4.11)$$

with the given essential or natural boundary conditions. Then the weak formulation of the problem (4.11) can be stated as: Find $\mathbf{u} \in V = H_0^1(\Omega)^2$, $\mathbf{B} \in M = H^1(\Omega)^2$ and $p \in W = L_0^2(\Omega)$ such that

$$B(\mathbf{u}, \mathbf{B}, p; \mathbf{v}, \mathbf{C}, q) = L(\mathbf{f}), \quad \forall (\mathbf{v}, \mathbf{C}, q) \in (V, M, W) \quad (4.12)$$

where

$$\begin{aligned} B(\mathbf{u}, \mathbf{B}, p; \mathbf{v}, \mathbf{C}, q) &= (\mathbf{u} \cdot \nabla \mathbf{u}, \mathbf{v}) + \frac{1}{Re} (\nabla \mathbf{u}, \nabla \mathbf{v}) - (p, \nabla \mathbf{v}) - S((\nabla \times \mathbf{B}) \times \mathbf{B}, \mathbf{v}) \\ &\quad - (\nabla \times (\mathbf{u} \times \mathbf{B}), \mathbf{C}) + \frac{1}{Rem} (\nabla \mathbf{B}, \nabla \mathbf{C}) + (q, \nabla \cdot \mathbf{u}) \end{aligned}$$

and

$$L(\mathbf{f}) = (\mathbf{f}, \mathbf{v}).$$

To introduce a finite element application, we begin by partitioning the domain into elements (triangles or quadrangles) in a standard way (e.g. no overlapping, no vertex on the edge of a neighboring elements, etc.). And the following finite element spaces are defined over an element K as follows [31]:

$$X_h^k = \{v_h \in C^0(\bar{\Omega}), v_h|_K \in (P_k(K) \text{ or } Q_k(K)), \forall K \in \Omega_h\}$$

where, $P_k(K)$ and $Q_k(K)$ correspond to the spaces for triangular and rectangular elements, respectively. Then, for the velocity component \mathbf{u} ; $V_h = (X_h^k \cap H_0^1(\Omega))^2$, for the magnetic field \mathbf{B} ; $M_h = (X_h^l)^2 \cap H^1(\Omega)^2$ and for the pressure p ; $W_h = X_h^m \cap L_0^2(\Omega)$ finite element spaces are selected. Galerkin finite element variational formulation of the problem reads; find $(\mathbf{u}_h, \mathbf{B}_h, p_h) \in (V_h, M_h, W_h)$ such that

$$B(\mathbf{u}_h, \mathbf{B}_h, p_h; \mathbf{v}_h, \mathbf{C}_h, q_h) = L(\mathbf{f}), \quad \forall (\mathbf{v}_h, \mathbf{C}_h, q_h) \in (V_h, W_h, M_h) \quad (4.13)$$

where

$$\begin{aligned} B(\mathbf{u}_h, \mathbf{B}_h, p_h; \mathbf{v}_h, \mathbf{C}_h, q_h) &= (\mathbf{u}_h \cdot \nabla \mathbf{u}_h, \mathbf{v}_h) + \frac{1}{Re} (\nabla \mathbf{u}_h, \nabla \mathbf{v}_h) - (p_h, \nabla \mathbf{v}_h) - S((\nabla \times \mathbf{B}_h) \times \mathbf{B}_h, \mathbf{v}_h) \\ &\quad - (\nabla \times (\mathbf{u}_h \times \mathbf{B}_h), \mathbf{C}_h) + \frac{1}{Rem} (\nabla \mathbf{B}_h, \nabla \mathbf{C}_h) + (q_h, \nabla \cdot \mathbf{u}_h) \end{aligned}$$

and

$$L(\mathbf{f}) = (\mathbf{f}, \mathbf{v}_h).$$

We impose an iterative procedure as is done for the Navier-Stokes equations in Chapters 2 and 3

$$\mathbf{u}^{n+1} = \mathbf{u}^n + \hat{\mathbf{u}} \quad \text{and} \quad \mathbf{B}^{n+1} = \mathbf{B}^n + \hat{\mathbf{B}}$$

where \mathbf{u}^n , \mathbf{B}^n and $\hat{\mathbf{u}}$, $\hat{\mathbf{B}}$ are the previous iteration and correction values of the velocity and the magnetic field, respectively. Then, the nonlinearity in the equations can be eliminated as

$$\begin{aligned} \mathbf{u}^{n+1} \cdot \nabla \mathbf{u}^{n+1} &\approx \mathbf{u}^n \cdot \nabla \mathbf{u}^n + \hat{\mathbf{u}} \cdot \nabla \mathbf{u}^n + \mathbf{u}^n \cdot \nabla \hat{\mathbf{u}} \\ (\nabla \times \mathbf{B}^{n+1}) \times \mathbf{B}^{n+1} &\approx (\nabla \times \mathbf{B}^n) \times \mathbf{B}^n + (\nabla \times \mathbf{B}^n) \times \hat{\mathbf{B}} + (\nabla \times \hat{\mathbf{B}}) \times \mathbf{B}^n \\ \nabla \times (\mathbf{u}^{n+1} \times \mathbf{B}^{n+1}) &\approx \nabla \times (\mathbf{u}^n \times \mathbf{B}^n) + \nabla \times (\mathbf{u}^n \times \hat{\mathbf{B}}) + \nabla \times (\hat{\mathbf{u}} \times \mathbf{B}^n). \end{aligned}$$

4.2 SUPG formulation for the MHD equations

It is known that, the existence of the pressure term in the MHD equations, brings some oscillations in the solution when the standard Galerkin finite element method is used. In order to eliminate these numerical difficulties, either some restricted finite element spaces must be used satisfying certain conditions (Babuska-Brezzi condition, which implies the use of quadratic shape functions for both the velocity and the magnetic field, and linear for the pressure) or some stabilized finite element methods should be used in the solution procedure which allows to use equal order shape functions.

SUPG type stabilized finite element formulation for of the MHD equations using linear elements is given in [31] as; find $(\mathbf{u}_h, \mathbf{B}_h, p_h) \in (V_h, M_h, W_h)$ such that

$$\begin{aligned} &B(\mathbf{u}_h, \mathbf{B}_h, p_h; \mathbf{v}_h, \mathbf{C}_h, q_h) + \\ &\tau_u((\mathbf{u}_h \cdot \nabla \mathbf{u}_h + \nabla p_h - S(\nabla \times \mathbf{B}_h) \times \mathbf{B}_h - \mathbf{f}), (\mathbf{u}_h \cdot \nabla \mathbf{v}_h + \nabla q_h + S\mathbf{B}_h \times (\nabla \times \mathbf{C}_h))) \\ &+ \tau_B((-\nabla \times (\mathbf{u}_h \times \mathbf{B}_h)), (-\nabla \times (\mathbf{v}_h \times \mathbf{B}_h))) = L(\mathbf{f}), \quad \forall (\mathbf{v}_h, \mathbf{C}_h, q_h) \in (V_h, M_h, W_h) \end{aligned} \quad (4.14)$$

with the stabilization parameters

$$\tau_u = \begin{cases} \frac{h_K}{2|\mathbf{u}_h^n|_K} & \text{if } Pe_K \geq 1 \\ \frac{h_K^2}{12\epsilon} & \text{if } Pe_K < 1 \end{cases} \quad \text{and} \quad \tau_B = \frac{h_K^2}{12\beta} \quad (4.15)$$

where h_K is the diameter of the element K , Pe_K is the Peclet number, $Pe_K = \frac{|\mathbf{u}_h^n|_K h_K}{6\epsilon}$ and $\epsilon = \frac{1}{Re}$, $\beta = \frac{1}{Rem}$.

In 2-D, the stabilized terms can be written explicitly as

$$\tau_u \left(\begin{array}{l} u_1 \frac{\partial u_1}{\partial x} + u_2 \frac{\partial u_1}{\partial y} + \frac{\partial p}{\partial x} - SB_2 \left(\frac{\partial B_1}{\partial y} - \frac{\partial B_2}{\partial x} \right) - f_1 \\ u_1 \frac{\partial u_2}{\partial x} + u_2 \frac{\partial u_2}{\partial y} + \frac{\partial p}{\partial y} + SB_1 \left(\frac{\partial B_1}{\partial y} - \frac{\partial B_2}{\partial x} \right) - f_2 \end{array} \right), \left(\begin{array}{l} u_1^n \frac{\partial v_1}{\partial x} + u_2^n \frac{\partial v_1}{\partial y} + \frac{\partial q}{\partial x} - SB_2^n \left(\frac{\partial C_1}{\partial y} - \frac{\partial C_2}{\partial x} \right) \\ u_1^n \frac{\partial v_2}{\partial x} + u_2^n \frac{\partial v_2}{\partial y} + \frac{\partial q}{\partial y} + SB_1^n \left(\frac{\partial C_1}{\partial y} - \frac{\partial C_2}{\partial x} \right) \end{array} \right) \\ + \tau_B \left(\begin{array}{l} -\frac{\partial}{\partial y} (u_1 B_2 - u_2 B_1) \\ \frac{\partial}{\partial x} (u_1 B_2 - u_2 B_1) \end{array} \right), \left(\begin{array}{l} -\frac{\partial}{\partial y} (v_1 B_2^n - v_2 B_1^n) \\ \frac{\partial}{\partial x} (v_1 B_2^n - v_2 B_1^n) \end{array} \right).$$

In order to obtain the stabilized terms for each component of the equation (4.14), the following procedure is used. For the first component, the inner products given above are performed by using only the terms containing v_1 in the second terms of the inner products. Similarly, for the second component v_2 , for the third one C_1 , for the fourth one C_2 and for the last component q is used. Therefore, for each component we will obtain the following stabilized terms additional to the standard Galerkin finite element formulation

$$\int_{\Omega} \left\{ \tau_u T_{11} \left(u_1^n \frac{\partial v_1}{\partial x} + u_2^n \frac{\partial v_1}{\partial y} \right) + \tau_B \left[-T_{21} \frac{\partial}{\partial y} (v_1 B_2^n) + T_{22} \frac{\partial}{\partial x} (v_1 B_2^n) \right] \right\} d\Omega \\ \int_{\Omega} \left\{ \tau_u T_{12} \left(u_1^n \frac{\partial v_2}{\partial x} + u_2^n \frac{\partial v_2}{\partial y} \right) + \tau_B \left[+T_{21} \frac{\partial}{\partial y} (v_2 B_1^n) - T_{22} \frac{\partial}{\partial x} (v_2 B_1^n) \right] \right\} d\Omega \\ \int_{\Omega} \tau_u \left[-T_{11} SB_2^n \frac{\partial C_1}{\partial y} + T_{12} SB_1^n \frac{\partial C_1}{\partial y} \right] d\Omega \\ \int_{\Omega} \tau_u \left[T_{11} SB_2^n \frac{\partial C_2}{\partial x} - T_{12} SB_1^n \frac{\partial C_2}{\partial x} \right] d\Omega \\ \int_{\Omega} \tau_u \left[T_{11} \frac{\partial q}{\partial x} + T_{12} \frac{\partial q}{\partial y} \right] d\Omega$$

where

$$T_{11} = u_1 \frac{\partial u_1}{\partial x} + u_2 \frac{\partial u_1}{\partial y} + \frac{\partial p}{\partial x} - SB_2 \left(\frac{\partial B_1}{\partial y} - \frac{\partial B_2}{\partial x} \right) - f_1 \\ T_{12} = u_1 \frac{\partial u_2}{\partial x} + u_2 \frac{\partial u_2}{\partial y} + \frac{\partial p}{\partial y} + SB_1 \left(\frac{\partial B_1}{\partial y} - \frac{\partial B_2}{\partial x} \right) - f_2 \\ T_{21} = -\frac{\partial}{\partial y} (u_1 B_2 - u_2 B_1) \\ T_{22} = \frac{\partial}{\partial x} (u_1 B_2 - u_2 B_1).$$

4.3 TLFEM for the MHD equations

The finite element approximation spaces for the velocity and the magnetic field are enriched by using bubble functions

$$V_h = V_1 \oplus V_B \quad \text{and} \quad M_h = M_1 \oplus M_B$$

$\forall \mathbf{u}_h \in V_h$ and $\mathbf{B}_h \in M_h$ where V_1 and M_1 are the linear spaces, V_B and M_B are the bubble spaces. Therefore, approximate solutions are decomposed as $\mathbf{u}_h = \mathbf{u}_1 + \mathbf{u}_b \in V_1 \oplus V_B$ and $\mathbf{B}_h = \mathbf{B}_1 + \mathbf{B}_b \in M_1 \oplus M_B$. Then, the MHD equations are rewritten as

$$\mathbf{u}_1 \cdot \nabla(\mathbf{u}_1 + \mathbf{u}_b) - \epsilon \nabla^2(\mathbf{u}_1 + \mathbf{u}_b) + \nabla p - S(\nabla \times \mathbf{B}_1) \times \mathbf{B}_1 = \mathbf{f} \quad (4.16)$$

$$\nabla \cdot (\mathbf{u}_1 + \mathbf{u}_b) = 0 \quad (4.17)$$

$$-\nabla \times (\mathbf{u}_1 \times \mathbf{B}_1) - \beta \nabla^2(\mathbf{B}_1 + \mathbf{B}_b) = 0 \quad (4.18)$$

and in variational form; find $\{\mathbf{u}_h, \mathbf{B}_h, p_1\} \in V_h \times M_h \times W_h$ as $\mathbf{u}_h = \mathbf{u}_1 + \mathbf{u}_b$ and $\mathbf{B}_h = \mathbf{B}_1 + \mathbf{B}_b$ such that

$$\begin{aligned} & (\mathbf{u}_1 \cdot \nabla(\mathbf{u}_1 + \mathbf{u}_b), \mathbf{v}_1) + \epsilon(\nabla(\mathbf{u}_1 + \mathbf{u}_b), \nabla \mathbf{v}_1) - (p_1, \nabla \mathbf{v}_1) - S((\nabla \times \mathbf{B}_1) \times \mathbf{B}_1, \mathbf{v}_1) \\ & - (\nabla \times (\mathbf{u}_1 \times \mathbf{B}_1), \mathbf{C}_1) + \beta(\nabla(\mathbf{B}_1 + \mathbf{B}_b), \nabla \mathbf{C}_1) + (q_1, \nabla \cdot (\mathbf{u}_1 + \mathbf{u}_b)) = (\mathbf{f}, \mathbf{v}_1) \end{aligned} \quad (4.19)$$

$\forall \{\mathbf{v}_1, \mathbf{C}_1, q_1\} \in V_h \times M_h \times W_h$ where $\epsilon = \frac{1}{Re}$, $\beta = \frac{1}{Rem}$.

Bubble part of the solutions \mathbf{u}_b and \mathbf{B}_b can be obtained from the solution of the following equations [52]

$$\begin{aligned} \mathbf{u}_1^n \cdot \nabla \mathbf{u}_b^{n+1} - \epsilon \nabla^2 \mathbf{u}_b^{n+1} &= \mathbf{f} - \mathbf{u}_1^n \cdot \nabla \mathbf{u}_1^{n+1} + \epsilon \nabla^2 \mathbf{u}_1^{n+1} - \nabla p_1^{n+1} + S(\nabla \times \mathbf{B}_1^{n+1}) \times \mathbf{B}_1^n & \text{in } K \\ \mathbf{u}_b &= 0 & \text{on } \partial K. \end{aligned} \quad (4.20)$$

and

$$\begin{aligned} -\beta \nabla^2 \mathbf{B}_b^{n+1} &= \beta \nabla^2 \mathbf{B}_1^{n+1} + \nabla \times (\mathbf{u}_1^n \times \mathbf{B}_1^{n+1}) & \text{in } K \\ \mathbf{B}_b &= 0 & \text{on } \partial K. \end{aligned} \quad (4.21)$$

In 2-D, explicit form of the bubble functions are

$$\begin{aligned} u_{1b} &= \sum_{i=1}^{\#nds} u_{1i} \varphi_i^{u_1} + \sum_{i=1}^{\#nds} B_{1i} \varphi_i^{B_1^1} + \sum_{i=1}^{\#nds} B_{2i} \varphi_i^{B_2^1} + \sum_{i=1}^{\#nds} p_i \varphi_i^{p_1} + \varphi^{f_1} \\ u_{2b} &= \sum_{i=1}^{\#nds} u_{2i} \varphi_i^{u_2} + \sum_{i=1}^{\#nds} B_{1i} \varphi_i^{B_1^2} + \sum_{i=1}^{\#nds} B_{2i} \varphi_i^{B_2^2} + \sum_{i=1}^{\#nds} p_i \varphi_i^{p_2} + \varphi^{f_2} \\ B_{1b} &= \sum_{i=1}^{\#nds} B_{1i} \varphi_i^{B_1^3} + \sum_{i=1}^{\#nds} B_{2i} \varphi_i^{B_2^3} \\ B_{2b} &= \sum_{i=1}^{\#nds} B_{1i} \varphi_i^{B_1^4} + \sum_{i=1}^{\#nds} B_{2i} \varphi_i^{B_2^4} \end{aligned} \quad (4.22)$$

where u_{1i} , u_{2i} , B_{1i} , B_{2i} , p_i denote the discrete values of the velocity, the magnetic field and the pressure, respectively. φ_i^u is the velocity part, $\varphi_i^{B_1^1}$, $\varphi_i^{B_2^1}$, $\varphi_i^{B_1^2}$ and $\varphi_i^{B_2^2}$ are the magnetic field

parts, φ_i^{p1} and φ_i^{p2} are the pressure parts, and φ^{f1} and φ^{f2} are external force parts of the bubble functions u_{1b} and u_{2b} . Similarly, $\varphi_i^{B1^3}$, $\varphi_i^{B2^3}$, $\varphi_i^{B1^4}$ and $\varphi_i^{B2^4}$ are the first and second components of the magnetic field parts of the bubble functions B_{1b} and B_{2b} .

Therefore, sub-mesh problems can be written using the operators $L_1 = -\epsilon\nabla^2 + \mathbf{u}_1^n$ and $L_2 = -\beta\nabla^2$ as follows;

Computation of \mathbf{u}_b :

It is seen from the equation (4.22) that \mathbf{u}_b consists of velocity parts, magnetic field parts, pressure part and body force part. Each part of the bubble functions are derived from the equation (4.20).

For the velocity parts u_{1b} and u_{2b} , the same sub-mesh problem will be solved

$$\begin{cases} L_1\varphi_i^{u1} = -(u_1^n \frac{\partial\phi_i}{\partial x} + u_2^n \frac{\partial\phi_i}{\partial y}) & \text{in } K \\ \varphi_i^{u1} = 0 & \text{on } \partial K. \end{cases} \quad (4.23)$$

For the magnetic field parts, there are four different sub-mesh problems

$$\begin{cases} L_1\varphi_i^{B1^1} = SB_2^n \frac{\partial\phi_i}{\partial y} & \text{in } K & , & L_1\varphi_i^{B2^1} = -SB_2^n \frac{\partial\phi_i}{\partial y} & \text{in } K \\ \varphi_i^{B1^1} = 0 & \text{on } \partial K & , & \varphi_i^{B2^1} = 0 & \text{on } \partial K \\ L_1\varphi_i^{B1^2} = -SB_1^n \frac{\partial\phi_i}{\partial y} & \text{in } K & , & L_1\varphi_i^{B2^2} = SB_1^n \frac{\partial\phi_i}{\partial y} & \text{in } K \\ \varphi_i^{B1^2} = 0 & \text{on } \partial K & , & \varphi_i^{B2^2} = 0 & \text{on } \partial K. \end{cases} \quad (4.24)$$

For the pressure part, there are two different sub-mesh problems

$$\begin{cases} L_1\varphi_i^{p1} = -\frac{\partial\phi_i}{\partial x} & \text{in } K & , & L_1\varphi_i^{p2} = -\frac{\partial\phi_i}{\partial y} & \text{in } K \\ \varphi_i^{p1} = 0 & \text{on } \partial K & , & \varphi_i^{p2} = 0 & \text{on } \partial K. \end{cases} \quad (4.25)$$

For the body force part of the bubbles, we have the following sub-mesh problems

$$\begin{cases} L_1\varphi^{f1} = f_1 & \text{in } K & , & L_1\varphi^{f2} = f_2 & \text{in } K \\ \varphi^{f1} = 0 & \text{on } \partial K & , & \varphi^{f2} = 0 & \text{on } \partial K. \end{cases} \quad (4.26)$$

Equations (4.23)-(4.26) should be solved on a sub-mesh with a non-standard method (such as SUPG). In all of the sub-mesh level problems for \mathbf{u}_b , left hand sides are common for each element. Therefore, it can be calculated only once and used for all the problems on an element level. Explicit form of the left hand side of the sub-mesh problems is given as

$$\int_{\Omega_{K^*}} \left\{ \epsilon(\nabla\phi_l^* \cdot \nabla\phi_m^*) + (u_1^n \frac{\partial\phi_l^*}{\partial x} + u_2^n \frac{\partial\phi_l^*}{\partial y})\phi_m^* + \tau_{K^*}(u_1^n \frac{\partial\phi_l^*}{\partial x} + u_2^n \frac{\partial\phi_l^*}{\partial y})(u_1^n \frac{\partial\phi_m^*}{\partial x} + u_2^n \frac{\partial\phi_m^*}{\partial y}) \right\} d\Omega_{K^*} \quad (4.27)$$

where ϕ^* denotes the basis function on the submesh.

Right hand sides of the equations (4.23)-(4.26) are respectively

velocity part

$$\int_{\Omega_{K^*}} \left\{ -(u_1^n \frac{\partial \phi_i}{\partial x} + u_2^n \frac{\partial \phi_i}{\partial y}) \phi_m^* - \tau_{K^*} (u_1^n \frac{\partial \phi_i}{\partial x} + u_2^n \frac{\partial \phi_i}{\partial y}) (u_1^n \frac{\partial \phi_m^*}{\partial x} + u_2^n \frac{\partial \phi_m^*}{\partial y}) \right\} d\Omega_{K^*} \quad (4.28)$$

magnetic field part

$$\int_{\Omega_{K^*}} \left\{ SB_2^n \frac{\partial \phi_i}{\partial y} \phi_m^* + \tau_{K^*} SB_2^n \frac{\partial \phi_i}{\partial y} (u_1^n \frac{\partial \phi_m^*}{\partial x} + u_2^n \frac{\partial \phi_m^*}{\partial y}) \right\} d\Omega_{K^*} \quad (4.29)$$

$$\int_{\Omega_{K^*}} \left\{ -SB_2^n \frac{\partial \phi_i}{\partial y} \phi_m^* - \tau_{K^*} SB_2^n \frac{\partial \phi_i}{\partial y} (u_1^n \frac{\partial \phi_m^*}{\partial x} + u_2^n \frac{\partial \phi_m^*}{\partial y}) \right\} d\Omega_{K^*} \quad (4.30)$$

$$\int_{\Omega_{K^*}} \left\{ -SB_1^n \frac{\partial \phi_i}{\partial y} \phi_m^* - \tau_{K^*} SB_1^n \frac{\partial \phi_i}{\partial y} (u_1^n \frac{\partial \phi_m^*}{\partial x} + u_2^n \frac{\partial \phi_m^*}{\partial y}) \right\} d\Omega_{K^*} \quad (4.31)$$

$$\int_{\Omega_{K^*}} \left\{ SB_1^n \frac{\partial \phi_i}{\partial y} \phi_m^* + \tau_{K^*} SB_1^n \frac{\partial \phi_i}{\partial y} (u_1^n \frac{\partial \phi_m^*}{\partial x} + u_2^n \frac{\partial \phi_m^*}{\partial y}) \right\} d\Omega_{K^*} \quad (4.32)$$

pressure part

$$\int_{\Omega_{K^*}} \left\{ -\frac{\partial \phi_i}{\partial x} \phi_m^* - \tau_{K^*} \frac{\partial \phi_i}{\partial x} (u_1^n \frac{\partial \phi_m^*}{\partial x} + u_2^n \frac{\partial \phi_m^*}{\partial y}) \right\} d\Omega_{K^*} \quad (4.33)$$

$$\int_{\Omega_{K^*}} \left\{ -\frac{\partial \phi_i}{\partial y} \phi_m^* - \tau_{K^*} \frac{\partial \phi_i}{\partial y} (u_1^n \frac{\partial \phi_m^*}{\partial x} + u_2^n \frac{\partial \phi_m^*}{\partial y}) \right\} d\Omega_{K^*} \quad (4.34)$$

body force part

$$\int_{\Omega_{K^*}} \left\{ f_1 \phi_m^* + \tau_{K^*} f_1 (u_1^n \frac{\partial \phi_m^*}{\partial x} + u_2^n \frac{\partial \phi_m^*}{\partial y}) \right\} d\Omega_{K^*} \quad (4.35)$$

$$\int_{\Omega_{K^*}} \left\{ f_2 \phi_m^* + \tau_{K^*} f_2 (u_1^n \frac{\partial \phi_m^*}{\partial x} + u_2^n \frac{\partial \phi_m^*}{\partial y}) \right\} d\Omega_{K^*} \quad (4.36)$$

with the stabilization parameter τ_{K^*} such that

$$\tau_{K^*} = \frac{h_{K^*}}{2|\mathbf{u}_1^n|_K} \varepsilon(Pe_K) \quad (4.37)$$

where

$$\varepsilon(Pe_K) = \begin{cases} Pe_k & \text{if } Pe_k < 1 \\ 1 & \text{if } Pe_k \geq 1 \end{cases}$$

and

$$Pe_K = \frac{|\mathbf{u}_1^n|_K h_{K^*}}{6\epsilon}.$$

Computation of \mathbf{B}_b :

Similar to \mathbf{u}_b , the following four sub-mesh problems are obtained from the equation (4.21) for \mathbf{B}_b

$$\left\{ \begin{array}{ll} L_2 \varphi_i^{B_1^3} = -(u_1^n \frac{\partial \phi_i}{\partial x} + u_2^n \frac{\partial \phi_i}{\partial y} + \frac{\partial u_2^n}{\partial y} \phi_i) & \text{in } K \\ \varphi_i^{B_1^3} = 0 & \text{on } \partial K \\ \\ L_2 \varphi_i^{B_2^3} = \frac{\partial u_1^n}{\partial y} \phi_i & \text{in } K \\ \varphi_i^{B_2^3} = 0 & \text{on } \partial K \\ \\ L_2 \varphi_i^{B_3^4} = \frac{\partial u_2^n}{\partial x} \phi_i & \text{in } K \\ \varphi_i^{B_3^4} = 0 & \text{on } \partial K \\ \\ L_2 \varphi_i^{B_4^4} = -(u_1^n \frac{\partial \phi_i}{\partial x} + u_2^n \frac{\partial \phi_i}{\partial y} + \frac{\partial u_1^n}{\partial x} \phi_i) & \text{in } K \\ \varphi_i^{B_4^4} = 0 & \text{on } \partial K. \end{array} \right. \quad (4.38)$$

Notice that, there is no need for the stabilization of the operator L_2 . Therefore, the solutions of the equations (4.38) are obtained from standard Galerkin finite element method with the common left hand side

$$\int_{\Omega_{K^*}} \beta (\nabla \phi_i^* \cdot \nabla \phi_m^*) d\Omega_{K^*} \quad (4.39)$$

and the following corresponding right hand sides

$$\int_{\Omega_{K^*}} \left\{ -(u_1^n \frac{\partial \phi_i}{\partial x} + u_2^n \frac{\partial \phi_i}{\partial y} + \frac{\partial u_2^n}{\partial y} \phi_i) \phi_m^* \right\} d\Omega_{K^*} \quad (4.40)$$

$$\int_{\Omega_{K^*}} \frac{\partial u_1^n}{\partial y} \phi_i \phi_m^* d\Omega_{K^*} \quad (4.41)$$

$$\int_{\Omega_{K^*}} \frac{\partial u_2^n}{\partial x} \phi_i \phi_m^* d\Omega_{K^*} \quad (4.42)$$

$$\int_{\Omega_{K^*}} \left\{ -(u_1^n \frac{\partial \phi_i}{\partial x} + u_2^n \frac{\partial \phi_i}{\partial y} + \frac{\partial u_1^n}{\partial x} \phi_i) \phi_m^* \right\} d\Omega_{K^*} \quad (4.43)$$

respectively.

Once all the bubble parts of the solutions are calculated, they will be substituted in the equations (4.16)-(4.18) and solved over the global mesh.

4.4 SSM for the MHD equations

The solution of the MHD equations with SSM is presented for the first time in this study. It is previously stated that SSM is related to the combination of the methods SUPG and residual-free-bubble functions.

The bubble parts of the MHD equations given in (4.20) and (4.21)

$$\begin{cases} \mathbf{u}_1^n \cdot \nabla \mathbf{u}_b^{n+1} - \epsilon \nabla^2 \mathbf{u}_b^{n+1} = \mathbf{f} - \mathbf{u}_1^n \cdot \nabla \mathbf{u}_1^{n+1} + \epsilon \nabla^2 \mathbf{u}_1^{n+1} - \nabla p_1^{n+1} + S(\nabla \times \mathbf{B}_1^{n+1}) \times \mathbf{B}_1^n & \text{in } K \\ \mathbf{u}_b = 0 & \text{on } \partial K \end{cases}$$

and

$$\begin{cases} -\beta \nabla^2 \mathbf{B}_b^{n+1} = \beta \nabla^2 \mathbf{B}_1^{n+1} + \nabla \times (\mathbf{u}_1^n \times \mathbf{B}_1^{n+1}) & \text{in } K \\ \mathbf{B}_b = 0 & \text{on } \partial K \end{cases}$$

are written by specifying the right hand sides as D_1 and D_2

$$\begin{cases} \mathbf{u}_1^n \cdot \nabla \mathbf{u}_b^{n+1} - \epsilon \nabla^2 \mathbf{u}_b^{n+1} = D_1 \\ -\beta \nabla^2 \mathbf{B}_b^{n+1} = D_2 \end{cases}$$

where

$$D_1(\mathbf{u}_1, \mathbf{B}_1, p_1, \mathbf{f}) = \mathbf{f} - \mathbf{u}_1^n \cdot \nabla \mathbf{u}_1^{n+1} + \epsilon \nabla^2 \mathbf{u}_1^{n+1} - \nabla p_1^{n+1} + S(\nabla \times \mathbf{B}_1^{n+1}) \times \mathbf{B}_1^n$$

and

$$D_2(\mathbf{u}_1, \mathbf{B}_1) = \beta \nabla^2 \mathbf{B}_1^{n+1} + \nabla \times (\mathbf{u}_1^n \times \mathbf{B}_1^{n+1}).$$

The **SSM** and the **SUPG** formulations of the MHD equations have the identical structure except for the value of the stabilization parameters τ_u and τ_B . In SSM, the stabilization parameters τ_u and τ_B are explicitly given by

$$\tau_u = \frac{1}{|K|} \int_K b_K^u dK \quad \text{and} \quad \tau_B = \frac{1}{|K|} \int_K b_K^B dK \quad (4.44)$$

where b_K^u are b_K^B are the unique solution of the following boundary value problems in an element K ,

$$\begin{cases} -\epsilon \nabla^2 b_K^u + \mathbf{u}_1^n \cdot \nabla b_K^u = 1 & \text{in } K \\ b_K^u = 0 & \text{on } \partial K \end{cases} \quad (4.45)$$

and

$$\begin{cases} -\beta \nabla^2 b_K^B = 1 & \text{in } K \\ b_K^B = 0 & \text{on } \partial K. \end{cases} \quad (4.46)$$

Using the integration by parts, observe that

$$\mathbf{u}_b = D_1 \frac{\int_K b_K^u dK}{\epsilon \int_K |\nabla b_K^u|^2 dK} \quad \text{and} \quad \mathbf{B}_b = D_2 \frac{\int_K b_K^B dK}{\beta \int_K |\nabla b_K^B|^2 dK}. \quad (4.47)$$

Note that, finding the exact solutions b_K^u using (4.45) and b_K^B using (4.46) may not be an easy task in an arbitrary triangular domain. Therefore, a cheap and efficient approximation to b_K^u and b_K^B that generates qualitatively the same behavior with the exact function b_K^u and b_K^B is required.

For this, we specify a subgrid which consists of three vertices of the triangle plus a single additional node in the interior of each element and approximate the bubble function over the specified subgrid by choosing the location of the additional node such that it gives the best approximation in L_1 norm.

Note that, the problem (4.45) is convective-diffusive type. Therefore, similar to the case in Navier-Stokes equations, the location of the subgrid point for \mathbf{u}_b is determined using the following two cases [10, 53].

In the first case where the inflow boundary makes up of two edges, let \mathbf{e}_2 and \mathbf{e}_3 be two inflow edges (Figure (2.1)). Then the value for t , we take

$$\begin{cases} t = 1 + \frac{\epsilon(|\mathbf{e}_1|^2)}{\epsilon(|\mathbf{e}_2 - \mathbf{e}_3|^2 - \frac{2}{3}|K|(\tilde{\mathbf{u}}_1^n, \nu_1))} & \text{if } \epsilon \leq \frac{2|K|(\tilde{\mathbf{u}}_1^n, \nu_1)/3}{3|\mathbf{e}_1|^2 + |\mathbf{e}_2 - \mathbf{e}_3|^2} \\ t = 2/3 & \text{otherwise.} \end{cases} \quad (4.48)$$

In the other case where the inflow boundary makes up of a single edge, let \mathbf{e}_1 be the inflow edge (Figure (2.1)). Then t is taken as

$$\begin{cases} t = \frac{\epsilon(|\mathbf{e}_2|^2 + |\mathbf{e}_3|^2)}{\epsilon(|\mathbf{e}_2 - \mathbf{e}_3|^2/2 - |K|(\tilde{\mathbf{u}}_1^n, \nu_1)/3)} & \text{if } \epsilon \leq \frac{-2|K|(\tilde{\mathbf{u}}_1^n, \nu_1)/3}{3(|\mathbf{e}_2|^2 + |\mathbf{e}_3|^2) - |\mathbf{e}_2 - \mathbf{e}_3|^2} \\ t = 2/3 & \text{otherwise.} \end{cases} \quad (4.49)$$

Once the location of the subgrid point is determined, a reasonably good approximation to the stabilization parameter τ_u can be obtained: The approximate value of τ_u is given by $\tilde{\tau}_u$ as

$$\tilde{\tau}_u = \frac{1}{|K|} \int_K b_K^{u*} = \frac{1}{|K|} \frac{(\int_K b_K^u)^2}{\epsilon \int_K |\nabla b_K^u|^2} = \frac{4|K|}{9\epsilon \sum_i |e_i|^2 / |K_i|} \quad (4.50)$$

where K_i is the area of the i^{th} sub-triangle.

For the solution of the problem (4.46), a subgrid point is selected on the body center of the triangle. Then, approximate value of the stabilization parameter τ_B is calculated as

$$\tilde{\tau}_B = \frac{1}{|K|} \int_K b_K^{B*} = \frac{1}{|K|} \frac{(\int_K b_K^B)^2}{\beta \int_K |\nabla b_K^B|^2} = \frac{4|K|}{9\beta \sum_i |e_i|^2 / |K_i|}. \quad (4.51)$$

After finding the values of τ_u and τ_B , similar to SUPG method, SSM formulation of the MHD equations is written as; find $(\mathbf{u}_h, \mathbf{B}_h, p_h) \in (V_h, M_h, W_h)$ such that

$$\begin{aligned} & B(\mathbf{u}_h, \mathbf{B}_h, p_h; \mathbf{v}_h, \mathbf{C}_h, q_h) + \\ & \tau_u((\mathbf{u}_h \cdot \nabla \mathbf{u}_h + \nabla p_h - S(\nabla \times \mathbf{B}_h) \times \mathbf{B}_h - \mathbf{f}), (\mathbf{u}_h \cdot \nabla \mathbf{v}_h + \nabla q_h - S(\nabla \times \mathbf{C}_h) \times \mathbf{B}_h)) \\ & + \tau_B((\nabla \times (\mathbf{u}_h \times \mathbf{B}_h)), (\nabla \times (\mathbf{v}_h \times \mathbf{B}_h))) = L(\mathbf{f}), \quad \forall (\mathbf{v}_h, \mathbf{C}_h, q_h) \in (V_h, M_h, W_h). \end{aligned} \quad (4.52)$$

4.5 Magnetic pressure in the MHD equations

It is possible to extend the two-dimensional MHD equations to the more general form by introducing a magnetic pressure r and a related external force \mathbf{g} as in [17, 34]

$$\mathbf{u} \cdot \nabla \mathbf{u} - \frac{1}{Re} \nabla^2 \mathbf{u} + \nabla p - \frac{Ha^2}{Re \cdot Rem} (\nabla \times \mathbf{B}) \times \mathbf{B} = \mathbf{f} \quad (4.53)$$

$$\nabla \cdot \mathbf{u} = 0 \quad (4.54)$$

$$-\nabla \times (\mathbf{u} \times \mathbf{B}) + \frac{1}{Rem} \nabla \times (\nabla \times \mathbf{B}) + \nabla r = \mathbf{g} \quad (4.55)$$

$$\nabla \cdot \mathbf{B} = 0. \quad (4.56)$$

In 2-D, if we define $\mathbf{g} = \begin{Bmatrix} g_1 \\ g_2 \end{Bmatrix}$, the following explicit equations will be obtained for the equations (4.53) - (4.56)

$$u_1 \frac{\partial u_1}{\partial x} + u_2 \frac{\partial u_1}{\partial y} + \frac{\partial p}{\partial x} - \frac{1}{Re} \left(\frac{\partial^2 u_1}{\partial x^2} + \frac{\partial^2 u_1}{\partial y^2} \right) - SB_2 \left(\frac{\partial B_1}{\partial y} - \frac{\partial B_2}{\partial x} \right) = f_1 \quad (4.57)$$

$$u_1 \frac{\partial u_2}{\partial x} + u_2 \frac{\partial u_2}{\partial y} + \frac{\partial p}{\partial y} - \frac{1}{Re} \left(\frac{\partial^2 u_2}{\partial x^2} + \frac{\partial^2 u_2}{\partial y^2} \right) + SB_1 \left(\frac{\partial B_1}{\partial y} - \frac{\partial B_2}{\partial x} \right) = f_2 \quad (4.58)$$

$$\frac{\partial u_1}{\partial x} + \frac{\partial u_2}{\partial y} = 0 \quad (4.59)$$

$$u_1 \frac{\partial B_1}{\partial x} + u_2 \frac{\partial B_1}{\partial y} + \frac{\partial u_2}{\partial y} B_1 - \frac{\partial u_1}{\partial y} B_2 + \frac{1}{Rem} \frac{\partial}{\partial y} \left(\frac{\partial B_2}{\partial x} - \frac{\partial B_1}{\partial y} \right) + \frac{\partial r}{\partial x} = g_1 \quad (4.60)$$

$$u_1 \frac{\partial B_2}{\partial x} + u_2 \frac{\partial B_2}{\partial y} + \frac{\partial u_1}{\partial x} B_2 - \frac{\partial u_2}{\partial x} B_1 - \frac{1}{Rem} \frac{\partial}{\partial x} \left(\frac{\partial B_2}{\partial x} - \frac{\partial B_1}{\partial y} \right) + \frac{\partial r}{\partial y} = g_2 \quad (4.61)$$

$$\frac{\partial B_1}{\partial x} + \frac{\partial B_2}{\partial y} = 0. \quad (4.62)$$

Variational Formulation

Before writing the variational formulation of MHD equations, we will define some finite element spaces over an element K as follows: $L^2(\Omega)$ is the space of square integrable functions, $H^1(\Omega)$ the space of functions such that they and their derivatives are in $L^2(\Omega)$, $L_0^2(\Omega)$ the subspace of functions in $L^2(\Omega)$ with zero mean, $H_0^1(\Omega)$ the subspace of functions in $H^1(\Omega)$ with zero trace on $\partial\Omega$, $H(\text{curl}, \Omega)$ the space of vector functions such that they and their curl are in the space $L^2(\Omega)$ and $H_0(\text{curl}, \Omega)$ the subspace of functions in the space $H(\text{curl}, \Omega)$ with zero tangential component on $\partial\Omega$. Then, define the functional space W as [17]

$$W := (H_0^1(\Omega))^2 \times L_0^2(\Omega) \times H_0(\text{curl}, \Omega) \times H_0^1(\Omega)$$

and

$$W_h = C^0(\bar{\Omega}) \cap W.$$

Also $\mathbf{f} \in (H^{-1}(\Omega))^2$, the dual of $(H_0^1(\Omega))^2$ and $\mathbf{g} \in (L^2(\Omega))^2$ with $\nabla \cdot \mathbf{g} = 0$ in $L^2(\Omega)$ are assumed for both \mathbf{f} and \mathbf{g} .

Importing a Dirichlet type boundary condition $r = 0$ on $\partial\Omega$ yields $r = 0$ as exact solution by taking the divergence of the equation (4.55)

$$\nabla^2 r = 0 \text{ in } \Omega.$$

Therefore, magnetic pressure (r) seems to be a dummy variable (in theory should be null). However, it satisfies the consistency of the system when the divergence free condition for the magnetic field (4.56) is used as an additional equation. Then, Galerkin FEM formulation of the problems reads [17]; find approximation for the unknowns $\mathbf{U} := (\mathbf{u}_h, p_h, \mathbf{B}_h, r_h) \in W_h$ such that

$$B(\mathbf{u}_h, p_h, \mathbf{B}_h, r_h; \mathbf{v}_h, q_h, \mathbf{C}_h, s_h) = L(\mathbf{f}, \mathbf{g}) \quad (4.63)$$

for all corresponding test functions $\mathbf{V} := (\mathbf{v}_h, q_h, \mathbf{C}_h, s_h) \in W_h$ where

$$\begin{aligned} B(\mathbf{u}_h, p_h, \mathbf{B}_h, r_h; \mathbf{v}_h, q_h, \mathbf{C}_h, s_h) = & \\ & (\mathbf{u}_h \cdot \nabla \mathbf{u}_h, \mathbf{v}_h) + \frac{1}{Re} (\nabla \mathbf{u}_h, \nabla \mathbf{v}_h) - (p_h, \nabla \cdot \mathbf{v}_h) + S(\mathbf{B}_h, \nabla \times (\mathbf{v}_h \times \mathbf{B}_h)) + (q_h, \nabla \cdot \mathbf{u}_h) \\ & - S(\mathbf{C}_h, \nabla \times (\mathbf{u}_h \times \mathbf{B}_h)) + \frac{S}{Rem} (\nabla \times \mathbf{B}_h, \nabla \times \mathbf{C}_h) + S(\nabla r_h, \mathbf{C}_h) - S(\mathbf{B}_h, \nabla s_h) \end{aligned}$$

and

$$L(\mathbf{f}, \mathbf{g}) = (\mathbf{f}, \mathbf{v}_h) + S(\mathbf{g}, \mathbf{C}_h).$$

Explicitly, in 2-D;

$$\int_{\Omega} \left\{ \left(u_1 \frac{\partial u_1}{\partial x} + u_2 \frac{\partial u_1}{\partial y} \right) v_1 + \frac{1}{Re} \left(\frac{\partial u_1}{\partial x} \frac{\partial v_1}{\partial x} + \frac{\partial u_1}{\partial y} \frac{\partial v_1}{\partial y} \right) - p \frac{\partial v_1}{\partial x} + S \left[B_1 \frac{\partial}{\partial y} (v_1 B_2) - B_2 \frac{\partial}{\partial x} (v_1 B_2) \right] \right\} d\Omega = \int_{\Omega} f_1 v_1 d\Omega$$

$$\int_{\Omega} \left\{ \left(u_1 \frac{\partial u_2}{\partial x} + u_2 \frac{\partial u_2}{\partial y} \right) v_2 + \frac{1}{Re} \left(\frac{\partial u_2}{\partial x} \frac{\partial v_2}{\partial x} + \frac{\partial u_2}{\partial y} \frac{\partial v_2}{\partial y} \right) - p \frac{\partial v_2}{\partial x} - S \left[B_1 \frac{\partial}{\partial y} (v_2 B_1) - B_2 \frac{\partial}{\partial x} (v_2 B_1) \right] \right\} d\Omega = \int_{\Omega} f_2 v_2 d\Omega$$

$$\int_{\Omega} \left(\frac{\partial u_1}{\partial x} + \frac{\partial u_2}{\partial y} \right) q d\Omega = 0$$

$$\int_{\Omega} \left\{ S \left(u_1 \frac{\partial B_1}{\partial x} + u_2 \frac{\partial B_1}{\partial y} - \frac{\partial u_1}{\partial y} B_2 + \frac{\partial u_2}{\partial y} B_1 \right) C_1 - \frac{S}{Rem} \left(\frac{\partial B_2}{\partial x} - \frac{\partial B_1}{\partial y} \right) \frac{\partial C_1}{\partial y} + S \frac{\partial r}{\partial x} C_1 \right\} d\Omega = \int_{\Omega} S g_1 C_1 d\Omega$$

$$\int_{\Omega} \left\{ S \left(u_1 \frac{\partial B_2}{\partial x} + u_2 \frac{\partial B_2}{\partial y} + \frac{\partial u_1}{\partial x} B_2 - \frac{\partial u_2}{\partial x} B_1 \right) C_2 + \frac{S}{Rem} \left(\frac{\partial B_2}{\partial x} - \frac{\partial B_1}{\partial y} \right) \frac{\partial C_2}{\partial x} + S \frac{\partial r}{\partial y} C_2 \right\} d\Omega = \int_{\Omega} S g_2 C_2 d\Omega$$

$$\int_{\Omega} -S \left(B_1 \frac{\partial s}{\partial x} + B_2 \frac{\partial s}{\partial y} \right) d\Omega = 0.$$

It is known that, the existence of the fluid pressure and magnetic pressure terms with first order derivatives in the MHD equations and convection dominated characteristic of the equations bring some oscillations in the solution using standard Galerkin finite element method. In order to eliminate these numerical difficulties some restricted finite element spaces must be used to satisfy certain conditions (Babuska-Brezzi condition, $(Q2, Q2, Q2, Q1)$ elements for $(\mathbf{u}, \mathbf{B}, r, p)$ respectively).

4.6 Numerical Results

In this section, we present some numerical results obtained by the stabilizing subgrid method (SSM) presented above and compare it with the exact one if exists, with SUPG type stabilized finite element method solution and with the solution obtained by Babuska-Brezzi condition which implies the use of Q2-Q2-Q1 elements for the velocity-magnetic field-pressure combinations respectively. We work on three problems: (1) test problem on a unit square with exact solution, (2) MHD flow inside a cavity and (3) MHD flow over a step. We use the tool VIGIE (Visualization Generale Interactive d'Ecoulements) to visualize the numerical results. The iteration cycle that resolve the nonlinearity of the problem stops when the maximum norm of the error is less than 10^{-6} .

4.6.1 Test problem

We have solved the MHD equations on the following test problem. Boundary conditions are obtained from the exact solution values of u_1 , u_2 , B_1 , B_2 and p which satisfy the equations (4.6)-(4.10) with $Re = 100$, $Rem = 10$ and $Ha = 10$ on the 2-D domain $[0, 1] \times [0, 1]$ given in [68] as,

$$\begin{cases} u_1 = 1 - \exp(x) \cos(2\pi y) \\ u_2 = \exp(x) \sin(2\pi y)/(2\pi) \\ B_1 = \cos(\pi x) \cos(\pi y) \\ B_2 = \sin(\pi x) \sin(\pi y) \\ p = (1 - \exp(2x))/2 + C \end{cases} \quad (4.64)$$

where C is any constant value. We have already noted that pressure is determined up to a constant. Therefore to satisfy the condition $\int_{\Omega} p = 0$ for the pressure, the value of C is selected as $C = 1.0972640247327$.

Solution of the MHD equations with equal order shape functions

The test problem is first solved by using linear shape functions for all unknowns. From the Figures (4.1),(4.2) and (4.3) it is seen that, there are oscillations in the pressure solutions,

although the velocity and the magnetic field components agree well with the exact solutions.

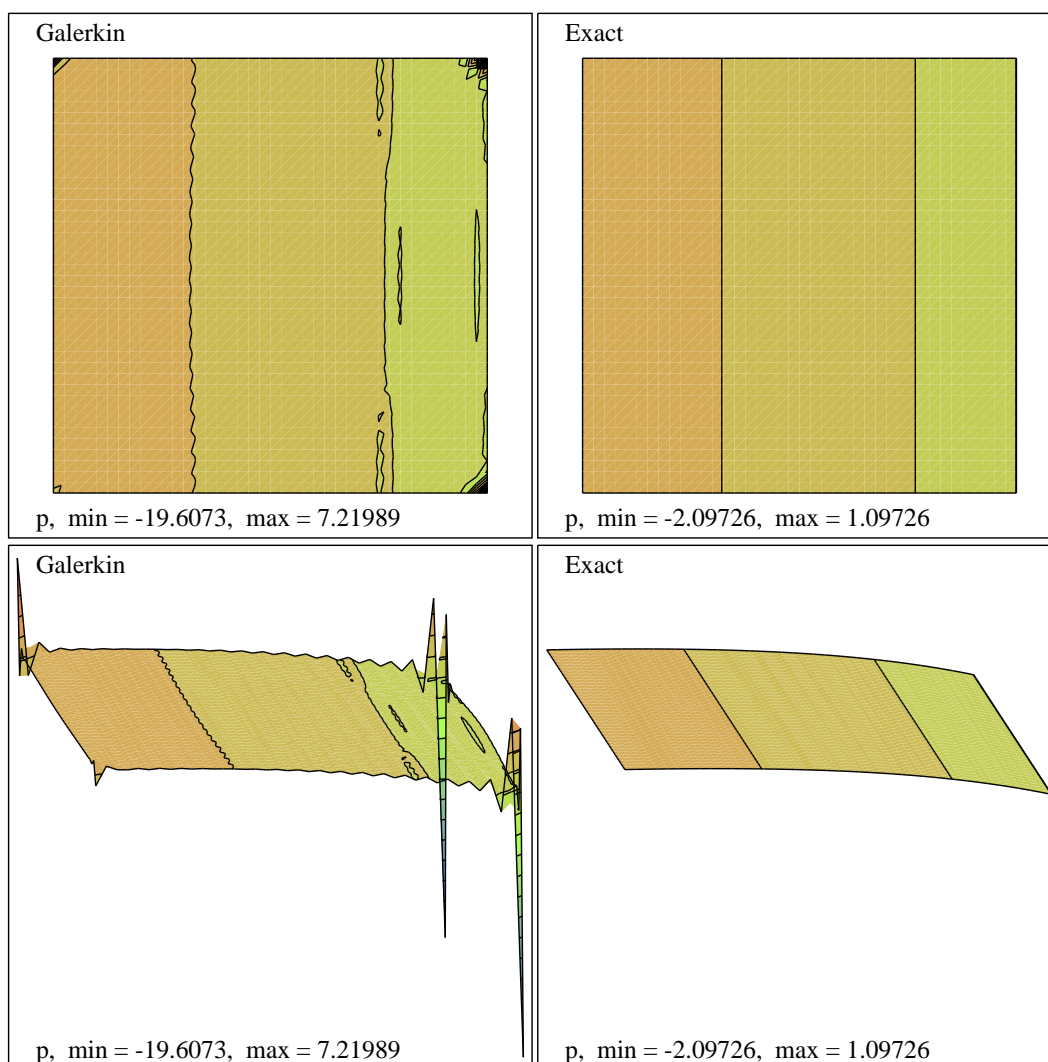


Figure 4.1: Pressure contours and elevations obtained from standard Galerkin FEM and exact solutions

Solution of the MHD equations with Babuska-Brezzi condition

We have solved the same test problem by using Q2-Q2-Q1 elements for the velocity-magnetic field-pressure combinations respectively with the Babuska-Brezzi condition. From the Figure (4.4) it seen that oscillations in the pressure solution disappeared.

Magnetic pressure in the MHD equations

Magnetic pressure also shows oscillations when the solution is obtain from the standard Galerkin finite element method. Although magnetic pressure plays similar role as the fluid pres-

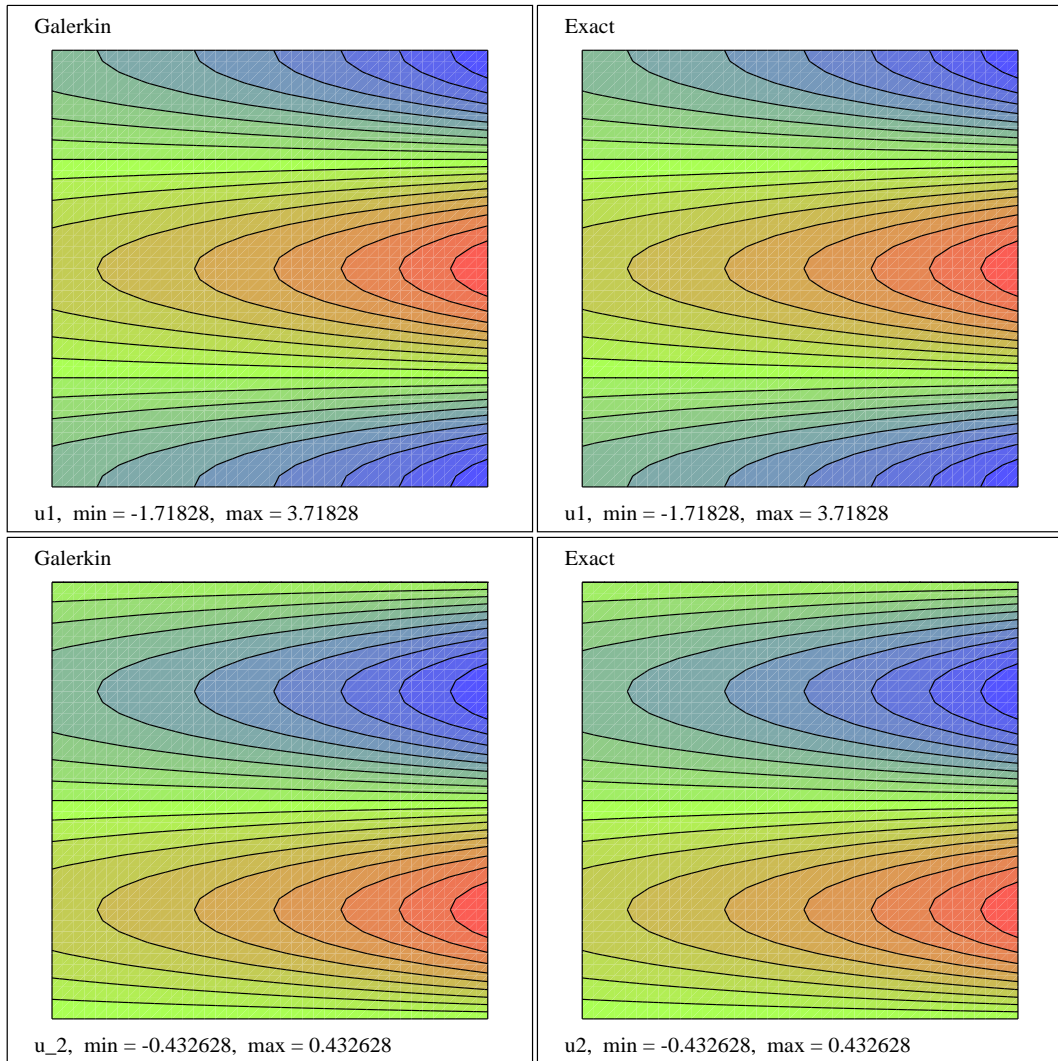


Figure 4.2: Standard Galerkin FEM and exact solutions for the velocity(u_1, u_2)

sure in the equations, the function spaces and conditions imposed are more stronger. Therefore, in order to obtain stable solutions from the magnetic pressure formulation of the MHD equations ((4.57) - (4.62)), quadratic elements should also be used for the magnetic pressure as used for the velocity and the magnetic field components. It is already stated that, magnetic pressure is a dummy variable. Therefore, in theory, it is null (i.e. zero value). Standard Galerkin FEM solutions and solutions obtained by using the stability condition (Babuska-Brezzi condition) using Q2-Q2-Q2-Q1 elements are displayed in the Figure (4.5). It is seen that, oscillations disappeared and the solution is almost zero.

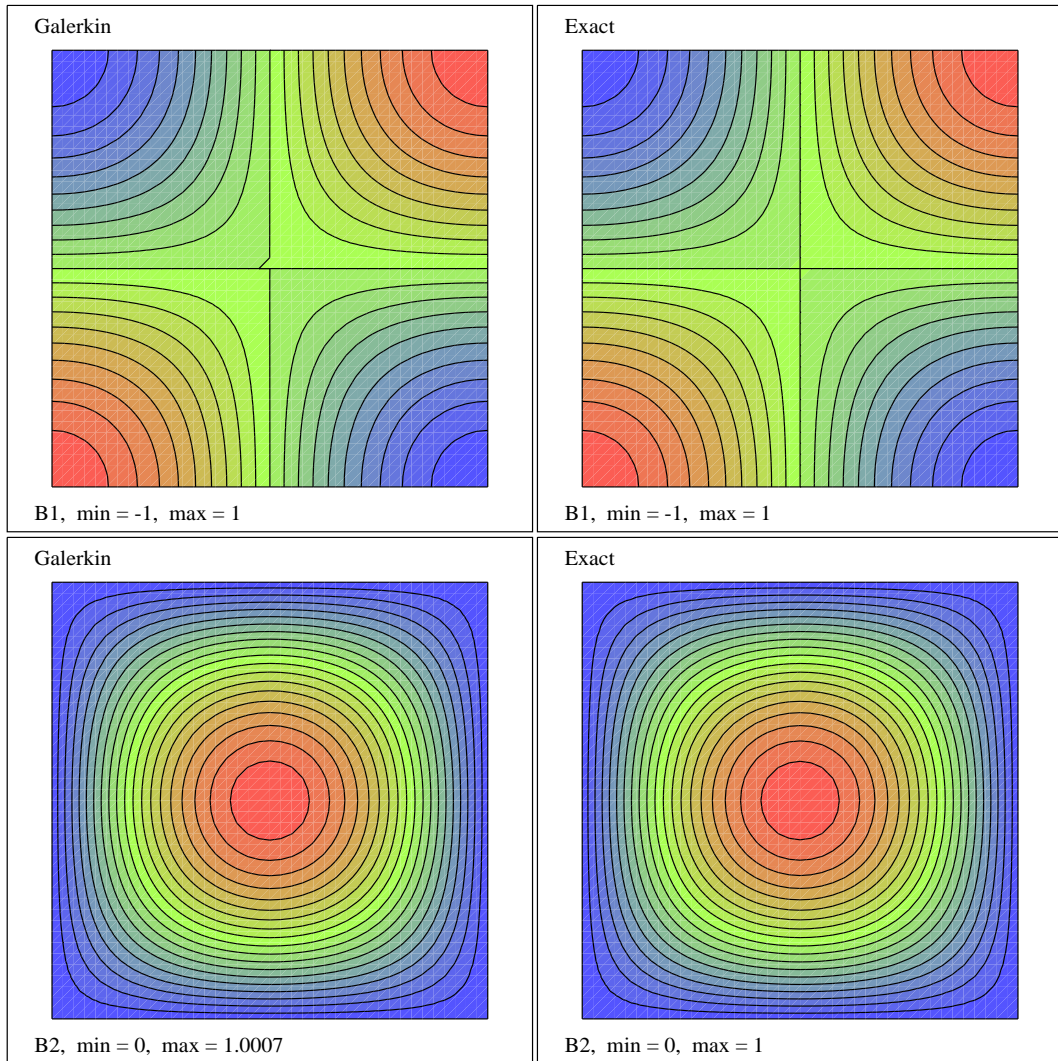


Figure 4.3: Standard Galerkin FEM and exact solutions for the magnetic field(B_1, B_2)

Solution of the MHD equations with stabilized finite element methods (SUPG, SSM)

Another alternative for obtaining stable solutions for the MHD equations is to use stabilized finite element methods. The same test problem is solved by using SUPG and SSM methods and obtained solutions are compared with the exact one. We will concentrate on the pressure solutions in which the stabilization is more effective.

It is seen from the Figure (4.6) that, SSM gets more accurate solutions compared to SUPG method although the stabilization is pronounced in both of the methods. The SSM is more effective in the elimination of the disturbances and oscillations in the pressure solution. This can be observed clearly from the Figure (4.7). Notice that, pressure contours obtained from SSM is more accurate compared to solutions obtained from SUPG.

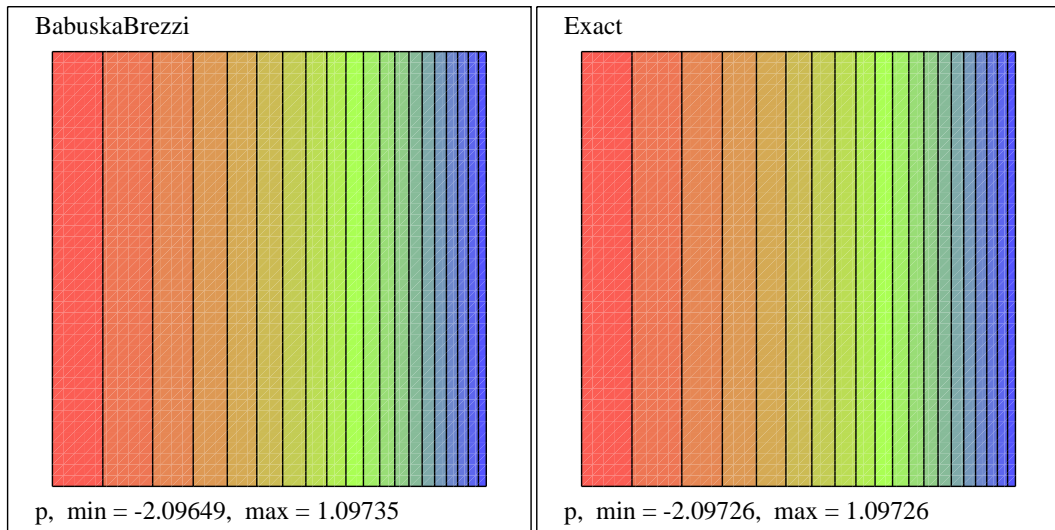


Figure 4.4: Pressure contours obtained from FEM with Babuska-Brezzi condition and exact solutions

As stated in the solution of the Navier-Stokes equations, the location of the subgrid point is effective in the stabilization. The position of the subgrid point is determined by the direction and magnitude of the velocity flow vector during the iteration process. In Figure (4.8), the resulting velocity flow vector and the location of the subgrid point which plays the main role in the stabilization, for each element are displayed over the global mesh. It is seen that in the regions where the magnitude of the velocity is effective, the subgrid point is located through the flow direction.

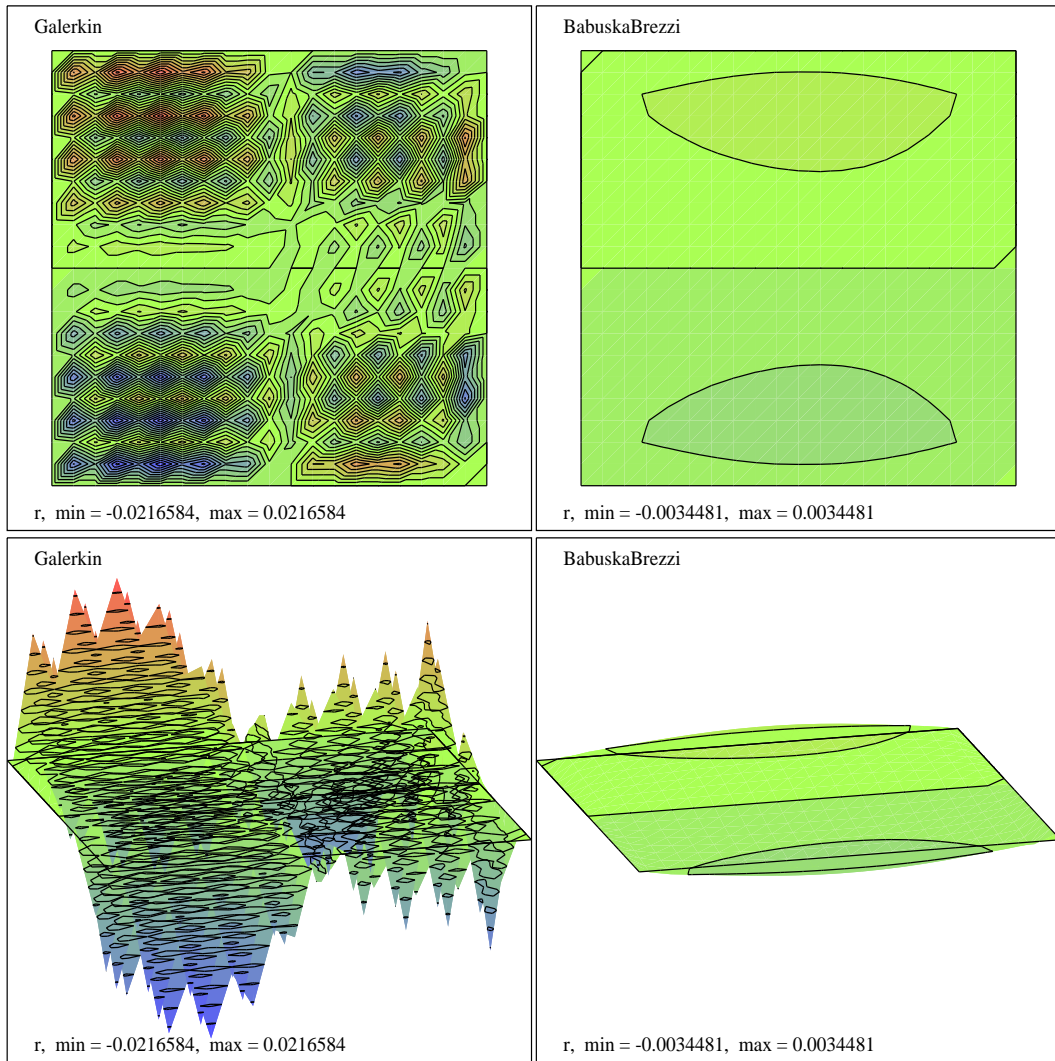


Figure 4.5: Magnetic pressure contours and elevations obtained from standard Galerkin FEM and Babuska-Brezzi condition (Q2-Q2-Q2-Q1 elements)

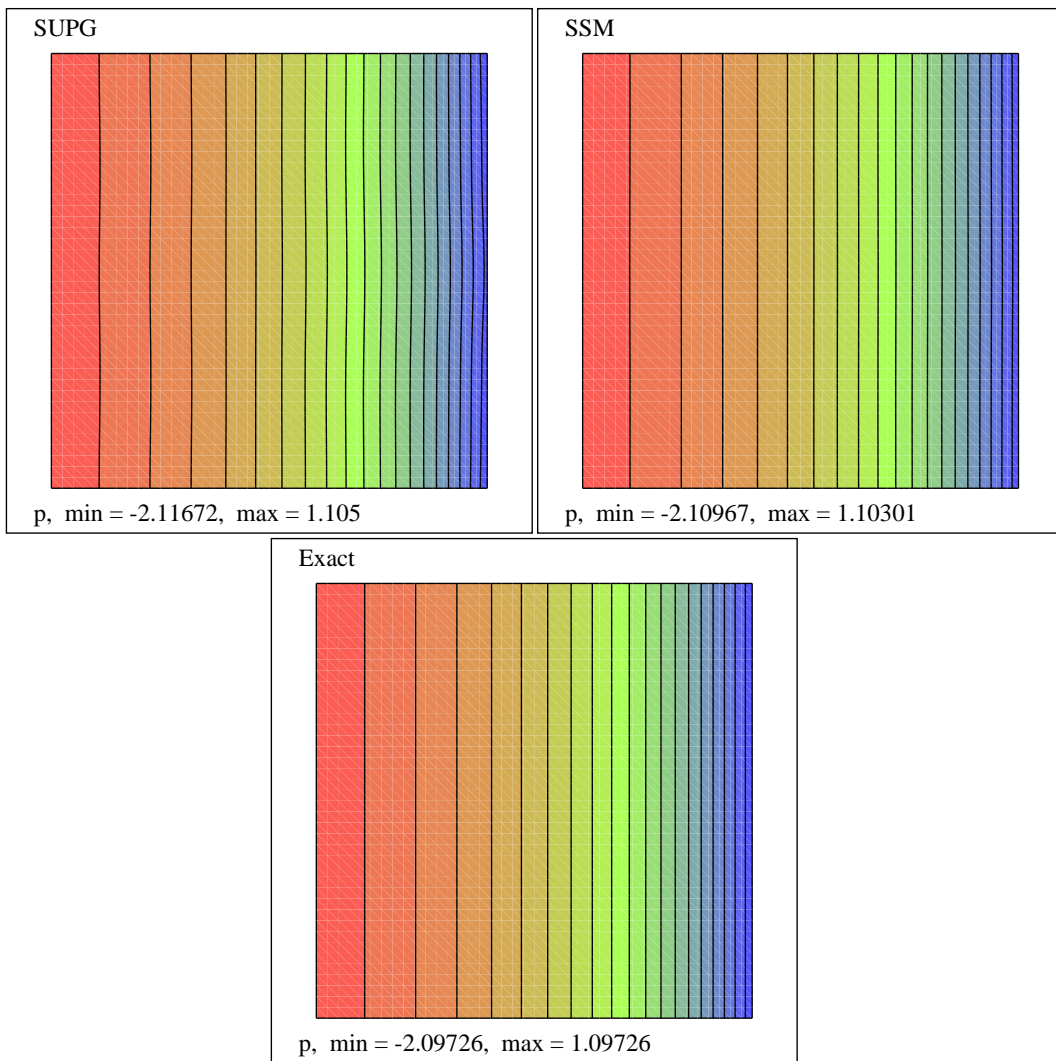


Figure 4.6: Pressure contours obtained from SUPG, SSM and exact solutions

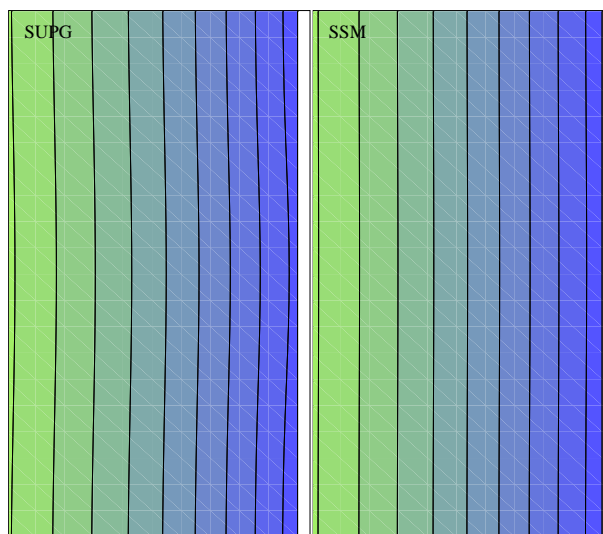


Figure 4.7: Zoom for the pressure contours obtained from SUPG, SSM

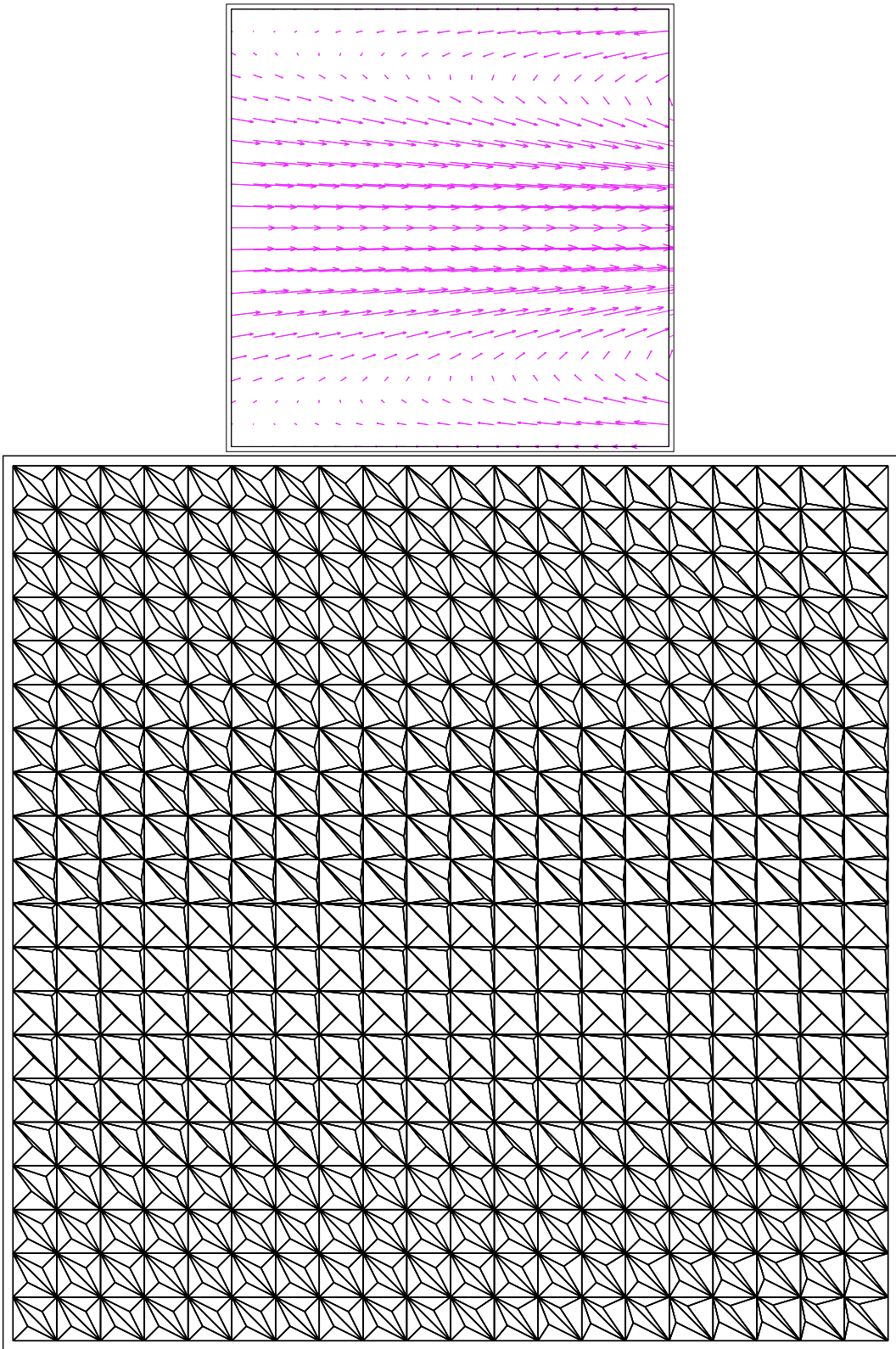


Figure 4.8: Velocity flow vectors and adaption of the position of the subgrid point

4.6.2 MHD Cavity flow

MHD equations (4.6)-(4.10) are solved in a square cavity (Figure (4.9)). Fluid Reynolds number and the magnetic Reynolds numbers are fixed as $Re = 400$, $Rem = 40$ in the calculations. The effect of the different values in the Hartmann number ($Ha = 0, 10, 100$) is observed in the flow under applied magnetic field through $+x$ -direction.

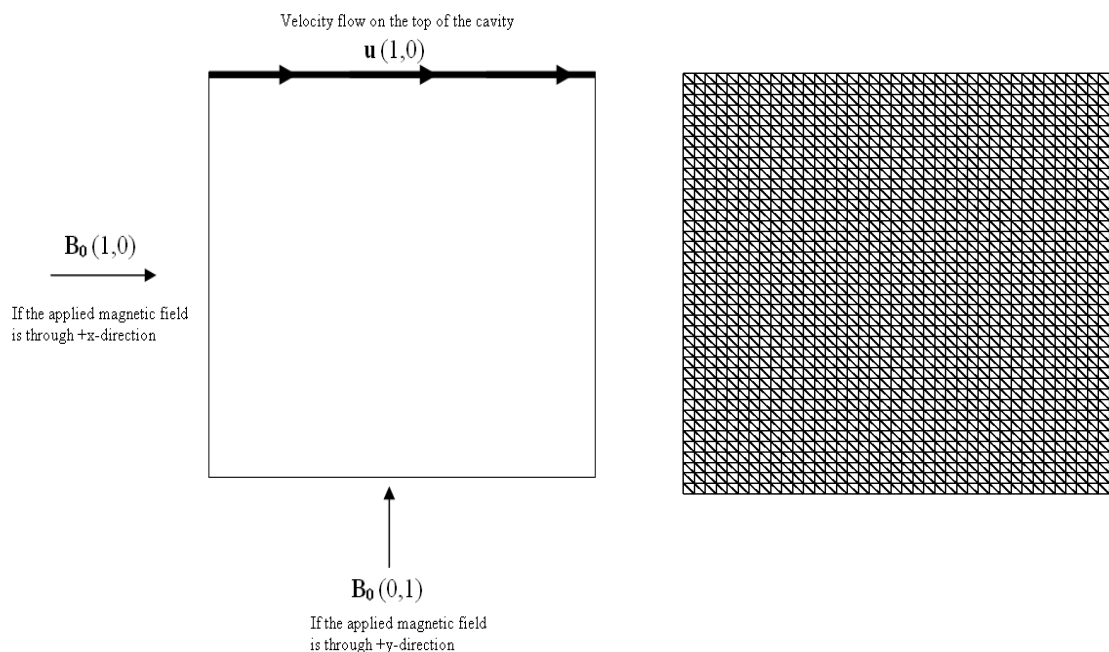


Figure 4.9: The problem statement and a uniform mesh with 3200 triangular elements for MHD cavity flow

In Figures (4.10) and (4.11), changes in the flow for different values of the Hartmann number are displayed in terms of pressure contours and elevations with the solutions obtained by SUPG, SSM and Babuska-Brezzi formulations. It is seen that, SSM again predicts the solution more accurately comparing to SUPG method in the sense of maximum and minimum values and captures the characteristic behavior of the pressure at the peak points which are located at right and left upper sides of the cavity. The existence of the boundary layer formation which is the well-known behaviour of the MHD flows, is displayed in the Figure (4.12) in terms of the first component of the velocity as Hartmann number increases. Also streamlines for the velocity and flow vectors for the magnetic field are displayed in the Figures (4.13) and (4.14), respectively. Obtained solutions which are compatible with the solutions in the literature, show the validity of the proposed method.

The cavity flow problem is also solved with SSM when the magnetic field is applied through $+y$ -direction for the same fluid Reynolds number, magnetic Reynolds number and Hartmann

numbers 10 and 100. In the Figure (4.15), it is seen that as Hartmann number increases, pressure contours are getting perpendicular to the y - axis and boundary layer formation in the velocity and in the magnetic field is pronounced more clearly. The same behaviour is observed from the streamlines of the velocity and flow vectors of the magnetic field in Figure (4.16). The square cavity problem was solved with a finite element method of a biharmonic mathematical model with stream function / magnetic potential form in [45], using stream function-vorticity approach for the unsteady case in [51], and for the 3-D case in [61]. Our solutions show the similar behaviour with these solutions.

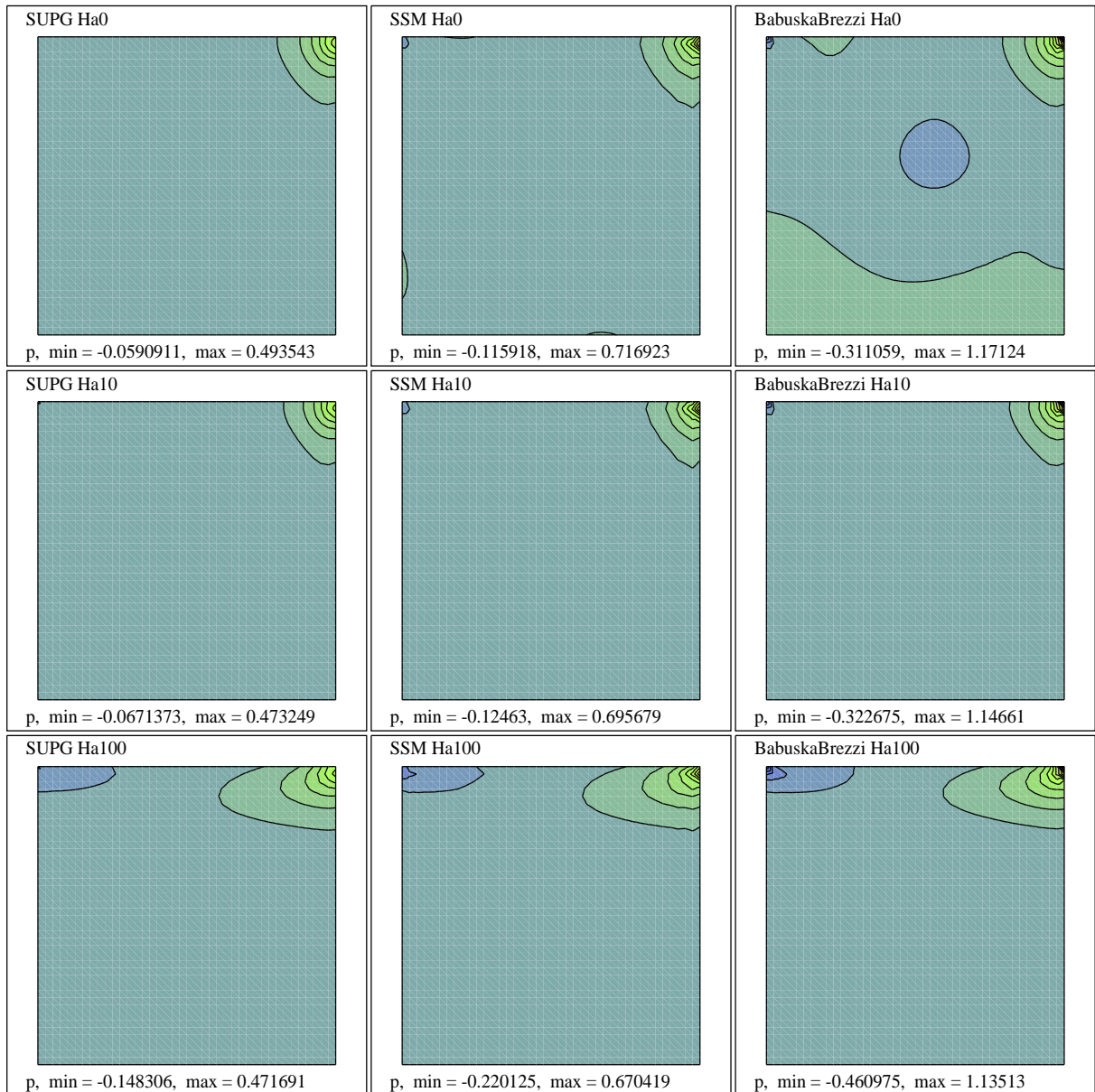


Figure 4.10: Pressure contours obtained from SUPG, SSM and Babuska-Brezzi formulations for $Ha = 0$, $Ha = 10$ and $Ha = 100$; applied magnetic field is through $+x$ direction

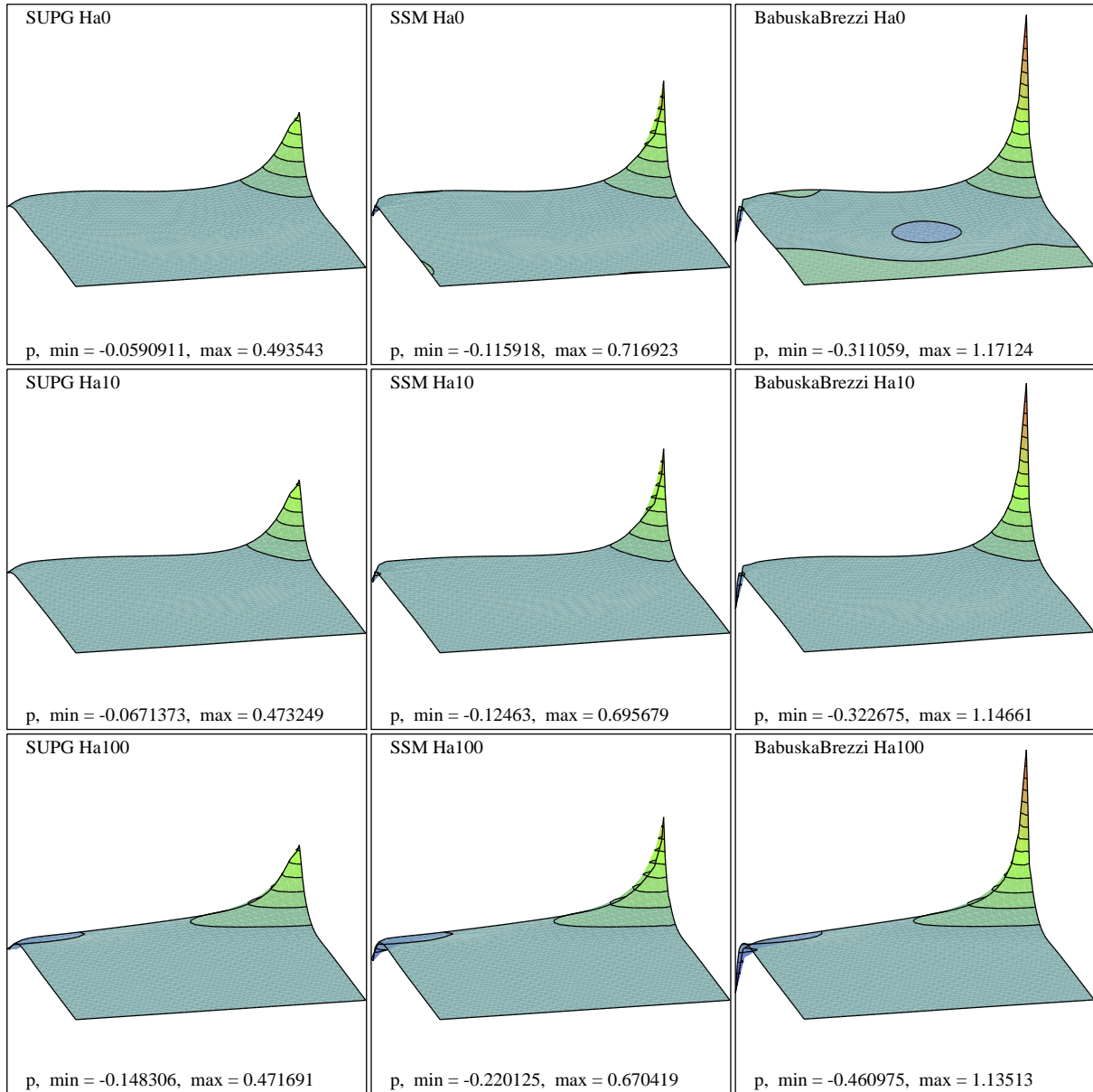


Figure 4.11: Pressure elevations obtained from SUPG, SSM and Babuska-Brezzi formulations for $Ha = 0$, $Ha = 10$ and $Ha = 100$; applied magnetic field is through $+x$ direction

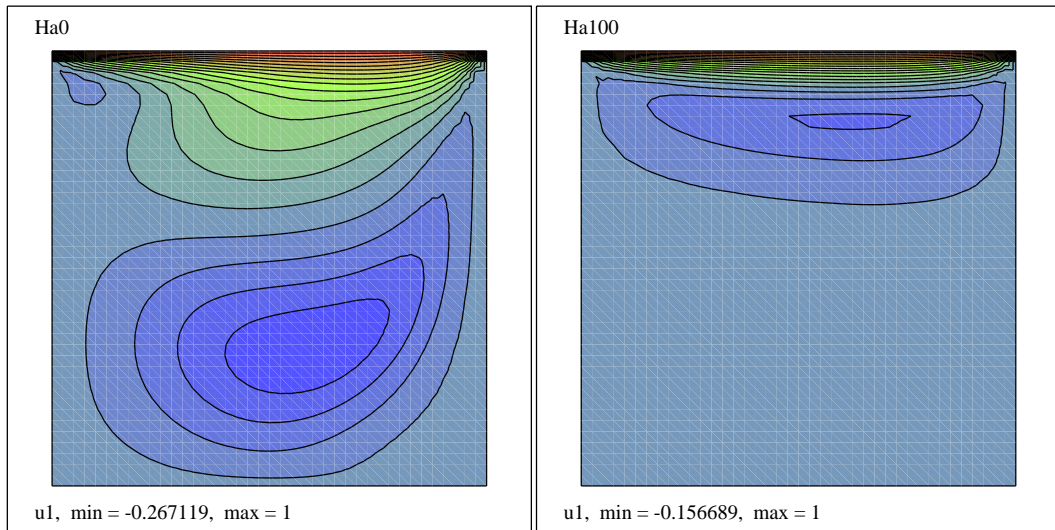


Figure 4.12: Velocity component (u_1) contours for $Ha = 0$ and $Ha = 100$ with SSM; applied magnetic field is through $+x$ direction

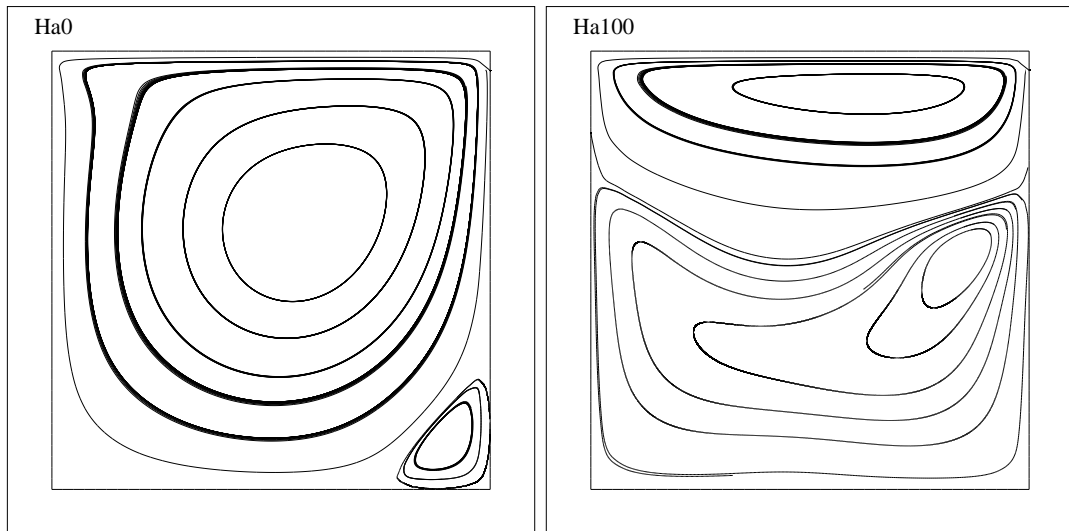


Figure 4.13: Streamlines of the velocity for $Ha = 0$ and $Ha = 100$ with SSM; applied magnetic field is through $+x$ direction

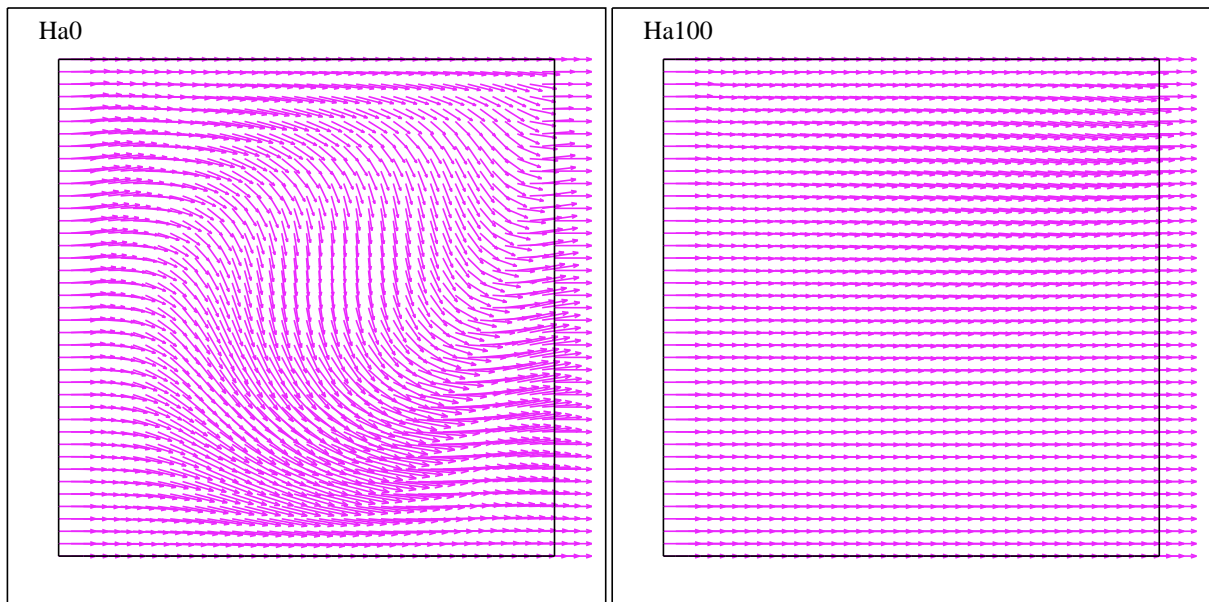


Figure 4.14: Flow vectors of the magnetic field for $Ha = 0$ and $Ha = 100$ with SSM; applied magnetic field is through $+x$ direction

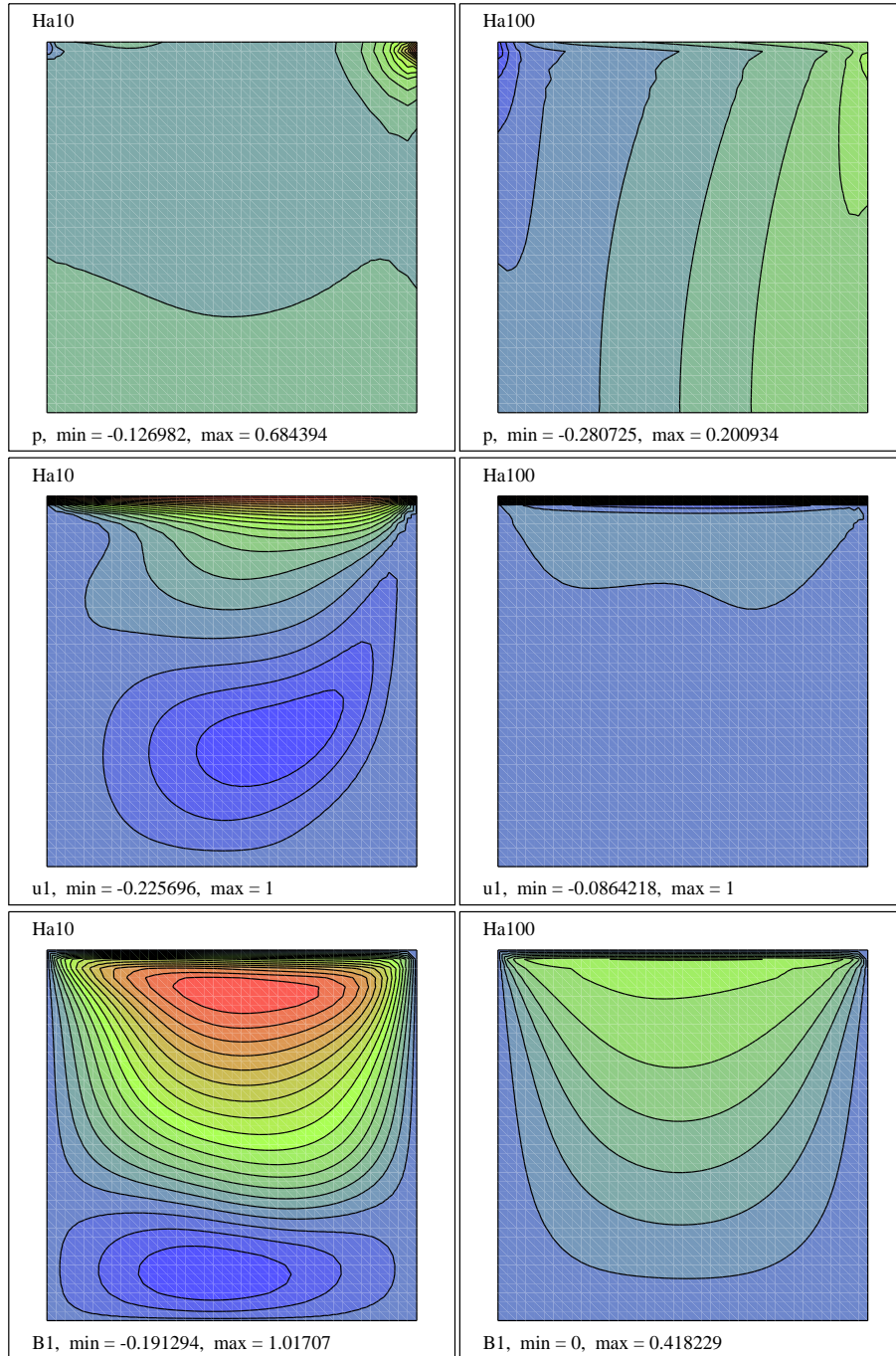


Figure 4.15: Pressure, first component of the velocity and magnetic field contours for $Ha = 10$ and $Ha = 100$ with SSM; applied magnetic field is through $+y$ direction

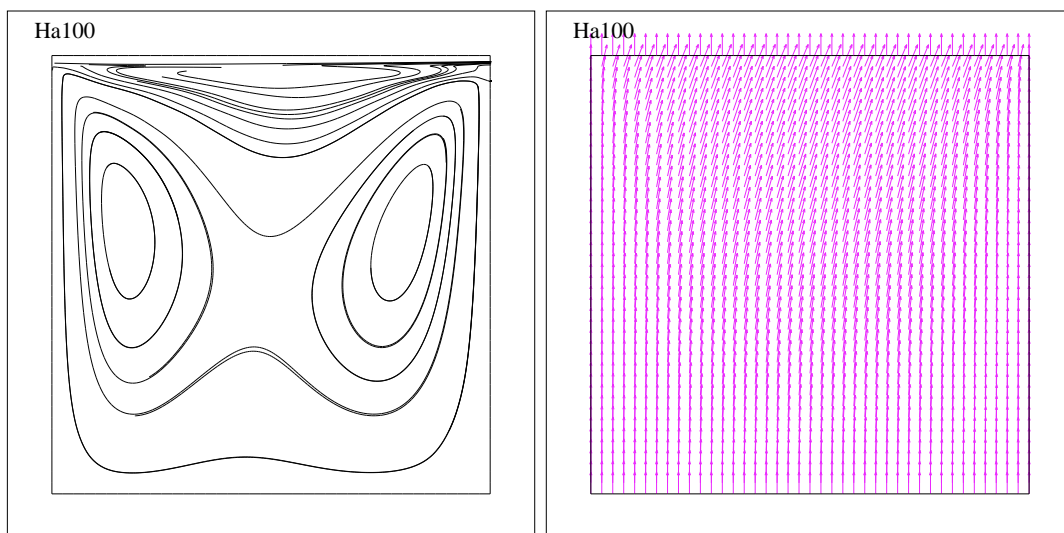


Figure 4.16: Streamlines of the velocity and flow vectors of the magnetic field for $Ha = 100$ with SSM; applied magnetic field is through $+y$ direction

4.6.3 MHD flow over a step

This is another standard benchmark problem. The statement of the problem and the mesh is given in Figure (4.17). The flow of the fluid is through $+x$ -direction and applied magnetic field is through $+y$ direction. The walls of the pipe are considered as perfect conductors. The velocity is prescribed at the inlet and outlet to a Poiseuille profile such that $\mathbf{u}_{\text{out}} = \frac{1}{2}\mathbf{u}_{\text{in}}$. The problem is solved with SSM for $Re = 100$, $Rem = 1$ and Hartmann numbers 0, 5 and 10.

Figures (4.18) and (4.19) show the magnetic field effect in the pressure and in the x -component of the magnetic field as Hartmann number changes, respectively. It is displayed in terms of streamlines in the Figure (4.20) that, the recirculation after the step decreases as Hartmann number increases. Obtained solutions are in good agreement with the other solutions in the literature [17, 31].

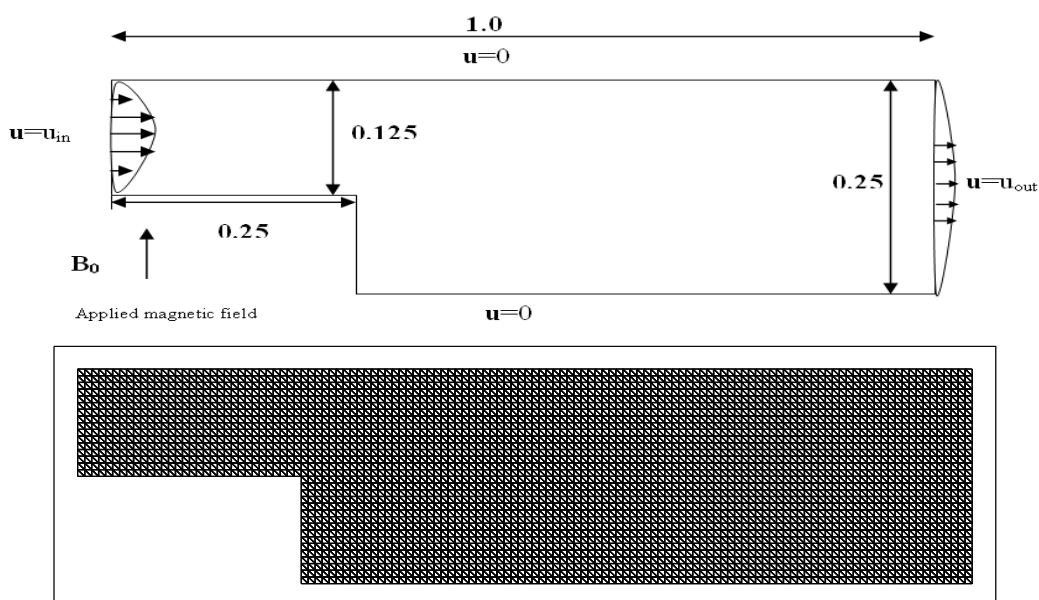


Figure 4.17: The problem statement and a uniform mesh with 7168 triangular elements for the MHD step flow

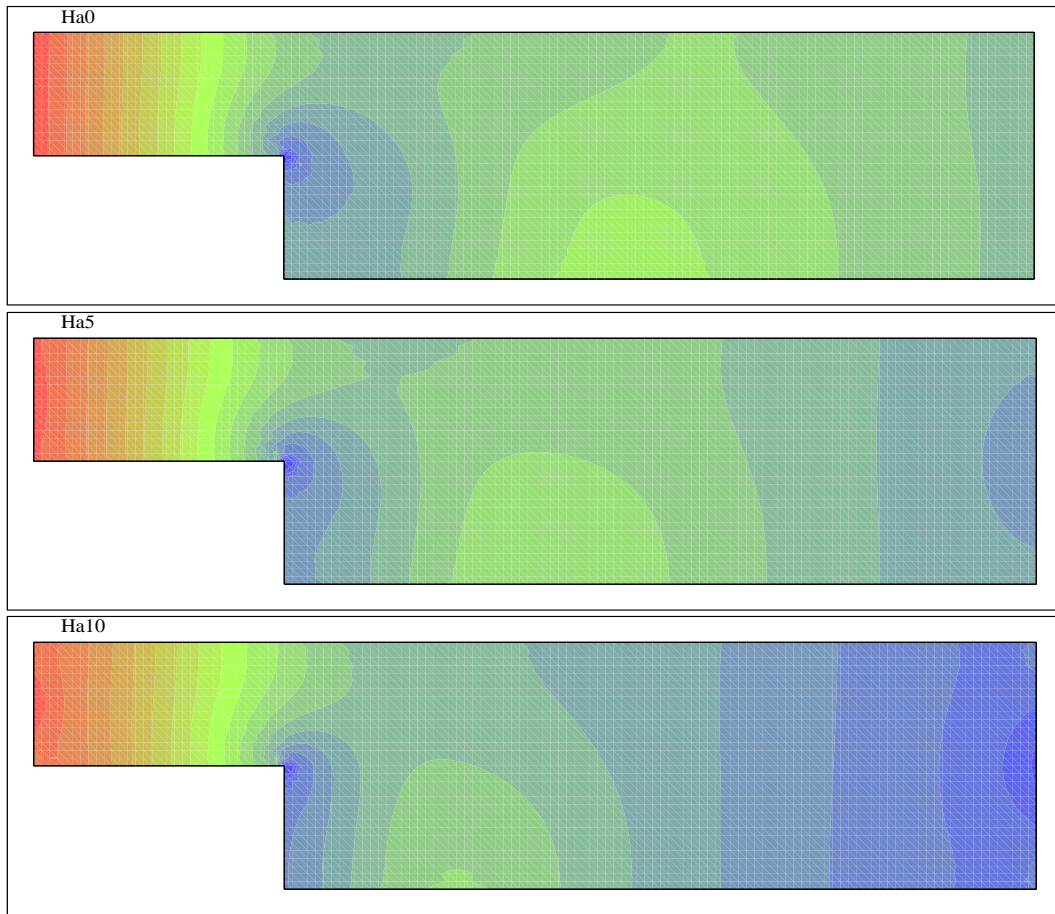


Figure 4.18: Pressure contours for $Ha = 0$, $Ha = 5$ and $Ha = 10$

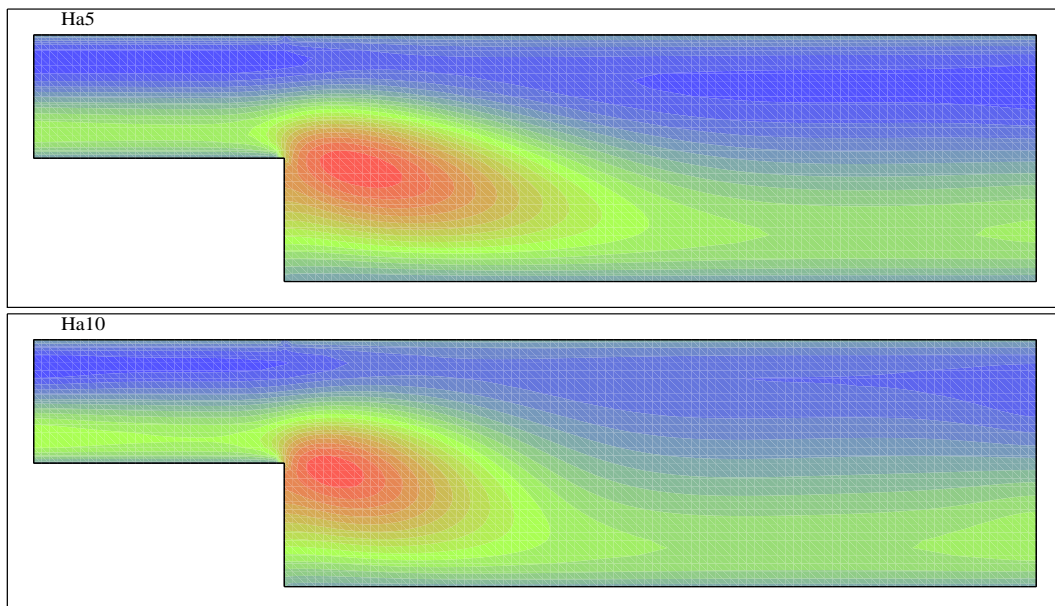


Figure 4.19: x-component (B_1 contours) of the magnetic field for $Ha = 5$ and $Ha = 10$

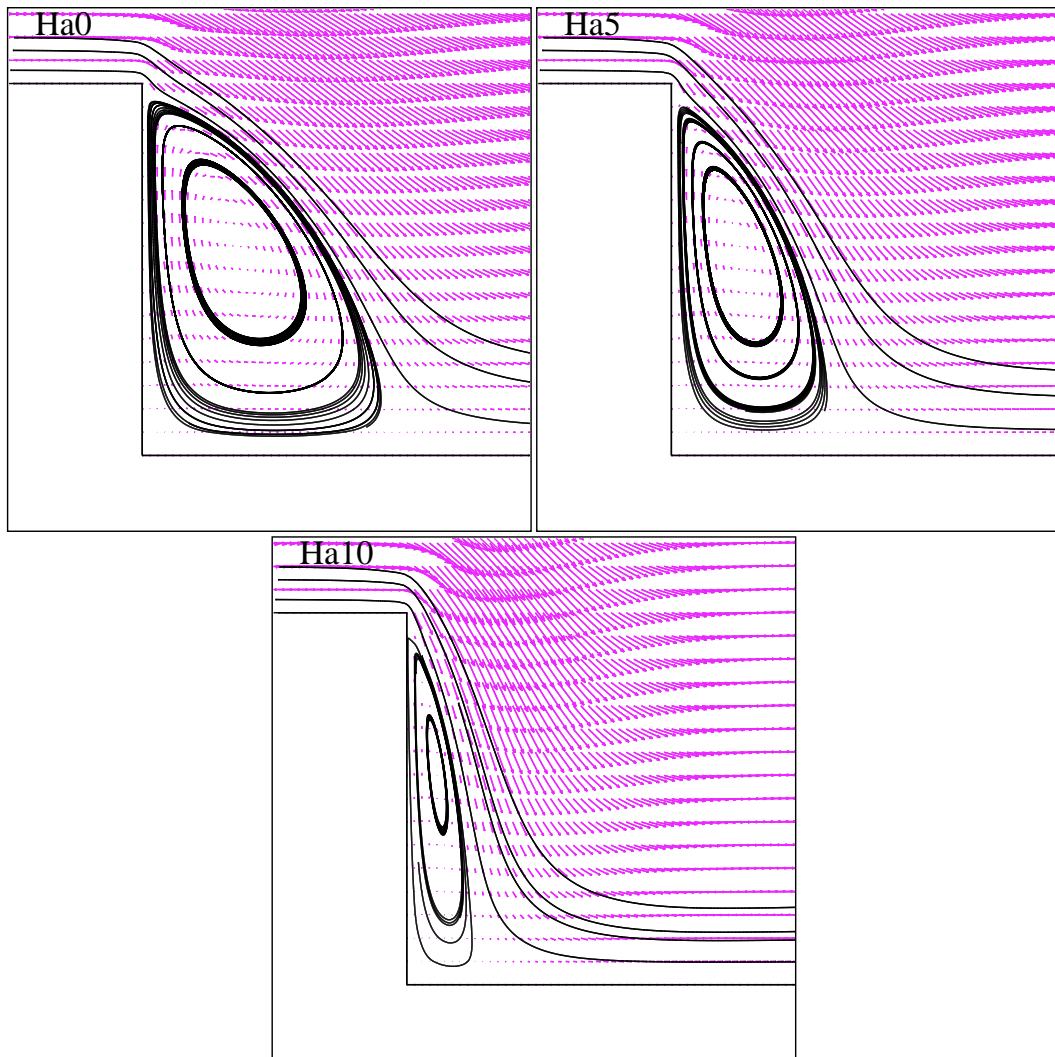


Figure 4.20: Velocity flow vectors and streamlines (zoom in behind the step) for $Ha = 0$, $Ha = 5$ and $Ha = 10$

4.6.4 MHD Duct flow

In this example, we consider the simplified form of the unsteady magnetohydrodynamic equations when the flow is considered in a rectangular duct with a cross-section in the xy -plane. The flow is in the direction of the duct axis which is the z -axis.

The governing equations of MHD flow are obtained from Maxwell equations of electromagnetism and the basic equations of fluid mechanics. The unsteady, laminar, fully developed flow of viscous, incompressible and electrically conducting fluid in a rectangular duct, subject to a constant and uniform applied magnetic field B_0 which is parallel to x -axis are expressed in non-dimensional form with the equations [20]

$$\begin{cases} \nabla^2 V + M \frac{\partial B}{\partial x} = -1 + \frac{\partial V}{\partial t} \\ \nabla^2 B + M \frac{\partial V}{\partial x} = \frac{\partial B}{\partial t} \end{cases} \quad (4.65)$$

in $\Omega \times [0, \infty)$ with the boundary conditions and the initial condition

$$\begin{cases} V(x, y, t) = 0 & B(x, y, t) = 0 & (x, y) \in \partial\Omega \\ V(x, y, 0) = 0 & B(x, y, 0) = 0 & (x, y) \in \Omega \end{cases} \quad (4.66)$$

where the boundaries are assumed to be insulating, M is the Hartmann number and $V(x, y, t)$ and $B(x, y, t)$ are the velocity and the induced magnetic field respectively. Here, there are only z -components of the velocity and the induced magnetic field.

Equations (4.65) are first decoupled using the following transformation

$$U_1 = V + B \quad U_2 = V - B. \quad (4.67)$$

Addition and subtraction of equations (4.65) and substituting the new variables defined in Equation (4.67) yield

$$\begin{cases} \nabla^2 U_1 + M \frac{\partial U_1}{\partial x} = -1 + \frac{\partial U_1}{\partial t} \\ \nabla^2 U_2 - M \frac{\partial U_2}{\partial x} = -1 + \frac{\partial U_2}{\partial t} \end{cases} \quad \text{in } \Omega \times [0, \infty) \quad (4.68)$$

and homogeneous boundary and initial conditions

$$\begin{cases} U_1(x, y, t) = 0 & U_2(x, y, t) = 0 & (x, y) \in \partial\Omega \\ U_1(x, y, 0) = 0 & U_2(x, y, 0) = 0 & (x, y) \in \Omega. \end{cases} \quad (4.69)$$

Notice that, the resulting equations are convection-diffusion type with the only difference between them is $+M$ and $-M$, and for high values of Hartmann number, it takes the convection

dominated form. Therefore, in order to obtain accurate result, equations (4.68) should be solved using a stabilized finite element method in spatial domain.

The time dependent MHD equations defining viscous, laminar flow of an incompressible electrically conducting fluid in a square duct [3] $-1 \leq x, y \leq 1$ for the time domain $[0, T]$ are solved for moderate ($M = 100$) and high values(1000, 10000) of Hartmann number. The space discretization is performed using 1600 uniformly distributed rectangular elements for moderate values of Hartmann number and 6400 elements for high values of Hartmann number. The combination of the shape functions are bilinear in spatial domain and linear in time direction. Increasing the number of elements is not sufficient for obtaining stable results. Therefore, SUPG stabilized finite element method is made use of in space dimensions throughout the computations especially for high Hartmann number. It is also well known that, as time increases, the flow behaves as in steady MHD flow. Therefore, it is possible to compare the results in steady-state with the Shercliff's [67] exact solution. The unsteady MHD flow problem has been solved by Tezer and Bozkaya [3] using the combination of DQM time-DRBEM in space formulations for moderate Hartmann number. Here the combination of stabilized FEM in space-FEM in time formulation made it possible to increase M up to 10000.

In Figures (4.21), velocity(V) and induced magnetic field(B) lines(contours) are displayed for moderate($M = 100$) value of Hartmann number at the time levels $t = 0.01$ and $t = 0.03$. The selected time step through the iterations is $\Delta t = 0.01$. It is seen that, in the third iteration, steady-state case is reached. Results are compared with the exact solutions and the agreement is observed. Also, existence of boundary layer formation as M increases and time increases which is the well-known behavior of MHD duct flow is also seen from the figures.

As the Hartmann number increases, small time steps should be used in order to capture the behavior of the flow. Therefore for Hartmann number 1000, Δt is selected as 0.001. Obtained results at the time level $t = 0.001$ and $t = 0.003$ at which flow reaches steady-state, are displayed in Figure (4.22). Also, boundary layer formation is shown more clearly.

For Hartmann number 10000, stable results are obtained and displayed in Figure (4.23). Although, small time step ($\Delta t = 0.001$) is used, steady-state results are obtained just in the first iteration. Results agree very well with the previously obtained results and exact solution of steady MHD duct flow problem, [54, 67].

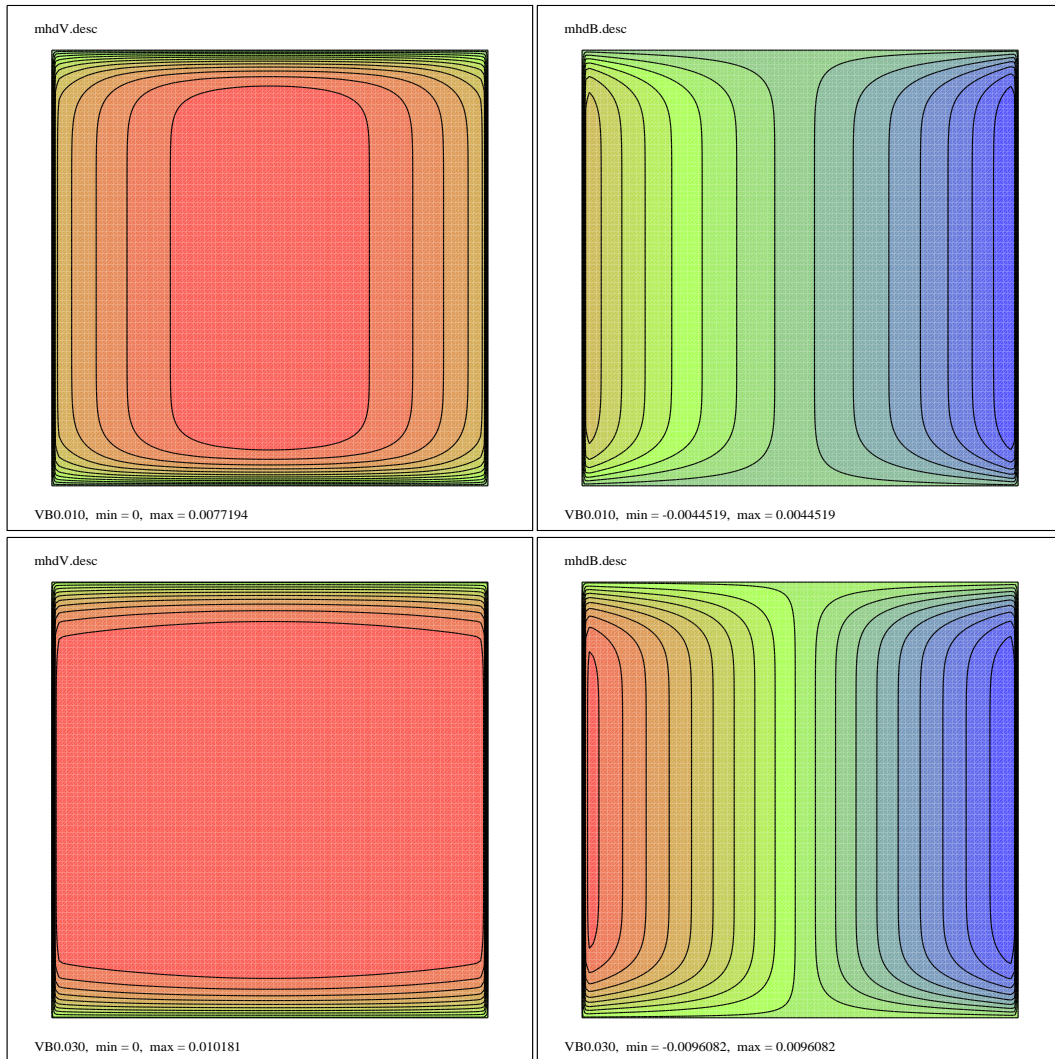


Figure 4.21: Velocity and induced magnetic field contours at $t = 0.01$ and $t = 0.03$ for $M = 100$

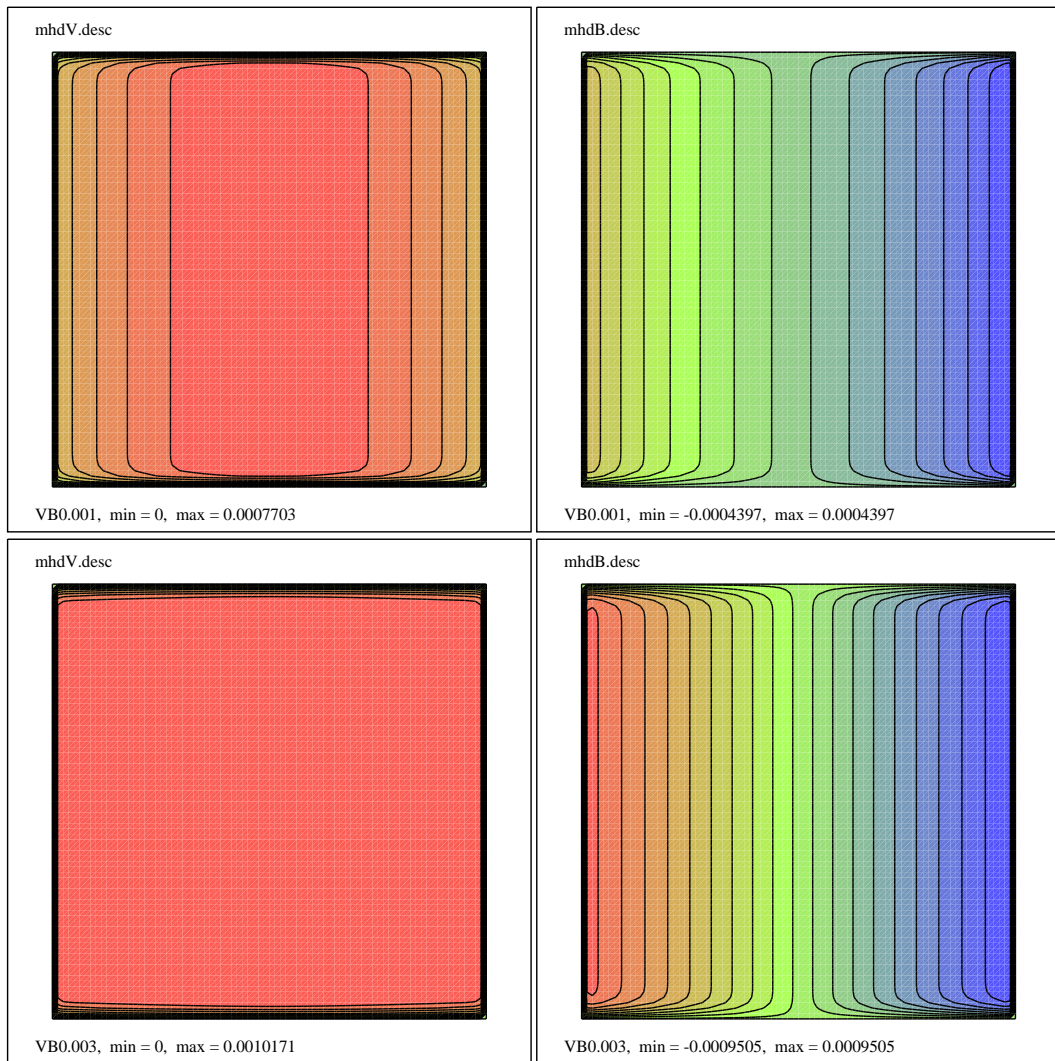


Figure 4.22: Velocity and induced magnetic field contours at $t = 0.001$ and $t = 0.003$ for $M = 1000$

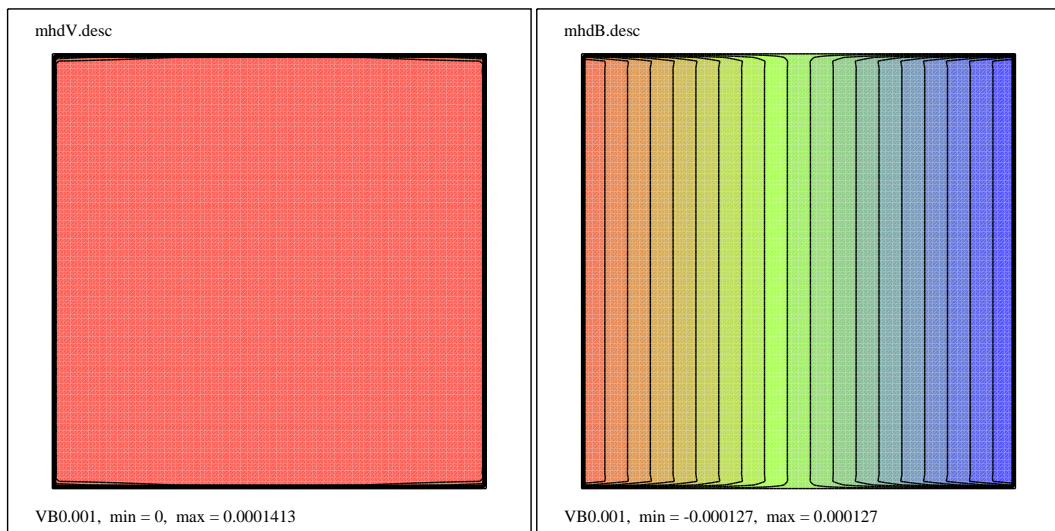


Figure 4.23: Velocity and induced magnetic field contours at $t = 0.001$ for $M = 10000$

CHAPTER 5

CONCLUSION

In this thesis, a stabilizing subgrid method, in the framework of a two-level finite element method with a stabilizing subgrid of a single node, is described for solving the incompressible Navier-Stokes equations as well as the magnetohydrodynamic equations. The domain is planar and the discretization is triangular. The presentation above shows that the TLFEM with the stabilizing subgrid produces stable and accurate approximations in a variety of problem configurations. Applications include convection dominated L-Shape flow and rotating flow field problems defined by convection-diffusion equation. The Navier-Stokes equations are solved for lid-driven cavity flow, backward facing step flow and flow past a cylinder. It is observed that the oscillations in the pressure disappeared when the stabilized FEM methods are used. The SSM is preferred in the sense of computational cost and accuracy. Numerical experiments further indicate that the proper choice of the subgrid node may play a significant role in obtaining more accurate approximations, especially for high values of Reynolds number.

The stabilized FEM methods (SUPG, TLFEM and SSM) are applied for solving the incompressible MHD equations in terms of the velocity, the induced magnetic field and the pressure. Applications on the test problems as MHD cavity flow and MHD flow over a step verified that SSM predicts the solution more accurately comparing to SUPG and captures the characteristic behaviour of the pressure. All these stabilized methods exhibit the well known behaviour of the velocity and the induced magnetic field in the MHD flow.

The stabilized FEM of SUPG type in space - the FEM in the time domain formulation is used in solving transient flow governed by incompressible Navier-Stokes equations. The approximation is based on the idea of separation of variables in terms of the shape functions corresponding to the space and time. The proposed stabilized FEM in space - FEM in time domain procedure enables one to circumvent the oscillations in the solution and eliminates the need of using very small time steps concerning stability. Applications include vortex flow and flow around a cylinder problems. The unsteady MHD equations which are simplified for the case of fully developed flow are also solved in a rectangular duct with insulated walls by using FEM in time - stabilized

FEM in space procedure. The velocity and the induced magnetic field values are obtained for high values of Hartmann number.

Further studies should be concentrated on obtaining solutions to the Navier-Stokes and MHD equations by combining the stabilized subgrid and adaptive grid ideas in the finite element method. Extensions of these stabilized FEMs to 3-dimensional Navier-Stokes and magnetohydrodynamic equations are still continuing research problems.

REFERENCES

- [1] Babuska I. The finite element method with Lagrangian multipliers. *Numer. Math.* 1973; **20**: 179–192.
- [2] Biros G, Ying L, Zorin D. *An embedded boundary integral solver for the unsteady incompressible Navier-Stokes equations*. New York University, Computer Science, Technical Reports, TR2003-838, November 2002.
- [3] Bozkaya C, Tezer-Sezgin M. Boundary element solution of unsteady magnetohydrodynamic duct flow with differential quadrature time integration scheme. *Int. J. Numer. Meth. Fluids* 2006; **51**: 567–584.
- [4] Brezzi F. On the existence, uniqueness and approximation of saddle-point problems arising from Lagrange multipliers. *RAIRO Ser. Rouge* 1974; **8**: 129–151.
- [5] Brezzi F, Bristeau MO, Franca LP, Mallet M, Rogé G. A relationship between stabilized finite element methods and the Galerkin method with bubble functions. *Comput. Methods Appl. Mech. Engrg.* 1992; **96**: 117–129.
- [6] Brezzi F, Franca LP, Hughes TJR, Russo A. Stabilization techniques and subgrid scales capturing. *In the Proceedings of the Conference “State of the Art in Numerical Analysis”*. York, England, April 1-4, 1996.
- [7] Brezzi F, Franca LP, Russo A. Further considerations on residual-free bubbles for advective-diffusive equations. *Comput. Methods Appl. Mech. Engrg.* 1998; **166**: 25-33.
- [8] Brezzi F, Hughes TJR, Marini LD, Russo A, Suli E. A priori error analysis of residual-free bubbles for advection-diffusion problems. *SIAM J. Numer. Anal.* 1999; **36**: 1933–1948.
- [9] Brezzi F, Marini D, Russo A. Applications of the pseudo residual-free bubbles to the stabilization of convection-diffusion problems. *Comput. Methods Appl. Mech. Engrg.* 1998; **166**: 51–63.
- [10] Brezzi F, Marini D, Russo A. On the choice of a stabilizing subgrid for convection-diffusion problems. *Comput. Methods Appl. Mech. Engrg.* 2005; **194**: 127–148.

- [11] Brezzi F, Marini LD, Suli E. The residual-free bubbles for advection-diffusion problems: The general error analysis. *Numer. Math.* 2000; **85**: 31–47.
- [12] Brezzi F, Russo A. Choosing bubbles for advection-diffusion problems. *Math. Mod. Meth. Appl. Sci.* 1994; **4**: 571–587.
- [13] Brooks AN, Hughes TJR. Streamline upwind/Petrov-Galerkin formulations for convection dominated flows with particular emphasis on the incompressible Navier-Stokes equations. *Comput. Methods Appl. Mech. Engrg.* 1982; **32**: 199–259.
- [14] Ciarlet PG. *The Finite Element Methods for Elliptic Problems*. North-Holland, Amsterdam, 1978.
- [15] Chawla MM, Al-Zanaidi MA. An extended trapezoidal formula for the diffusion equation in two space dimensions. *Comput. Math. Appl.* 2001; **42**: 157–168.
- [16] Codina R, Blasco J, Buscaglia GC, Huerta A. Implementation of a stabilized finite element formulation for the incompressible Navier-Stokes equations based on a pressure gradient projection. *Int. J. Numer. Meth. Fluids* 2001; **37**: 419–444.
- [17] Codina R, Silva NH. Stabilized finite element approximation of the stationary magneto-hydrodynamics equations. *Comput. Mech.* 2006; **38**: 344–355.
- [18] Dettmer W, Perić D. An analysis of the time integration algorithms for the finite element solutions of incompressible Navier-Stokes equations based on a stabilized formulation. *Comput. Methods Appl. Mech. Engrg.* 2003; **192**: 1117–1226.
- [19] Donea J, Huerta A. *Finite Element Methods for Flow Problems*, John Wiley & Sons, Ltd., England, 2003.
- [20] Dragos L. *Magnetofluid Dynamics*. Abacus Press, 1975.
- [21] Fornberg B. Computing steady incompressible flows past blunt bodies: A historical overview, *Numerical methods for fluid dynamics 4*, M.J. Baines and K.W. Morton, Clarendon Press, London, 1993; 115–133.
- [22] Franca LP, Dutra do Carmo EG. The Galerkin Gradient Least-squares method. *Comput. Methods Appl. Mech. Engrg.* 1989; **74**: 41–54.
- [23] Franca LP, Farhat C. Bubble functions prompt unusual stabilized finite element methods. *Comput. Methods Appl. Mech. Engrg.* 1995; **123**: 299–308.
- [24] Franca LP, Frey SL. Stabilized finite element methods: II. The incompressible Navier-Stokes equations. *Comput. Methods Appl. Mech. Engrg.* 1992; **99**: 209–233.

- [25] Franca LP, Frey SL, Hughes TJR. Stabilized finite element methods: I. Application to the advective-diffusive mode. *Comput. Methods Appl. Mech. Engrg.* 1992; **95**: 253–276.
- [26] Franca LP, Macedo AP. A two-level finite element method and its application to the Helmholtz equation. *Int. J. Numer. Meth. Engrg.* 1998; **43**: 23–32.
- [27] Franca LP, Neslitürk A. On a two-level finite element method for the incompressible Navier-Stokes equations. *Int. J. Numer. Meth. Engrg.* 2001; **52**: 433–453.
- [28] Franca LP, Neslitürk A, Stynes M. On the stability of residual-free bubbles for convection-diffusion problems and their approximation by a two-level finite element method. *Comput. Methods Appl. Mech. Engrg.* 1998; **166**: 35–49.
- [29] Franca LP, Valentin F. On an improved unusual stabilized finite element method for the advective-reactive-diffusive equation. *Comput. Methods Appl. Mech. Engrg.* 2000; **190 (13-14)**: 1785–1800.
- [30] Galeão AC, Dutra do Carmo G. A consistent approximate upwind Petrov-Galerkin method for convection-dominated problems. *Comput. Methods Appl. Mech. Engrg.* 1988; **68**: 83–95.
- [31] Gerbeau JF. A stabilized finite element method for the incompressible magnetohydrodynamic equations. *Numer. Math.* 2000; **87**: 83–111.
- [32] Ghia U, Ghia KN, Shin CT. High-resolutions for incompressible flow using the Navier-Stokes equations and a multigrid method. *J. Comput. Phys.* 1982; **48**: 387–411.
- [33] Gunzburger MD, Meir AJ, Peterson JS. On the existence, uniqueness, and finite element approximation of solutions of the equations of stationary, incompressible magnetohydrodynamics. *Math. Comp.* 1991; **56 (194)**: 523–563.
- [34] Hasler U, Schneebeli A, Schötzau D. Mixed finite element approximation of incompressible MHD problems based of weighted regularization. *Appl. Numer. Math.* 2004; **51**: 19–45.
- [35] Houston P, Süli E. Adaptive Lagrange-Galerkin Methods for Unsteady Convection-Diffusion Problems. *Math. Comp.* 2000; **70 (233)**: 77–106.
- [36] Hughes, TJR. Streamline Upwind/Petrov-Galerkin formulations for convection dominated flows with particular emphasis on the incompressible Navier-Stokes equations. *Comput. Methods Appl. Mech. Engrg.* 1982; **32**: 199–259.
- [37] Hughes TJR. Multiscale phenomena: Green’s functions, the Dirichlet-to-Neumann formulation, subgrid scale models, bubbles and the origin of stabilized methods. *Comput. Methods Appl. Mech. Engrg.* 1995; **127**: 387–401.

- [38] Hughes TJR, Brooks AN. A multidimensional upwind scheme with no crosswind diffusion, Finite Element Methods for Convection Dominated Flows. *Amer. Soc. Mech. Eng.* 1979; 19–35.
- [39] Hughes TJR, Franca LP, Mallet M. A new finite element formulation for computational fluid dynamics: VI. Convergence analysis of the generalized SUPG formulation for linear time-dependent multidimensional advective-diffusive systems. *Comput. Methods Appl. Mech. Engrg.* 1987; **63**: 97–112.
- [40] Hughes TJR, Franca LP, Hulbert GM. A new finite element formulation for computational fluid dynamics: VIII. The Galerkin/least squares method for advective-diffusive equations. *Comput. Methods Appl. Mech. Engrg.* 1989; **73**: 173–189.
- [41] John V. Reference values for drag and lift of a two dimensional time-dependent flow around a cylinder. *Int. J. Numer. Meth. Fluids* 2004; **44**: 777–788.
- [42] John V, Matthies G, Rang J. A comparison of time-discretization/linearization approaches for the incompressible Navier-Stokes equations. *Comput. Methods Appl. Mech. Engrg.* 2006; **195**: 5995–6010.
- [43] Johnson C, Nävert U, Pitkäranta J. Finite element methods for linear hyperbolic problem. *Comput. Methods Appl. Mech. Engrg.* 1984; **45**: 285–312.
- [44] Krzeminski SK, Cala A, Smialek M. Numerical Simulation of 2D MHD Flows Ψ - ξ - \mathbf{A} Method. *IEEE Trans. Magn.* 1996; **32 (3)**: 990–993.
- [45] Krzeminski SK, Smialek M, Wlodarczyk M. Finite element approximation of biharmonic mathematical model for MHD flow using Ψ - \mathbf{A} approach. *IEEE Trans. Magn.* 2000; **36 (4)**: 1313–1318.
- [46] Kumamaru H, Kodama S, Hirano H, Itoh K. Three-dimensional numerical calculations on liquid-metal magnetohydrodynamic flow in magnetic-field inlet-region. *J. Nucl. Sci. Technol.* 2004; **41 (5)**: 624–631.
- [47] Layton WJ, Meir AJ, Schmidt PG. A two-level discretization method for the stationary MHD equations. *ETNA* 1997; **6**: 198–210.
- [48] Liu CH, Leung DYK. Development of a finite element solution for the unsteady Navier-Stokes equations using projection method and fractional- θ -scheme. *Comput. Methods Appl. Mech. Engrg.* 2001; **190**: 4301–4317.
- [49] Meir AJ, Schmidt PG. Analysis and numerical approximation of a stationary MHD flow problem with nonideal boundary. *SIAM J. Numer. Anal.* 1999; **36(4)**: 1304–1332.

- [50] Mittal S, Tezduyar TE. A finite element study of incompressible flow past oscillating cylinders and aerofoils. *Int. J. Numer. Meth. Fluids* 1992; **15**:1703–1118.
- [51] Navarro HA, Cabezas-Gómez L, César da Silva R, Montagnoli AN. A generalized alternating-direction implicit scheme for incompressible magnetohydrodynamic viscous flows at low magnetic Reynolds number. *Appl. Math. Comput.* 2007; **189**: 1601–1613.
- [52] Nesliturk A. Approximating the incompressible Navier-Stokes equations using a two level finite element method. *Ph.D. Thesis*, University of Colorado, Denver, 1999.
- [53] Nesliturk A.I. A Stabilizing subgrid for convection-diffusion problem. *Math. Mod. Meth. Appl. Sci.* 2006; **16 (2)**: 211–231.
- [54] Nesliturk AI, Tezer-Sezgin M. The finite element method for MHD flow at high Hartmann numbers. *Comput. Methods Appl. Mech. Engrg.* 2005; **194**: 1201–1224.
- [55] Nesliturk AI, Tezer-Sezgin M. Finite element method solution of electrically driven magnetohydrodynamic flow. *J. Comput. Appl. Math.* 2006; **192**: 339–352.
- [56] Nesliturk AI, Aydin SH, Tezer-Sezgin M. Two-level finite element method with a stabilizing subgrid for the incompressible Navier-Stokes equations. *Int. J. Numer. Meth. Fluids*, in press.
- [57] Peterson AR. *A first course in fluid dynamics*, Cambridge University Press, 1983.
- [58] Reddy JN. *An Introduction to the Finite Element Method*, McGraw-Hill, 1993.
- [59] Roos HG, Stynes M, Tobiska L. Numerical methods for singularly perturbed differential equations. *Springer Series in Computational Mechanics*, vol.24, Springer-Verlag, Berlin, New-York, 1996.
- [60] Russo A. Bubble Stabilization of Finite Element Methods for the Linearized Incompressible Navier-Stokes Equations. *Comput. Methods Appl. Mech. Engrg.* 1996; **132**: 335-343.
- [61] Salah NB, Soulaïmani A, Habashi WG. A finite element method for magnetohydrodynamics. *Comput. Methods Appl. Mech. Engrg.* 2001; **190**: 5867–5892.
- [62] Salah NB, Soulaïmani A, Habashi WG, Fortin M. A conservative stabilized finite element method for the magneto-hydrodynamic equations. *Int. J. Numer. Meth. Fluids* 1999; **29**: 535–554.
- [63] Sangalli G. Global and local error analysis for the residual-free bubbles method applied to advection-dominated problems. *SIAM J. Numer. Anal.*, 2000; **38**: 1496-1522.

- [64] Schötzau D. Mixed finite element methods for stationary incompressible magneto-hydrodynamics. *Numer. Math.* 2004; **96**: 771–800.
- [65] Segerlind LJ. Weighted residual solutions in the time domain. *Int. J. Numer. Meth. Engng.* 1989; **28**: 679–685.
- [66] Sekhar TVS, Ravikumar TVR, Kumar H. MHD flow past a sphere at low and moderate Reynolds numbers. *Comput. Mech.* 2003; **31**: 437–444.
- [67] Shercliff JA. The motion of conducting fluids in pipes under transverse fields. *Proceedings of the Cambridge Philosophy Society* 1953; **49**: 136–144.
- [68] Sheu TWH, Lin RK. Development of a convection-diffusion-reaction magnetohydrodynamic solver on a non-staggered grids. *Int. J. Numer. Meth. Fluids* 2004; **45**: 1209–1233.
- [69] Sing KM, Kalra MS. Three and four step least squares finite element schemes in the time domain. *Commun. Numer. Meth. Engrg.* 1996; **12**: 425–431.
- [70] Sing KM, Kalra MS. Least-squares finite element schemes in the time domain. *Comput. Methods Appl. Mech. Engrg.* 2000; **190**: 111–131.
- [71] Tezduyar TE, Behr M, Liou J. A new strategy for finite element computations involving moving boundaries and interfaces – The deforming-spatial-domain/space-time procedure: I. The concept and the preliminary numerical tests*. *Comput. Methods Appl. Mech. Engrg.* 1992; **94**: 339–351.
- [72] Tezduyar TE, Behr M, Liou J. A new strategy for finite element computations involving moving boundaries and interfaces – The deforming-spatial-domain/space-time procedure: II. Computation of free-surface flows, two-liquid flows, and flows with drifting clinders*. *Comput. Methods Appl. Mech. Engrg.* 1992; **94**: 353–371.
- [73] Tezduyar TE, Shih R, Mittal S, Ray SE. Incompressible flow computations with stabilized bilinear and linear equal-order-interpolation velocity-pressure elements. *Comput. Methods Appl. Mech. Engrg.* 1992; **95**: 221–242.
- [74] Tezer-Sezgin M, Koksals S. FEM for solving MHD flow in a rectangular duct. *Int. J. Numer. Methods Engrg.* 1989; **28**: 445–459.
- [75] Verardi SLL, Cardoso JR. A solution of two-dimensional magnetohydrodynamic flow using the finite element method. *IEEE Trans. Magn.* 1998; **34** (5): 3134–3137.
- [76] Verardi SLL, Cardoso JR. Three-dimensional finite element analysis of MHD duct flow by the penalty function formulation. *IEEE Trans. Magn.* 2001; **37** (5): 3384–3387.

- [77] Wiedmer M. Finite element approximation for equations of magnetohydrodynamics. *Math. Comp.* 1999; **69 (229)**: 83–101.
- [78] Wood WL. *Practical time stepping schemes*, Clarendon Press, Oxford, 1990.
- [79] Zienkiewicz OC. *The Finite Element Method, 3rd*. McGraw-Hill, Newyork, 1977.

VITA

PERSONAL INFORMATION

Surname, Name : Aydın, Selçuk Han
Nationality : Turkish (TC)
Date and Place of Birth : May 23, 1975, Maçka
Marital Status : Married to Burcu Tuncer Aydın
Phone : +90 312 210 33 11
Fax : +90 312 210 33 02
e@mail : saydin@metu.edu.tr

ACADEMIC DEGREES

- Ph.D.** Department of Scientific Computing, 2008 May
Institute of Applied Mathematics
Middle East Technical University-Ankara
Supervisor: Prof. Dr. Münevver Tezer-Sezgin
Co-Supervisor: Assoc. Prof. Dr. Ali İhsan Neslitürk
Thesis Title: The Finite Element Method Over a Simple Stabilizing Grid
Applied to Fluid Flow Problems
- M.Sc.** Department of Mathematics, 2000 September
Middle East Technical University-Ankara
Supervisor: Prof. Dr. Münevver Tezer-Sezgin
Thesis Title: Dual Reciprocity Boundary Element Method for Poisson's Equation
Using Osculatory Radial Basis Functions
- B.S.** Department of Mathematics, June 1997
Middle East Technical University-Ankara

EMPLOYMENT

2002-	Researcher	Computer Center, Middle East Technical University
2001	Military Service	(8 months)
1998-2001	Researcher	Computer Center, Middle East Technical University

ADMINISTRATIVE RESPONSIBILITIES

User Support-PC Group Coordinator, Computer Center, Middle East Technical University.

NUMERICAL METHODS

Finite Difference Method (FDM), Boundary Element Method (BEM), Finite Element Method (FEM), Differential Quadrature Method (DQM).

PROGRAMMING LANGUAGES

Fortran, C, C++, PHP, Shell Programming, Matlab, Mathematica.

PUBLICATIONS

A. Papers published in International Journals:

A1. M. Tezer-Sezgin and S. Han Aydın, Dual Reciprocity Boundary Element Method for MHD Flows Using Radial Basis Functions, *Inter.Jour.of Comput. Fluid Dyns.*, 2002; **1**: 49–63.

A2. M. Tezer-Sezgin and S. Han Aydın, Numerical solution of magnetohydrodynamic flow problems using boundary element method, *WIT Transaction on Modeling and Simulation*, 2005; **39**.

A3. M. Tezer-Sezgin and S. Han Aydın, Solution of MHD Flow Problems using the Boundary Element Method, *Engrg. Analy. with Bound. Elem.*, 2006; **30**: 411–418.

A4. A. I. Neslitürk, S. Han Aydın and M. Tezer-Sezgin, Two-level finite element method with a stabilizing subgrid for the incompressible Navier-Stokes equations, *Int. J. Numer. Meth. Fluids* (in press).

B. Papers published in International Conference Proceedings:

B1. M. Tezer-Sezgin, S. Han Aydın; Numerical Solution of MHD Flow Problems Using Boundary Element Method BEM/MRM 27 World Conf. *On Boundary Elements and Other Mesh Reduction Methods*, 15-17 March 2005, Orlando, Florida, USA.

B2. S. Han Aydın; Dual Reciprocity BEM Solution of Grad-Shafranov Equation for the Distribution of Magnetic Flux in Nuclear Fusion Devices, *International Association for Boundary Element Methods 2006*, IABEM-2006, July 10-12, 2006, Graz, Austria.

B3. S. Han Aydın; BEM Solution of MHD Flow in Ducts with Arbitrarily Conducting Walls, *UKBIM 6 Proceedings of the 6th UK Conference on Boundary Integral Methods*, September 17-18 2007, Durham University, Durham, UK.

C. Presentations in International Conferences:

C1. S. Han Aydın, M. Tezer-Sezgin; Dual Reciprocity BEM for MHD Flow Using Radial Basis Functions, *2nd Inter. Conf. On Boundary Integral Methods: Theory and Applications*, 12-16 Sept. 2000, University of Bath, Bath, UK.

C2. S. Han Aydın, Sevin Gümgüm, M. Tezer-Sezgin; Dual Reciprocity BEM Solution of Diffusion Equation, *3rd Inter. Conf. On Boundary Integral Methods: Theory and Applications*, 14-18 September 2004, University of Reading, UK.

D. Presentations in National Conferences:

D1. S. Han Aydın; Multidimensional Interpolation Using Osculatory Radial Basis Functions, *Dynamical Systems*, Cumhuriyet Üniversitesi, Sivas, 1999.

D2. S. Han Aydın; Numerical solution of magnetohydrodynamic flow problems using boundary element method, *Dynamical Systems*, Ege Üniversitesi, İzmir, 2002.

D3. S. Han Aydın; Dual Reciprocity BEM Solution of Grad-Shafranov Equation for the Distribution of Magnetic Flux in Nuclear Fusion Devices, *Workshop on Numerical Methods Differential Equations*, İzmir Yüksek Teknoloji Enstitüsü, İzmir, 2006.

E. Projects:

Boundary element method solution of Nuclear Fusion problems, TÜBİTAK Project No: 105T091, Oct 2005 - Oct 2007.